



universität
wien

DIPLOMARBEIT

Titel der Diplomarbeit

Investigating the quaternary structure of the FMDV Leader protease

angestrebter akademischer Grad

Magistra der Naturwissenschaften (Mag. rer.nat.)

Verfasserin / Verfasser:	Jutta Steinberger
Matrikel-Nummer:	0345395
Studienrichtung /Studienzweig (lt. Studienblatt):	A 441 Diplomstudium Genetik - Mikrobiologie
Betreuerin / Betreuer:	Ao. Univ.-Prof. Dr. Timothy Skern

Wien, am 08. Juni 2009

Acknowledgements

First of all, I want to thank my supervisor Tim Skern for giving me the chance to work on this great project and for the support and motivation during my work.

I want to thank my lab members David Neubauer, Tina Kurz, Chiara Rancan, Carla Sousa, Kathi Ruzicska and Sabine Schultes for the friendship and the fun we had together. I enjoyed our common events like hiking, barbecue, Vienna Night Run, Italian dinner and Vienna City Marathon very much.

I also want to thank Georg Kontaxis for the help with NMR and Irene Gösler for introducing me to cell culture.

It was a great pleasure for me to work with you all, particularly due to the motivating and constructive ambience in the lab.

Furthermore, I want to thank my family and friends for making life interesting.

Special thanks to my father who always supported me and gave me the chance to study the subject of my choice.

At last, I want to thank Werner Steinmetz for the help, patience and motivation during the years of studies. Thank you for believing in me and always being there when I need you.

Index

1 Introduction	9
1.1 Picornaviruses	9
1.2 Foot-and-mouth disease virus	9
1.3 The virion	10
1.3.1 Genome organisation	10
1.3.2 Capsid organisation	11
1.4 Picornaviral life cycle	12
1.4.1 Attachment and cell entry	13
1.4.2 Translation and processing of the viral polyprotein	13
1.4.3 Viral replication	15
1.4.4 Virus assembly and release	16
1.4.5 Host cell shut off	17
1.5 Leader protease	19
1.5.1 Structure of Lb ^{PFO}	19
1.5.2 Enzymatic activities	23
1.5.2.1 Self-processing	23
1.5.2.2 eIF4G cleavage	24
1.5.3 Nuclear localisation	25
2 Aim of the work	27
3 Materials and Methods	29
3.1 Tissue culture	29
3.1.1 Cell lines	29
3.1.2 Media and Solutions	29
3.1.3 Cell culture	29
3.1.4 Cell splitting	30
3.1.5 Cell counting	30
3.1.6 Thawing of cells	30
3.1.7 Freezing of cells	30
3.2 Bacterial culture	31
3.2.1 Bacterial strains	31
3.2.1.1 E. coli Top 10F'	31
3.2.1.2 E. coli BL21 (DE3) LysS	31
3.2.1.3 Media and solutions	31
3.2.2 Preparation of competent cells	32
3.2.3 Transformation of competent cells	32
3.3 DNA methods	33
3.3.1 Plasmids	33
3.3.1.1 Plasmids used for <i>in vitro</i> experiments and protein expression	33
3.3.1.2 Plasmids used for cell culture experiments	33
3.3.2 Preparation of plasmid DNA from bacteria	34
3.3.2.1 DNA miniprep	34
3.3.2.2 DNA midiprep	34
3.3.3 DNA gelelectrophoresis	35
3.3.4 DNA quantification	35
3.3.5 Restriction digestion of DNA	35
3.3.6 DNA dephosphorylation	36
3.3.7 Phosphorylation and annealing of oligonucleotides	36
3.3.8 Extraction of DNA from agarose gel	36

3.3.9 DNA ligation.....	37
3.3.10 DNA purification	37
3.3.10.1 Wizard SV Gel and PCR Clean-Up System (Promega).....	37
3.3.10.2 Phenol/chloroform extraction	38
3.3.11 Site-directed PCR mutagenesis.....	38
3.3.12 Cassette cloning	39
3.3.13 DNA sequencing	39
3.3.14 Primers.....	39
3.3.14.1 Primers used for site-directed PCR mutagenesis.....	39
3.3.14.2 Oligonucleotides used for cassette cloning	40
3.3.14.3 Primers used for sequencing	40
3.4 RNA methods.....	41
3.4.1 <i>In vitro</i> transcription	41
3.4.2 RNA gelelectrophoresis	42
3.4.3 <i>In vitro</i> translation.....	42
3.5 Protein methods.....	43
3.5.1 Protein expression in HEK 293T cells.....	43
3.5.1.1 Ecdysone-Inducible Mammalian Expression System (Invitrogen)	43
3.5.1.2 Transfection and protein expression	43
3.5.2 Protein expression in E. coli BL 21 (DE3) LysS.....	44
3.5.2.1 Protein expression in LB medium	44
3.5.2.2 Protein expression in minimal medium.....	44
3.5.3 Preparation of HEK 293T cell extracts.....	45
3.5.4 Preparation of BL 21(DE3) LysS cell extracts.....	45
3.5.5 Protein purification	46
3.5.5.1 Ammonium sulfate precipitation	46
3.5.5.2 Dialysis	46
3.5.5.3 FPLC.....	46
3.5.5.3.1 Anion exchange chromatography	47
3.5.5.3.2 Size exclusion chromatography	47
3.5.6 Protein concentration.....	47
3.5.7 Protein quantification.....	47
3.5.8 SDS PAGE (Sodiumdodecylsulfate Polyacrylamide Gelelectrophoresis)	48
3.5.8.1 SDS PAGE (Laemmli, 1970)	48
3.5.8.2 SDS PAGE (Dasso et al., 1989)	49
3.5.9 Coomassie Staining	49
3.5.10 Fluorography.....	50
3.5.11 Western blot analysis.....	50
3.6 NMR (Nuclear Magnetic Resonance)	52
3.6.1 Principles.....	52
3.6.1.1 Chemical shift.....	53
3.6.1.2 Spin relaxation	53
3.6.2 NMR sample	53
3.6.3 NMR experiments	54
3.6.3.1 2D ¹ H- ¹⁵ N HSQC	54
3.6.3.2 3D triple resonance experiments	54

4 Results	57
4.1 Investigating intramolecular self-processing of Lb ^{pro}	57
4.1.1 Lb ^{pro} wildtype and shortened Lb ^{pro}	57
4.1.1.1 Enzymatic activity of Lb ^{pro} WT.....	57
4.1.1.2 Oligomerisation state of Lb ^{pro} WT and sLb ^{pro}	59
4.1.2 Effects of mutations at the interface on dimerisation.....	61
4.1.2.1 Enzymatic activities of interface mutants.....	62
4.1.2.2 Oligomerisation state of interface mutants.....	64
4.1.3 Effects of mutations in the CTE on dimerisation.....	65
4.1.3.1 Enzymatic activities of CTE mutants.....	66
4.1.3.2 Oligomerisation state of CTE mutants.....	68
4.1.3.3 NMR studies of CTE mutants.....	69
4.1.3.3.1 T ₂ transverse relaxation times of CTE mutants.....	70
4.1.3.3.2 2D ¹ H- ¹⁵ N HSQC spectra of CTE mutants.....	72
4.1.3.3.3 3D triple resonance experiments of Lb ^{pro} L200F.....	78
4.2 Investigating the nuclear localisation of Lb ^{pro}	81
5 Discussion	85
5.1 Investigating intramolecular self-processing of Lb ^{pro}	85
5.1.1 Interface mutants.....	85
5.1.2 CTE mutants.....	87
5.2 Investigating the nuclear localisation of Lb ^{pro}	93
6 Summary	95
7 Zusammenfassung	97
8 Appendix	99
8.1 Amino acids.....	99
8.2 Abbreviations.....	100
9 References	103
Curriculum vitae	107
Lebenslauf	109

1 Introduction

1.1 Picornaviruses

Picornaviruses are small (30 nm diameter), non-enveloped viruses with a single-stranded RNA genome of positive sense. The particles are simple, consisting of an icosahedral protein shell surrounding the naked RNA genome. This virus family contains many human and animal pathogens of particular importance, including poliovirus, hepatitis A virus, rhinoviruses and foot-and-mouth disease virus (Fields *et al.*, 2007).

1.2 Foot-and-mouth disease virus

Foot-and-mouth disease virus (FMDV) is a member of the aphthovirus genus of the picornavirus family (Pringle, 1997). There are seven serotypes (A, O, C, Asia 1 and South African Territories 1, 2 and 3) known which contain multiple subtypes (Bachrach, 1968). FMDV is the causative agent of a devastating viral disease affecting cloven-hoofed animals including cattle, swine, sheep and goats. In addition, more than 70 species of wild animals can be infected by FMDV (Fenner, 1993). The disease is characterised by fever, lameness and vesicular lesions on the tongue, feet, snout and teats (Donaldson, 1987). Although foot-and-mouth disease does not result in high mortality in adult animals, the disease has debilitating effects including the failure to gain weight, decrease in milk production and breeding problems (Bachrach, 1968). In fact, the FMDV epidemic in the United Kingdom in 2001 claimed expenses of £ 2.7 billion and the destruction of four million animals (Davies, 2002).

This thesis discusses experiments with the Leader protease of FMDV. Therefore, the further introduction is focused on FMDV. However, some aspects of the viral life cycle of FMDV have not been investigated in detail. Therefore, many references refer to experiments with other picornaviruses which are thought to show similar characteristics.

1.3 The virion

1.3.1 Genome organisation

Picornaviruses encode their genetic information on a single-stranded RNA genome of positive sense. Figure 1 shows the organisation of the FMDV genome which reflects a typical picornaviral genome (Mason *et al.*, 2003).

The viral protein VPg (viral protein genome linked) is covalently linked to the 5' end of the viral genome (Lee *et al.*, 1977; Sangar *et al.*, 1977) and is thought to play an important role in genome replication (Wimmer, 1982).

Upstream and downstream of the single open reading frame (ORF) the viral RNA contains untranslated regions (UTRs). The 5' UTR as well as the 3' UTR contain highly ordered structures important for cap independent translation and genome replication. The 5' UTR of FMDV is more than 1300 nucleotides in length and contains secondary structures such as the IRES (internal ribosome entry site) important for translation initiation (Belsham & Brangwyn, 1990) or the cre (*cis* replicative element) important for replication (Mason *et al.*, 2002). The 3' UTR is followed by a genetically encoded poly(A) tract. The stem-loop structure found in the 3' UTR of FMDV was shown to be important for genome replication (Saiz *et al.*, 2001).

The single ORF of picornaviruses is organised into three regions, designated as P1, P2 and P3 (Rueckert & Wimmer, 1984). The P1 region encodes the four structural viral proteins (VP) VP4, VP2, VP3 and VP1, whereas the P2 region encodes the three non-structural proteins 2A, 2B and 2C. Furthermore, the P3 region encodes the non-structural proteins 3A, 3B, the 3C protease (3C^{pro}) and the 3D polymerase (3D^{pol}) (Fields *et al.*, 2007). In contrast to other picornaviruses, such as poliovirus or human rhinoviruses (HRVs) (Toyoda *et al.*, 1986; Sommergruber *et al.*, 1989), the protein 2A of FMDV has no enzymatic activity. Instead, the FMDV genome encodes an additional protein, the Leader protease (L^{pro}), which is the first protein encoded on the open reading frame (Sangar *et al.*, 1987).

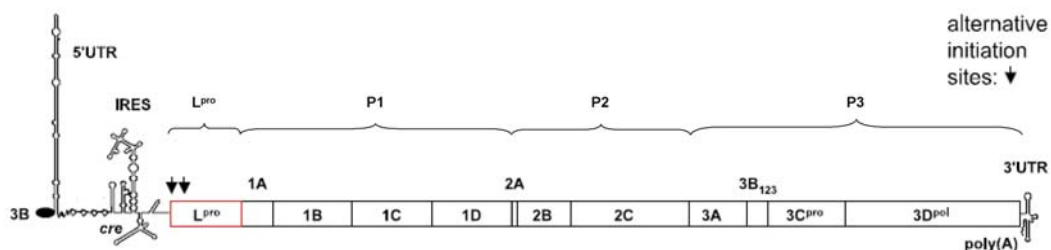


Figure 1 Organisation of the FMDV RNA genome. The viral protein VPg is linked to the 5' end of the viral RNA. The genome is composed of the 5' untranslated region (UTR), the protein coding region, the 3' UTR and a poly(A) tract. The 5' and 3' UTR contain several secondary structure elements such as IRES (internal ribosome entry site) and cre (*cis* replicative element) important for viral translation and replication. The protein coding region is composed of the regions L^{pro} (Leader protease), P1 (1A=VP4, 1B=VP2, 1C=VP3 and 1D=VP1), P2 (2A, 2B and 2C) and P3 (3A, three copies of 3B, 3C^{pro} and 3D^{pol}). Adapted from Mason *et al.*, 2003.

1.3.2 Capsid organisation

Picornaviral capsids consist of 60 protomers, each composed of the four structural proteins VP1, VP2, VP3 and VP4. These four proteins are arranged in an icosahedral symmetry, displaying 20 threefold axis and 12 fivefold axis (Acharya *et al.*, 1989). Figure 2A shows the icosahedral structure of the FMDV capsid which is common to all picornaviral capsids. The three capsid proteins VP1-VP3 have molecular weights of about 30 kDa and form the external surface of the icosahedral shell, whereas the smaller protein VP4 lies on the inner surface (see Figure 2B). Though VP1, VP2 and VP3 share no sequence homology, they display the same structure of an eight-stranded, antiparallel β -sheet, also called a β -barrel jelly roll. This jelly roll forms a wedge-shaped structure that allows packing of structural units to form a dense, rigid protein shell (Fields *et al.*, 2007). Thereby, the N-termini of VP1, VP2, VP3 and VP4 form a network on the interior of the capsid contributing significantly to the stability of the virion. It has been shown for poliovirus that the interaction between the N-termini is mediated by the myristate group which is attached to the N-terminus of VP4 (Chow *et al.*, 1987). However, VP4 differs significantly from the other proteins in its extended conformation, thereby interacting with the viral RNA (Morrell *et al.*, 1987).

The FMDV virion appears as a round particle with a smooth surface and a diameter of about 25 nm (Bachrach, 1968), lacking a surface canyon (Acharya *et al.*, 1989) (see Figure 2C). It was shown for other picornaviruses, such as poliovirus and human rhinoviruses, that the viral capsid displays a prominent, star-shaped plateau which is found at the fivefold axis surrounded by a deep depression, called the canyon. This canyon has been shown to be the receptor binding site for cell entry for entero- and cardioviruses (Rossmann *et al.*, 1985; Luo *et al.*, 1987; Kolatkar *et al.*, 1999; Belnap *et al.*, 2000). In contrast, FMDV attaches to cell receptors via an RGD sequence provided by the flexible β G- β H loop of the capsid protein VP1, as shown in Figure 2C (Neff *et al.*, 1998) (see chapter 1.4.1).

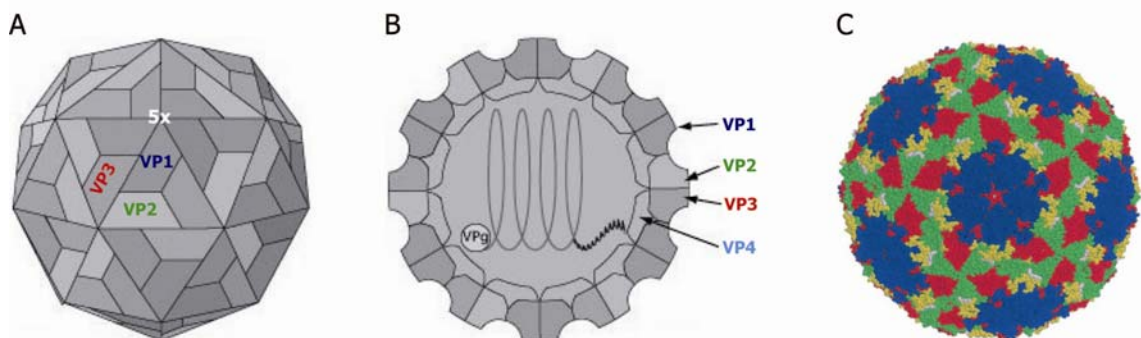


Figure 2 Structure of the FMDV capsid. (A) Schematic representation of the FMDV capsid which is composed of 60 copies of each of the structural proteins VP1, VP2, VP3 and VP4 (on the interior). Protomer proteins that are displayed on the surface are labelled. A fivefold axis is labelled. (B) Cross-section of the FMDV capsid. VP1-3 are displayed on the outer surface, whereas VP4 is located on the inside connecting the viral RNA genome to the capsid. (B) + (C) Adapted from http://www.expasy.org/viralzone/all_by_protein/98.html. (C) Structure of the mature type O₁BFS FMD virion based on crystal data. The capsid proteins VP1 (blue), VP2 (green) and VP3 (red) are displayed on the surface. The β G- β H loop (yellow) providing the RGD sequence (white) important for cell attachment is shown (Grubman & Baxt, 2004).

1.4 Picornaviral life cycle

Figure 3 shows an overview of the picornaviral life cycle.

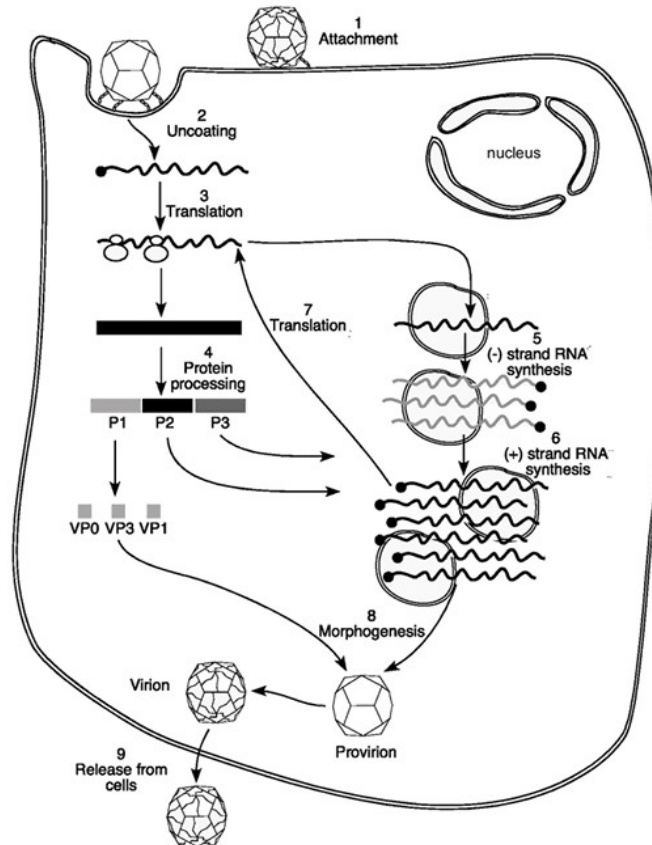


Figure 3 The picornaviral life cycle. After attachment of the virus to a cellular receptor (1), the viral RNA genome is uncoated (2) and released into the cytoplasm. The VPg is removed from the RNA which is subsequently translated into a long polyprotein (3). Subsequently, the polyprotein is proteolytically processed by viral proteases (4). RNA synthesis takes place on membranous vesicles induced by viral proteins once the viral RNA polymerase is translated. In this process, the polymerase copies the (+) strand RNA to form a full length (-) strand RNA (5) which is used to produce additional (+) strand RNA (6). This newly synthesised (+) strand RNA is either used for further translation (early in infection) (7) or packed into viral particles (late in infection) (8). Finally, newly synthesised virus particles are released from the cell upon cell lysis (9). (Fields *et al.*, 2007)

1.4.1 Attachment and cell entry

A picornavirus infection starts with the attachment of the virus to a receptor on the host cell membrane. For some picornaviruses, such as major group human rhinoviruses, it has been shown that the canyon on the viral capsid mediates the interaction with host cell receptors (Olson *et al.*, 1993). In contrast, the FMDV capsid does not exhibit prominent canyons that can be used for cell attachment. Instead, FMDV binds to host cell receptors via a conserved Arg-Gly-Asp (RGD) sequence in the flexible β G- β H loop of the capsid protein VP1 (Neff *et al.*, 1998). FMDV binds to one of the four different α_v integrins ($\alpha_v\beta_1$, $\alpha_v\beta_3$, $\alpha_v\beta_6$ or $\alpha_v\beta_8$) to infect animal cells (Jackson *et al.*, 2004). However, *in vitro* experiments revealed that FMDV can also use heparan sulfate as an alternative receptor for the attachment to cultured cells (O'Donnell *et al.*, 2008).

After attachment to the cell, the virus is internalised via endocytosis. It was found for FMDV that the attachment to the cell by binding to integrin is followed by clathrin-mediated endocytosis (Berryman *et al.*, 2005), whereas the binding to the alternative receptor heparan sulfate leads to caveola-mediated endocytosis (Berryman *et al.*, 2005; O'Donnell *et al.*, 2005; O'Donnell *et al.*, 2008).

It was shown for FMDV that uncoating of the viral RNA genome is dependent on the acidification of endocytic vesicles. The low pH leads to a breakdown of the viral capsid structure, converting 140S virion particles to 12S pentameric subunits. This would suggest that FMDV uncoating resembles the mechanism used by minor group human rhinoviruses which are dependent on low pH-induced virion degradation for the release of the viral genome (O'Donnell *et al.*, 2005). However, the mechanism of FMDV genome release into the cytoplasm is yet unknown.

1.4.2 Translation and processing of the viral polyprotein

As soon as the genome is released into the cytoplasm, the picornaviral RNA is translated. As the replication of the viral genome is dependent on the virally encoded RNA-dependent RNA-polymerase 3D^{pol} the genome has to be translated before replication can occur.

The viral RNA lacks the 5' cap-structure found on cellular mRNAs but has the VPg covalently linked to its 5' end. However, it has been shown for poliovirus that VPg is cleaved off the viral RNA by a cellular enzyme before translation is initiated (Ambros & Baltimore, 1980).

In contrast to the cap-dependent translation initiation of cellular mRNAs, the translation of the viral RNA is initiated via an internal ribosome entry site (IRES) found in the 5' UTR of the viral genome (Belsham & Brangwyn, 1990) (see chapter 1.3.1). This cap-independent mechanism of translation initiation allows the translation of viral RNA during infection while cap-dependent translation of the host cell is inhibited (Devaney *et al.*, 1988) (see chapter 1.4.5).

The picornaviral genome contains only one open reading frame which is translated into a long polyprotein. Subsequently, the polyprotein is processed by viral proteases to form the mature structural and non-structural proteins (Toyoda *et al.*, 1986).

The translation of the single open reading frame of FMDV can be initiated at one of two AUG codons lying 84 nucleotides apart. Consequently, two forms of the first protein encoded on the polyprotein (L^{PRO}) are created, designated as Lab^{PRO} and Lb^{PRO} (Sangar *et al.*, 1987). Although Lb^{PRO} is 28 amino acids shorter than Lab^{PRO}, both variants were found to possess the same enzymatic activities (Medina *et al.*, 1993). However, it was shown that Lb^{PRO} is the physiologically active protease (Cao *et al.*, 1995). Therefore, most studies were performed with the Lb^{PRO} form.

The processing of the FMDV polyprotein is shown in Figure 4. The processing of the viral polyprotein is initiated by L^{PRO} cleaving autocatalytically between its own C-terminus and the N-terminus of the subsequent viral protein VP4 (Strebel & Beck, 1986) (see chapter 1.5.2.1).

The protein 2A of FMDV is only 18 amino acids in length and has no enzymatic activity. However, it frees itself from the subsequent protein 2B by mediating a putative ribosomal skip between its own C-terminus and the N-terminus of 2B (Donnelly *et al.*, 2001). In contrast, in other picornaviruses, such as poliovirus and human rhinoviruses, the 2A protease is about 17 kDa in size and is enzymatically active cleaving the nascent polyprotein at its own N-terminus. The separation from the subsequent 2B protein is not mediated by a ribosomal skip, which is unique to FMDV, but is performed by the 3C protease (Toyoda *et al.*, 1986; Sommergruber *et al.*, 1989).

All other cleavage reactions are performed by the chymotrypsin-like cysteine protease 3C^{PRO} (Clarke & Sangar, 1988).

The last step in polyprotein processing is the cleavage of VP0 into VP4 and VP2. This cleavage reaction is a maturation step during the assembly of new viral particles (see chapter 1.4.4). However, the mechanism that results in the maturation cleavage has yet not been identified.

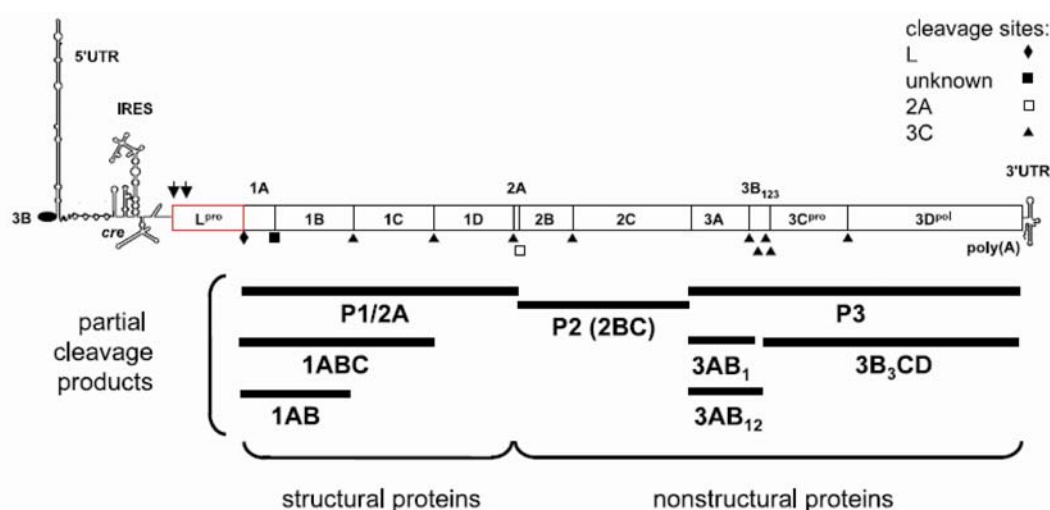


Figure 4 Processing of the FMDV polyprotein. Translation of the single ORF results in the production of a long polyprotein which is processed by viral proteases. The 3C protease (3C^{PRO}) performs most of the cleavage events of post-translational processing. However, the Leader protease (L^{PRO}) autocatalytically cleaves itself off, whereas the 2A protein is N-terminally cleaved by 3C^{PRO} and induces a ribosomal skip at its C-terminus to free itself from the polyprotein. The protease responsible for the cleavage of VP0 has yet not been identified. The partial cleavage products are indicated. Adapted from Mason *et al.*, 2003.

1.4.3 Viral replication

Viral RNA replication takes place on membranous vesicles, composed of material from lysosomes, Golgi and endoplasmic reticulum induced by the viral proteins (Bienz *et al.*, 1990).

Upon translation, the virally encoded RNA-dependent RNA polymerase 3D^{pol} (3D polymerase) initiates replication of the viral genome by the synthesis of a minus-strand RNA transcript. The switch mechanism from translation to replication is unclear. However, it has been suggested for poliovirus infected cells that the switch is caused by the accumulation of the polymerase precursor 3CD (Garmarnik & Andino, 1998). Whether 3CD plays a similar role in FMDV RNA replication is not known. It has been shown in FMDV-infected cells that the polymerase precursor is rapidly cleaved to 3C^{pro} and 3D^{pol} (Grubman, 1984), arguing against a role for 3CD in replication control.

Currently, a model for minus-strand RNA synthesis has been proposed that suggests a circularisation of the positive-strand RNA genome (Herold & Andino, 2001). Thereby, VPg is thought to act as a primer for the RNA polymerase (Crawford & Baltimore, 1983). The alternative model suggests that minus-strand synthesis is primed on the poly(A) tail. Thereby, double-stranded RNA molecules are formed which are used for the synthesis of plus-strand RNA (Novak & Kirkegaard, 1991).

Specific secondary structures, such as the cloverleaf found in the 5' UTR (Rivera *et al.*, 1988) or the single stem loop found in the 3' UTR (Pilipenko *et al.*, 1992) ensure that the viral RNA is specifically recruited to the replicative complex.

The cre (*cis* replicative element), found in the 5' UTR of the FMDV genome, was found to play an important role in genome replication (Mason *et al.*, 2002). The cre, a stem-loop structure, contains a conserved AAACA motif which functions as a template for the addition of U residues to the protein primer VPg. Interestingly, in other picornaviruses these elements, being responsible for the same function, are located in different regions of the genomes. In poliovirus the cre sequence was found to be embedded within the protein-encoding region for the protein 2C (Goodfellow *et al.*, 2000), whereas in human rhinovirus 2 the cre sequence was found in the sequence encoding the 2A protease (Gerber *et al.*, 2001).

1.4.4 Virus assembly and release

The final steps in the replication cycle are the assembly of the viral particle and the encapsidation of the plus-stranded RNA genome. Figure 5 shows a schematic overview of the assembly of picornaviral particles. The viral capsid is composed of the structural proteins that are created as a result of 3C^{pro} cleavage of the P1 region (see chapter 1.4.2). The smallest intermediate block is the 5S protomer which contains one copy each of the proteins VP0, VP1 and VP3. In the mature capsid, the C-termini of the structural proteins are located on the outer surface, whereas the N-termini point to the interior and form a network of interactions connecting single protomers (Palmenberg, 1982). Five protomers form the 14S pentamer, which then build up the complete capsid. Currently, there are two models of picornavirus assembly. One model suggests that pentamers assemble into empty capsids (80S), followed by insertion of the RNA (Jacobson & Baltimore, 1968). In contrast, the second model proposes that pentamers directly interact with the RNA to form the provirion (150S) (Nugent & Kirkegarrd, 1995). However, it was shown that only viral positive-strand RNA linked to VPg is encapsidated (Nugent & Kirkegarrd, 1995). In the presence of viral RNA, the maturation cleavage of VP0 into VP4 and VP2 takes place resulting in a fully infectious 160S virion (Basavappa et al., 1994).

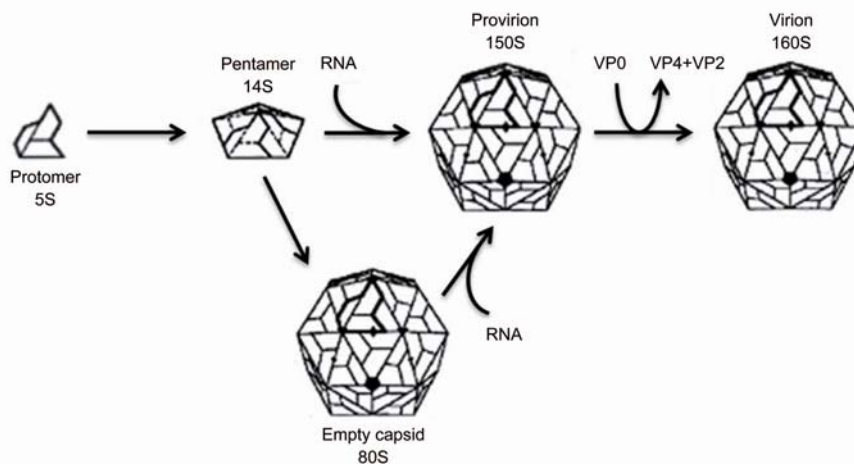


Figure 5 Assembly of picornavirus particles. 5S protomers composed of VP0, VP1 and VP3, self-assemble into 14S pentamers which can fit into the 80S capsid (no RNA encapsidated) or 150S provirion (RNA encapsidated). The maturation cleavage of VP0 into VP4 and VP2 results in fully infective 160S virions. Adapted from Fields *et al.*, 2007.

1.4.5 Host cell shut off

The term 'host cell shut off' describes the collapse of protein synthesis of virus infected cells (Etchison *et al.*, 1982; Etchison & Fout, 1985; Devaney *et al.*, 1988). In contrast, viral protein synthesis is not affected, enabling the virus to replicate and take over the host cell.

Figure 6A gives an overview of cellular initiation factors involved in cap-dependent translation initiation. An important feature of cellular mRNAs is the 7-methyl-guanosine at the 5' end. This cap structure as an anchor for the cap binding complex eIF4F, composed of the eukaryotic initiation factors (eIFs) 4E, 4G and 4A. eIF4E (also designated as cap binding protein) is able to bind to the cap structure of mRNAs (Sonenberg *et al.*, 1978). eIF4A acts as an RNA helicase, whereas eIF4G acts as a central scaffold protein mediating interactions between several initiation factors. The binding of eIF4G to eIF4E and the poly(A) binding protein (PABP) results in the circularisation of the mRNA which constitutes an important event in translation initiation (Imataka *et al.*, 1998). Beside eIF4A, eIF4G also binds eIF3, thereby recruiting the 40S ribosomal subunit to the mRNA.

During picornaviral infection eIF4G is cleaved by a viral protease, thus separating the domain binding the cap-binding protein eIF4E from the domain which binds eIF3 complexed to the 40S ribosomal subunit. In case of FMDV infection, this cleavage reaction is performed by the Leader protease (Devaney *et al.*, 1988) (see chapter 1.5.2.2). Consequently, the translation machinery of the host cell is not able to recruit ribosomes to mRNAs any more, resulting in inhibited protein synthesis (see Figure 6B). However, viral mRNA translation remains unaffected as it initiates protein synthesis internally via an internal ribosome entry site (IRES). IRES mediated translation initiation includes interactions with a number of cellular proteins, including translation initiation factors important for cap-dependent cellular mRNA translation (Borman *et al.*, 1997).

It was shown by Gradi and colleagues that there are two homologues of eIF4G, termed eIF4GI and eIF4GII (Gradi *et al.*, 1998a). Though the two homologues share only 46 % sequence identity, both homologues have to be cleaved for full host-cell shut off (Gradi *et al.*, 1998b).

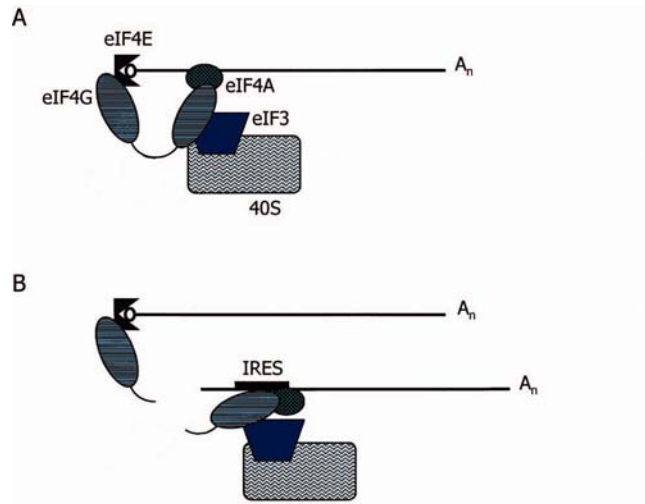


Figure 6 eIF4G cleavage during viral infection. (A) eIF4G plays an important role in cap-dependent translation initiation acting as a scaffold protein for eIF4E (cap binding protein), eIF4A and eIF3, thereby recruiting the ribosome to the mRNA. (B) During infection, eIF4G is cleaved by a viral protease, thus disrupting cap-dependent translation initiation. Viral RNA translation is not affected as translation is initiated via an internal ribosome entry site (IRES). Adapted from Guarne *et al.*, 1998.

1.5 Leader protease

The Leader protease (L^{pro}), the first protein on the polyprotein, is an important determinant of virulence in FMDV infection. It was shown that L^{pro} is responsible for the inhibition of translation in the host cell, also designated as 'host cell shut off' (Devaney *et al.*, 1988) (see chapter 1.4.5). L^{pro} is also related with the degradation of NF- κ B during FMDV infection, thus antagonising the cellular innate immune system (de Los Santos *et al.*, 2007). Furthermore, it has been shown that a virus lacking the Leader sequence was avirulent when injected into cattle and pigs and unable to spread to cohoused animals (Chinsangaram *et al.*, 1998).

Therefore, L^{pro} represents an interesting target for antiviral therapy (Kleina & Grubman, 1992).

1.5.1 Structure of Lb^{pro}

Lb^{pro} is a cysteine protease displaying a papain-like fold which is adapted for self-processing and the recognition of the eukaryotic initiation factor 4G (Guarne *et al.*, 1998). Figure 7 shows the protein structures of Lb^{pro} and papain. Like papain, Lb^{pro} consists of a globular region divided into two subdomains, an α -helical N-terminal domain and a β -sheet C-terminal domain. The active site residues, Cys 51 and His 148 in case of Lb^{pro} and Cys 25 and His 149 in case of papain, are positioned on opposite sides of a cleft separating the two domains (Guarne *et al.*, 1998). The third residue of the catalytic triad of Lb^{pro} is Asp 163, in contrast with all other cysteine proteases that have Asn at this position (Guarne *et al.*, 2000).

A unique feature of Lb^{pro} is the flexible 18 amino acid long C-terminal extension (CTE) which has no equivalent in papain (Guarne *et al.*, 1998). The CTE was shown to be involved in self-processing and the recognition of eIF4GI (Glaser *et al.*, 2001).

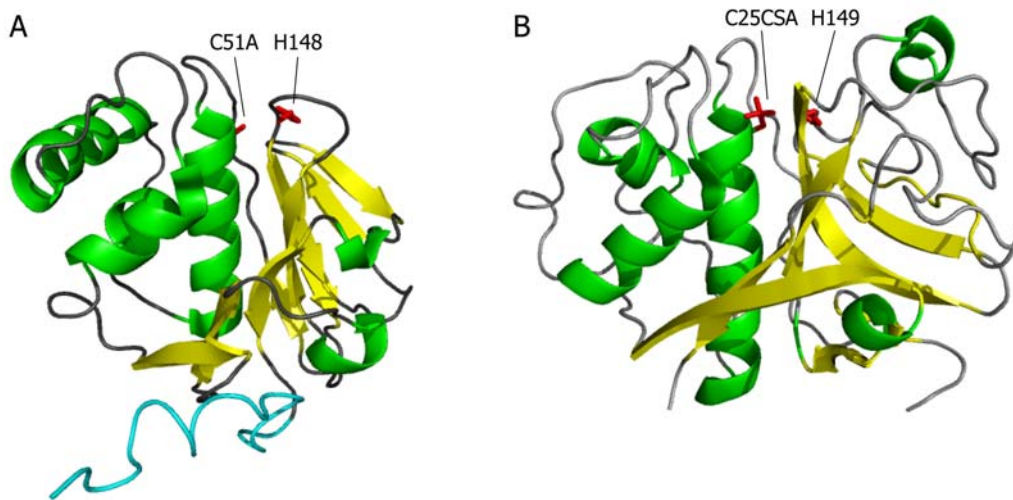


Figure 7 Structures of Lb^{P^{ro}} (A) and papain (B). α -helices are shown in green, β -sheets in yellow. The globular domains of Lb^{P^{ro}} and papain show high similarity, displaying an α -helical N-terminal domain and a β -sheet C-terminal domain. The CTE of Lb^{P^{ro}}, shown in cyan, has no equivalent in papain. The active site residues are shown in red. The active site of Lb^{P^{ro}} is built of Cys 51 and His 148 (H148), whereas Cys 51 was mutated to Ala (C51A) for crystallisation. In papain, Cys 25 and His 159 (H159) form the active site, whereas Cys 25 was mutated to cysteinesulfonic acid (C25CSA) for crystallisation. Created with PyMOL (DeLano, 2002) using the PDB ID codes 1QOL (A) and 9PAP (B).

Crystallography studies showed that Lb^{P^{ro}} forms stable dimers in solution by inserting the CTE into the active site of the neighbouring molecule and *vice versa* (Guarne *et al.*, 1998), as shown in Figure 8A. However, it was shown in NMR studies that one half of the dimer in the crystal structure is rotated about 25-30° away from the crystal structure, thus showing the formation of a complete symmetric arrangement of the dimer. Therefore, it is likely that crystal packing constraints forced the dimer into an asymmetric arrangement (Cencic *et al.*, 2007).

It was demonstrated by Santos and colleagues that the last seven residues of the CTE interact with residues of the substrate binding site (Santos *et al.*, 2009). Figure 8A shows the interaction between the CTE and the active site of a neighbouring Lb^{P^{ro}} molecule, resulting in the formation of stable dimers in solution. Figure 8B shows the interaction between CTE and active site in respect to the electrostatic interactions. For clarity, the residues of one molecule of the dimer are designated Met 29 (M29) to Lys 201 (K201), whereas the residues of the other molecule are designated Met 29' (M29') to Lys 201' (K201').

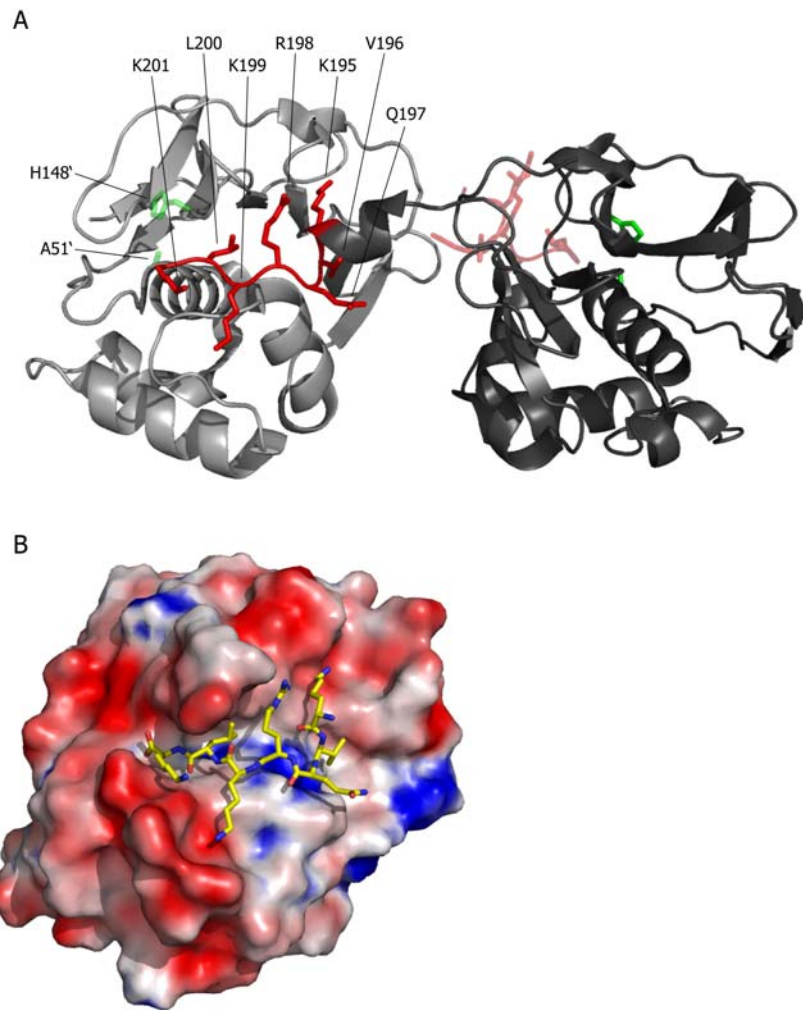


Figure 8 Interaction between the CTE and the active site of neighbouring Lb^{D70} molecules. (A) Dimerised proteases are shown in light and dark grey. The last seven amino acids of the CTE (shown in red) bind into the active site of the adjacent molecule (shown in green), thus forming a stable dimer. (B) The last seven C-terminal amino acids (shown as sticks) bound to the active site of the neighbouring molecule are shown. The carbon atoms of the CTE are coloured yellow, the nitrogen atoms are coloured blue and the oxygen atoms are coloured red. The electrostatic potential of the globular domain of one molecule is shown. A blue colour indicates regions of positive potential (5 kT/e), whereas red depicts negative potential (-30 kT/e). Created with PyMOL (DeLano, 2002) using the PDB ID code 1QOL. The electrostatic potential was calculated using the APBS tool (Baker *et al.*, 2001).

Residues P₁ to P₃ are bound in an extended conformation whereas residues P₄ to P₇ are bound in a short 3₁₀ helix (Santos *et al.*, 2009).

The S₁ subsite of Lb^{PRO} displays a deep, narrow cleft which clearly prefers Lys at P₁ in the self-processing reaction. Lys 201' was found to point away from the substrate binding cleft and is sandwiched by Glu 96 and Glu 147, enabling the formation of electrostatic interactions (Kirchweger *et al.*, 1994; Gradi *et al.*, 2004).

The major determinant of specificity is the S₂ subsite which constitutes a deep hydrophobic pocket accepting only Val, Leu and to a certain extent Ile (Santos *et al.*, 2009). It was previously shown by Mayer and colleagues that the substitution of Leu 200 at position P₂ to Phe results in the inability of Lb^{PRO} to cleave itself off the polyprotein. The discrimination against Phe at position 200 was shown to be due to sterical hindrance from Leu 143'. When leucine 143' was substituted with Ala, more space was provided in the S₂ pocket allowing Phe to fit into the pocket. This led to a complete recovery of Lb^{PRO} self-processing (Mayer *et al.*, 2008).

The side chain of Lys at position P₃ points away from the active site and was found to occupy a loose pocket (Kuehnel *et al.*, 2004).

Lb^{PRO} clearly prefers Arg at position P₄ that is involved in hydrogen bonds and Van der Waals interactions. There is no real binding site for Gln at position P₅. However, it is possible that Gln is involved in making the 3₁₀-turn referred to above. The P₆ subsite is composed of hydrophobic residues which can accept the wildtype Val, but also Phe and Pro. Also Ser is well accepted, probably because it does not fully enter into the pocket. The Lys residue at position P₇ of the CTE builds Van der Waals and ionic interactions with residues of the active site (Santos *et al.*, 2009).

Interestingly, the two residues Leu 143 and Leu 178 are involved in more than one interaction with the CTE of the neighbouring molecule, fitting with the strategy of viruses to conserve genome space. Leu 143 is involved in the S₂ and the S₄ subsite as well as in Van der Waals interactions with Lys at position P₇. Leu 178 is involved in the S₂ as well as the S₆ subsite (Santos *et al.*, 2009).

It was shown by Cencic and colleagues that the dimer is indeed very stable as several attempts to inhibit dimer formation failed. Dilution of the enzyme to 0.3 mM as well as increasing the sodium chloride concentration to 2 M did not affect dimer formation. In a further attempt, 12mer oligopeptides were designed containing either the cleavage sequence of the polyprotein or that of eIF4G. Titration with these model peptides mimicking the substrates destabilised the dimer. Transient peptide binding led to a chemical shift of residues in essentially two regions of Lb^{PRO}. One region lies in the dimer interface between the two globular domains of dimerised molecules (Trp 105, Thr 113, Thr 117 and Ser 119) and the second region contains certain residues of the CTE (Tyr 183, Asp 184, Gln 185 and Glu 93) (Cencic *et al.*, 2007). However, it was not possible to dissociate the dimer.

1.5.2 Enzymatic activities

In contrast to papain, Lb^{pro} is a very specific protease, cleaving only three known substrates, the viral polyprotein (Strebel & Beck, 1986) and the two homologues of the cellular eukaryotic initiation factor 4G (eIF4G) (Kirchweger *et al.*, 1994; Gradi *et al.*, 2004).

As shown in Table 1 the cleavage sequences vary strongly amongst substrates, not allowing the determination of a consensus sequence. In contrast to Lb^{pro}, papain has a broad range of specificity which is mainly caused by the architecture of the S₁ subsite. The S₁ subsite of papain is a wide, unrestricted pocket which exerts relatively little influence on the substrate specificity. In contrast, the subsite of Lb^{pro} is narrower and deeper, resulting in increased substrate specificity (Guarne *et al.*, 1998) (see chapter 1.5.1).

Table 1 Cleavage sites recognized by Lb^{pro}

Substrate	Cleavage sequence	
	P	P'
	6 5 4 3 2 1	↓ 1 2 3 4 5 6
Lb ^{pro} /VP4	VQRKLK	↓GAGQSS
eIF4GI	SFANLG	↓RTTLST
eIF4GII	PLLNVG	↓SRRSQP

1.5.2.1 Self-processing

The unique role of Lb^{pro} in viral maturation is to free itself from the polyprotein by cleavage between its own C-terminus and the N-terminus of VP4 at the sequence VQRKLK↓GAGQSS, as shown in Figure 9. This self-processing event can either occur in an inter- or intramolecular process (Glaser *et al.*, 2001).

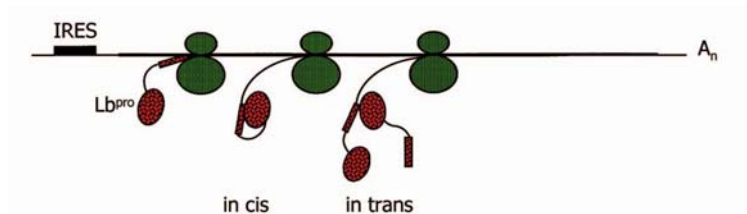


Figure 9 Lb^{pro} self-processing. Lb^{pro} (red) is translated by the ribosome (green) as the first protein from the single ORF. Still part of the polyprotein it is entirely folded and enzymatically active. Lb^{pro} can free itself from the polyprotein either by intramolecular (*in cis*) or intermolecular (*in trans*) processing. Adapted from Guarne *et al.*, 1998.

The presence of the CTE in the active site of neighbouring molecules found in the crystal and NMR structure argues for intermolecular self-processing; however, structural features of the CTE suggest for self-processing in *cis*. Since the interface between the globular domains of dimerised molecules is composed of weak interactions, this region does not seem to be designed to promote an intermolecular reaction (Guarne *et al.*, 1998).

Indeed, certain residues of the CTE favour a turn towards the own active site and promote interactions with the globular domain. Thus, the CTE would reach the active site where electrostatic and van der Waals interactions would maintain the correct orientation of the CTE for self-processing in *cis*. A model for intramolecular self-processing of the Lb^{pro} is presented by Guarne *et al.*, 1998.

Furthermore, it was shown by Glaser and colleagues that self-processing in *cis* is preferred to the *trans* cleavage reaction. Using an *in vitro* assay they could simultaneously investigate the inter- and intramolecular cleavage reaction of Lb^{pro}. Thereby, the intramolecular cleavage reaction of the polyprotein substrate was found to be performed much more rapid than the intermolecular one. This led to the conclusion that *cis* cleavage is preferred over the *trans* reaction (Glaser *et al.*, 2001).

1.5.2.2 eIF4G cleavage

During FMDV infection Lb^{pro} plays an important role in host cell shut off, as it completely disrupts the translation machinery by cleaving the two homologues of the eukaryotic initiation factors 4GI and 4GII (Devaney *et al.*, 1988) (see chapter 1.4.5). eIF4GI is cleaved at the sequence SFANLG⁶⁷⁴↓GRTTLST, whereas eIF4GII is cleaved at the sequence PLLNVG⁷⁰⁰↓SRRSQP (Kirchweger *et al.*, 1994; Gradi *et al.*, 2004). The amino acid sequence of the eIF4GII cleavage site differs significantly from the one of eIF4GI. Interestingly, the region of eIF4GII that corresponds to the cleavage site on eIF4GI is not recognised by Lb^{pro}, even when the correct site is blocked. However, this phenomenon remains to be investigated.

Interestingly, the CTE was shown to play an important role in the *trans* cleavage reaction. Investigations by Foeger and colleagues indicated that the cleavage of eIF4GI is a multistep-process that involves the binding of the C-terminal residues Tyr 183 to Lys 195 of Lb^{pro} to a distinct domain of eIF4GI which promotes cleavage of eIF4GI, presumably by bringing the active site into close proximity of the cleavage site (Foeger *et al.*, 2002).

1.5.3 Nuclear localisation

Upon uncoating, Lb^{pro} is subsequently translated from the viral RNA in the cytoplasm. However, it was previously shown that a small fraction of Lb^{pro} locates to the nucleus during infection and is directly associated with the degradation of accumulated p65/RelA in the nucleus. This prevents NF- κ B induced expression of IFN- β and other inflammatory cytokines, resembling a global strategy to counteract the immune system (de Los Santos *et al.*, 2007). Furthermore, de los Santos and colleagues reported that L^{pro} contains a SAP (SAF-A/B, Acinus and PIAS) domain. This protein structure is associated with the nuclear retention of molecules involved in transcriptional control in some cases (de los Santos *et al.*, 2009).

In principal, there are two possibilities how the Leader protease can enter the nucleus, either by passive diffusion or via receptor-mediated transport through the nuclear pore complex (NPC). In fact, small molecules such as ions and metabolites can freely diffuse between the cytoplasmic and the nucleic compartment. Also small proteins are able to translocate to the nucleus by simple diffusion. However, if the molecular weight of the proteins approach 20 - 40 kDa, diffusion becomes inefficient (Fried & Kutay, 2003).

Receptor-mediated transport across the NPC is dependent on a nuclear localisation signal (NLS). A nuclear localisation signal consists of one or two sequences that are rich in the positively charged amino acids Lys and Arg. The precise sequence is varying for different nuclear proteins and there are signals which are not yet characterised (Alberts, 2002). The import across the NPC is mediated by binding of the importin α - β heterodimer to the NLS of the import substrate in the cytoplasm. The transfer through the nuclear pore complex is energy-dependent and requires GTP-hydrolysis by Ran. In the nucleus, the cargo is released and importin subunits are separately returned to the cytoplasm for another round of transport (Gorlich, 1997).

De los Santos and colleagues showed that L^{pro} could be detected in the nucleus of infected cells three hours post infection. However, as the Leader protease was found to be distributed throughout the cytoplasm already two hours post infection (de Los Santos *et al.*, 2007), diffusion of the Leader protease into the nucleus could be excluded. In that case, Leader protease would already have been detected in the nucleus 2 hours post infection. We speculated that the Leader protease might possess a nuclear localisation signal to pass the nuclear pore complex. Therefore, we wanted to investigate the nucleocytoplasmic transport of Lb^{pro} more precisely.

2 Aim of the work

The overall aim of the work was to investigate the mechanism of intramolecular self-processing of FMDV Lb^{pro} in order to provide the background for an inhibition of this process. Consequently, Lb^{pro} would stay connected with VP4 which would no longer be able to fit correctly into the viral capsid structure. Therefore, we assumed that the inhibition of the intramolecular self-processing of Lb^{pro} would disrupt the formation of viable virus particles, as has previously been shown for poliovirus (Crowder & Kirkegaard, 2005).

However, due to stable dimer formation of Lb^{pro} this was not yet possible. Therefore, we attempted to inhibit dimer formation by site-directed mutagenesis in order to find mutants that appeared monomeric, but remained enzymatically active.

On the basis of previous studies, several residues that were thought to be involved in dimer stabilisation should be substituted with different residues. The mutated residues were either located in the interface region between dimeric molecules or in the interacting regions of the CTE and the active site. We then aimed to investigate the enzymatic activity of the different mutants by kinetic studies on self-processing and eIF4GI cleavage. At the same time the oligomerisation state of the Lb^{pro} mutants should be checked by size-exclusion chromatography and NMR analysis. Furthermore, NMR provides the possibility to investigate the structural and dynamic properties of the flexible CTE. Thus, NMR is a useful tool to investigate the interaction of the CTE with the active site in order to gain more information about intramolecular self-processing of Lb^{pro}.

As a side project, we set out to investigate the nucleocytoplasmic transport of Lb^{pro} more precisely. In this context, we addressed the question whether Lb^{pro} contains a nuclear localisation signal (NLS) in order to be transported through the nuclear pore complex. Therefore, Lb^{pro} was intended to be expressed in a human cell line and cellular localisation should be investigated via western blot analysis and immunodetection. Should Lb^{pro} appear in the nucleus, the putative NLS could be modified and the resulting effects on the localisation of Lb^{pro} could be investigated.

3 Materials and Methods

3.1 Tissue culture

3.1.1 Cell lines

Human embryonic kidney (HEK) 293T cells were used for cell culture experiments due to their easy handling and high transfectability. This variant of HEK 293 cells contains, in addition, the SV40 Large T antigen which allows episomal replication of transfected plasmids containing the SV40 origin of replication.

3.1.2 Media and Solutions

Dulbecco's Modified Eagle Medium (DMEM) (Gibco BRL) was supplemented with 10 % (v/v) Foetal Calf Serum (FCS) (Gibco BRL), 1 % (v/v) 200mM L-Glutamine (Gibco BRL) and 1 % (v/v) 100 x Penicillin/Streptomycin (Gibco BRL). This medium was used for monolayer culture of HEK 293T cells.

For the transfection of cells, DMEM was supplemented with 1 % (v/v) 200mM L-Glutamine (Gibco BRL) and varying concentrations of (v/v) Foetal Calf Serum (FCS) with or without the addition of 100 x Penicillin/Streptomycin (Gibco BRL).

The buffer used to wash the cells was Phosphate Buffered Saline (PBS) containing 1.4 mM KH_2PO_4 , 2.7 mM KCl, 4.3 mM Na_2HPO_4 and 137 mM NaCl dissolved in H_2O . PBST additionally contains 0.1 % (v/v) Tween 20.

3.1.3 Cell culture

Cells were cultured either in Petri dishes or flasks (Nunc, Corning) with DMEM supplemented with 10 % (v/v) FCS, 1 % (v/v) 200 mM L-Glutamine (Gibco BRL) and 1 % (v/v) 100 x Penicillin/Streptomycin (Gibco BRL) at 37°C in presence of 5 % CO_2 .

3.1.4 Cell splitting

When monolayer cells were about 90 % to 95 % confluent, they were split to avoid overgrowth. The old medium was removed and the cells were washed with PBS. Subsequently, the cells were treated with trypsin/EDTA and incubated for about 5 min at 37°C to dissociate the cells from the surface. Immediately, the cells were resuspended in 10 ml of medium. A part of the cell suspension was removed according to the desired splitting ratio. To the rest of the cells medium was added to the desired end volume.

3.1.5 Cell counting

Cells were trypsinised and taken up in a known volume of medium. 200 µl of the cell suspension were mixed with 800 µl of trypan blue. The cell number was counted using a haemocytometer (Neubauer improved counting chamber) under a light microscope.

3.1.6 Thawing of cells

For seeding fresh cells, cells were recovered from liquid nitrogen by quickly warming them to 37°C in a waterbath for a few min. Subsequently, the cells were transferred to 10 ml DMEM supplemented with 10 % (v/v) FCS, 1 % (v/v) 200 mM L-Glutamine (Gibco BRL) and 1 % (v/v) 100 x Penicillin/Streptomycin (Gibco BRL). After centrifugation at 1200 rpm for 3 min at RT the supernatant was removed and the cell pellet was washed with 10 ml PBS. After centrifugation at 1200 rpm for 3 min at RT the cell pellet was resuspended in 10 ml medium and transferred to a new flask. The cells were incubated at 37°C in the presence of 5 % CO₂.

3.1.7 Freezing of cells

The cells were grown and split as usual with the exception that the cells that are normally discarded were kept for freezing. They were centrifuged for 5 min at 1200 rpm at room temperature (RT). The supernatant was discarded and the cell pellet was resuspended in 2 ml FCS and 10 % (v/v) DMSO. 1 ml aliquots were transferred to cryo tubes (Nunc) and stored at -80°C in a freezing container (Nalgene) overnight or over the weekend. Afterwards, the cells were transferred to liquid nitrogen for long time storage.

3.2 Bacterial culture

3.2.1 Bacterial strains

3.2.1.1 E. coli Top 10F'

For modification and amplification of plasmids the strain E. coli Top10F' (F-mcrAD(mrr-hsdRMS-mrcBC) Φ 80lacZ Δ m15 Δ lacX74recA1deoRaraD139(ara-leu)7697 galU galK rpsL (StrR) endA1 nupG) (Invitrogen) was used.

3.2.1.2 E. coli BL21 (DE3) LysS

The expression of recombinant proteins was performed using E. coli BL21 (DE3) LysS (hsdD gal (λ clts857 ind1 Sam7 nin5 lacUV5-T7gene1) (Novagen). The gene for the T7 polymerase is cloned into the chromosome under the control of the lac operon. Therefore, protein expression can be induced by the addition of IPTG. Additionally, the genes for chloramphenicol resistance and the T7 lysozyme are episomally encoded. The T7 lysozyme protein has two effects. It degrades the cell wall and it inhibits T7 RNA polymerase. This inhibition helps to keep expression of the T7 promoter off until the IPTG is added. When IPTG is added, the amount of T7 RNA polymerase increases and overcomes the inhibition by lysozyme.

3.2.1.3 Media and solutions

Luria Bertani (LB) medium (Roth) is composed of 10 g/l of tryptone, 5 g/l of yeast extract and 10 g/l of NaCl, pH 7.0 \pm 0.2. The medium was autoclaved before use. Bacteria were grown in LB medium for amplification of DNA or the expression of proteins.

For the expression of isotope-labelled proteins, bacteria were grown in minimal medium containing 33.7 mM Na₂HPO₄ · 2H₂O, 22 mM KH₂PO₄, 8.5 mM NaCl and 18.7 mM ¹⁵NH₄Cl. This solution was autoclaved and added to a sterile filtered solution of 2 mM MgSO₄, 1 % trace elements, 0.4 % glucose or ¹³C labeled glucose in case of double-labelling, 0.3 mM CaCl₂, 1 μ g/ml biotine, 1 μ g/ml thiamine and 100 μ g/ml of each ampicillin and chloramphenicol.

To grow bacteria on solid medium, 1.5 % (w/v) Bacto-agar (Roth) was added to liquid LB medium before autoclaving. When the temperature of the medium was below 50°C, the antibiotics were added and the medium was subsequently poured into Petri dishes.

Ampicillin sodium salt (Sigma) dissolved in dH₂O (100 mg/ml) and Chloramphenicol (Calbiochem) dissolved in absolute ethanol (34 mg/ml) were used for working dilutions of 100 μ g/ml.

3.2.2 Preparation of competent cells

For the preparation of competent cells, a starter culture was set up by inoculation of 3 ml LB medium with the desired bacterial strain, shaking overnight at 37°C. 200 ml LB medium were inoculated with the starter culture on the next day. The culture was grown at 37°C for 2 - 4 h until an OD₆₀₀ of 0.4 - 0.5 had been reached. The cells were harvested by centrifugation in sterile Falcon tubes at 5000 rpm for 5 min at 4°C in a swinging bucket. After harvesting, cells were constantly kept at 4°C. Subsequently, the bacterial pellet was resuspended in 25 ml ice-cold 0.1 M CaCl₂ solution and incubated on ice for 25 min. After repeating the centrifugation, the pellet was again resuspended in 10 ml 0.1 M CaCl₂ solution and incubated at 4°C overnight. The next day the suspension was mixed gently with 2 ml sterile glycerol, portioned into 200 µl aliquots and frozen in liquid nitrogen. Competent cells were stored at -80°C.

3.2.3 Transformation of competent cells

For efficient introduction of foreign DNA into bacterial cells, an aliquot of 200 µl of competent cells was thawed on ice. Afterwards 10 µl of PCR product or 1 µl of a 1:50 diluted midiprep were added, mixed gently and left on ice for 10 to 15 min. After cells had been heat-shocked at 42°C for 30 - 60 seconds, 400 µl of pre-heated (37°C) LB medium were added quickly. Incubation at 37°C for 15 to 30 min was followed by plating of 100 to 150 µl on LB-Amp Agar-Agar plates. As a backup, the remaining bacterial cells were spun down at 4000 rpm for 60 seconds at RT. The supernatant was discarded except for 100 µl which were used to resuspend the pellet and subsequently plated.

3.3 DNA methods

3.3.1 Plasmids

3.3.1.1 Plasmids used for *in vitro* experiments and protein expression

The vector pCITE 1d (Novagen) was used for *in vitro* experiments. This vector is 4682 bp in size and contains a CITE (Cap-Independent Translation Enhancer) sequence allowing correct translation initiation and sites for T7 driven protein expression. The FMDV cDNA encoding the polypeptide Lb, VP4 and VP2 was introduced via the *Nco*I and *Pst*I restriction sites by Glaser *et al.*, 2001. For plasmid propagation in *E. coli* Top 10F', the ampicillin gene allows to screen for bacterial clones that carry the plasmid.

For the expression of proteins in *E. coli* BL21 (DE3) LysS, the vector pET 11d (Novagen) was used. This vector is 6165 bp in size and provides sequences for T7 driven protein expression as well as a lac operator region. Therefore, protein expression can be induced by the addition of IPTG. The Lb cDNA of FMDV was introduced via the *Nco*I and *Bam*HI restriction sites (Kirchweger *et al.*, 1994). An ampicillin gene allows screening for bacterial clones that carry the plasmid.

3.3.1.2 Plasmids used for cell culture experiments

For protein expression in HEK 293T cells the ecdysone-inducible mammalian expression system from Invitrogen was used (see chapter 3.5.1.1). Therefore, the vectors pMZI (developed by (Zeghouf *et al.*, 2004) and pVgRXR were transfected corporately.

The pVgRXR vector is 8.8 kb in size and contains the Zeocin gene as resistance gene for propagation in bacteria. Upon addition of the ecdysone analog ponasterone A, the expression of a receptor is induced.

The pMZI vector is 6856 bp in size and contains an ampicillin resistance gene for propagation in bacteria. The pMZI vector encodes the recombinant protein of interest, which is expressed upon binding of the pVgRXR encoded receptor to the ecdysone response element.

3.3.2 Preparation of plasmid DNA from bacteria

3.3.2.1 DNA miniprep

To screen for positive mutants, small scale DNA preparations (minipreps) from transformed *E. coli* were done using Solution I-III of the Nucleobond AX plasmid Midi Kit from Machery Nagel (see chapter 3.3.2.2).

To this end, 4 ml of LB-Amp were inoculated with a transformed bacterial colony and grown overnight, shaking at 37°C. The cells were harvested by centrifugation at 8000 rpm for 60 seconds at RT. The pellet was resuspended in 100 µl of Solution I. 200 µl of Solution II were added to lyse the cells. The suspension was mixed gently and incubated for not more than 5 min at RT. Proteins and chromosomal DNA were precipitated by addition of 150 µl Solution III and gentle mixing. The precipitate was separated by centrifugation for 5 min at 14000 rpm at 4°C. The supernatant containing the plasmid DNA was transferred to a new tube and the DNA was precipitated by addition of 1 ml icecold ethanol. Centrifugation was repeated as before and the supernatant was discarded. The DNA pellet was dissolved in 200 µl of TE buffer and mixed with 200 µl of 5 M LiCl. After centrifugation at 14000 rpm for 5 min at 4°C, the supernatant was transferred to a new eppendorf tube and the DNA was again precipitated with 1 ml icecold ethanol. Centrifugation was repeated as before and the supernatant was discarded. The DNA pellet was dried on air for about 1 h and then resuspended in 50 µl dH₂O.

Solution I:	50 mM Tris/HCl pH 8.0, 10 mM EDTA, 100 µg/ml RNase A
Solution II:	20 mM NaOH, 1 % (w/v) SDS
Solution III:	2.8 M potassiumacetate pH 5.1
TE buffer:	10 mM Tris/HCl pH 8.0, 1 mM EDTA

3.3.2.2 DNA midiprep

Higher amounts of pure plasmid DNA were obtained with the Nucleobond AX plasmid Midi Kit (Macherey-Nagel), used according to the instructions of the manufacturer. The DNA was resuspended in 200 µl of dH₂O and stored at -20°C before further use.

3.3.3 DNA gelelectrophoresis

To check the outcome of different reactions and procedures, DNA fragments were separated on gels composed of 1 % (w/v) agarose (GenXpress) melted in 0.5 x TAE buffer. The DNA samples were mixed in $1/_{10}$ volume of 10 x loading buffer. Gels were run at 90 to 110 V using a power pack 300 from Biorad. DNA was visualised by a UV-transilluminator after 20 - 30 min of ethidiumbromide staining. The size marker consisted of 1 μ g of *Hind*III digested λ -DNA (Promega).

0.5 x TAE buffer: 20 mM Tris base, 5 mM sodiumacetate, 1 mM EDTA
10 x Loading Buffer: 1 mM EDTA, 0.1 % Orange G, 10 % Ficoll in 0.5 x TAE
Ethidium bromide solution: 10^{-4} % ethidium bromide in 0.5 x TAE

3.3.4 DNA quantification

To quantify DNA concentrations the Nanodrop spectrophotometer ND-1000 from Peggab was used, following the instructions of the manufacturer.

3.3.5 Restriction digestion of DNA

Restriction endonucleases and 10 x reaction buffers (New England Biolabs) were used, following the instructions of the manufacturer. Analytical digestions were performed in a total volume of 20 μ l, composed of:

x	μ l	DNA
2	μ l	NE buffer (1-4)
0.3	μ l	enzyme
y	μ l	dH ₂ O
<hr/>		
20	μ l	

Preparative digestions were performed in a total volume of 100 μ l, composed of:

x	μ l	DNA
10	μ l	NE buffer (1-4)
0.5 -1.0	μ l	enzyme
y	μ l	dH ₂ O
<hr/>		
100	μ l	

Temperature and time of incubation were chosen according to the properties of the enzyme used.

3.3.6 DNA dephosphorylation

To avoid the religation of restricted plasmids the 5' end of the DNA was dephosphorylated.

The restricted vector (see chapter 3.3.5) was purified using the Clean-Up System (see chapter 3.3.10.1) and eluted in 44 μl dH_2O . Further, 5 μl NEB 3 (New England BioLabs) and 1 μl calf-intestine alkaline phosphatase (CIP) (New England BioLabs, 10 $\text{u}/\mu\text{l}$) were added. The dephosphorylation reaction was performed at 37°C for 60 min.

3.3.7 Phosphorylation and annealing of oligonucleotides

In order to insert synthetic oligonucleotides into a dephosphorylated vector, oligonucleotides were phosphorylated at the 5' end using the T4 polynucleotide kinase (PNK) (New England BioLabs, 10 $\text{u}/\mu\text{l}$). Phosphorylation reactions were performed in a total volume of 20 μl composed of:

2	μl	100 mM ATP
2	μl	10 x PNK buffer
1	μl	TIM XXXX (1 $\mu\text{g}/\mu\text{l}$)
1	μl	TIM XXXX (1 $\mu\text{g}/\mu\text{l}$)
1	μl	T4 PNK (New England BioLabs, 10 $\text{u}/\mu\text{l}$)
13	μl	dH_2O
<hr/>		
20	μl	

The phosphorylation and annealing reaction was performed using the T3 Thermocycler Biometra. The temperature program was as follows: 30 min at 37°C, 30 seconds at 90°C and 5 min at 37°C.

3.3.8 Extraction of DNA from agarose gel

DNA bands were visualised by UV light and cut out of the gel. The DNA was isolated from the gel using the Wizard SV Gel and PCR Clean-Up System from Promega (see chapter 3.3.10.1).

3.3.9 DNA ligation

Prior to ligation 1 μl of the dephosphorylated vector was loaded on an agarose gel to estimate the DNA concentration. The ligation reaction was performed at RT over night in a total volume of 20 μl composed of:

50	ng	vector
1	μl	phosphorylation mix
2	μl	10 x ligase buffer (Promega)
0.5	μl	T4 DNA ligase (Promega, 3 u/ μl)
x	μl	dH ₂ O
<hr/>		
20	μl	

3.3.10 DNA purification

3.3.10.1 Wizard SV Gel and PCR Clean-Up System (Promega)

The Wizard SV Gel and PCR Clean-Up System was used for the extraction of DNA from an agarose gel as well as for cleaning DNA.

To extract DNA from an agarose gel, the excised DNA band was transferred to an eppendorf tube and an equal volume of membrane binding solution was added. The mixture was vortexed and incubated at about 60°C until the gel slice was completely dissolved. To clean DNA, an equal volume of membrane binding solution was added to the DNA sample. The following steps were performed for both approaches.

The SV minicolumn was inserted into the collection tube before the prepared DNA sample was transferred to the minicolumn assembly. After incubation for 1 min at RT, the DNA sample was centrifuged at 14000 rpm for 1 min. The flow-through was discarded and the column reinserted into the collection tube. Afterwards, the minicolumn was washed once with 700 μl and another time with 500 μl of membrane wash solution. Centrifugation was carried out at 14000 rpm for 1 min and the flowthrough was discarded. The collection tube was then sucked dry and the minicolumn assembly was centrifuged at 14000 rpm for another 5 min. Afterwards the column was dried for 10 - 15 min on air. For elution, the minicolumn was transferred to a clean 1.5 ml eppendorf tube and 30 - 50 μl of dH₂O were added to the minicolumn. After incubation at RT for 1 min, centrifugation at 14000 rpm for 1 min was performed. The purified DNA sample was stored at -20°C.

3.3.10.2 Phenol/chloroform extraction

To purify DNA from enzymes or other contaminants, 2 - 3 μl of 0.5 M EDTA pH 8.0 per 100 μl of DNA sample were added. After the addition of one volume of phenol, the sample was vortexed and centrifuged at 14000 rpm for 2 min. The aqueous phase was transferred to a fresh eppendorf tube and one volume of chloroform was added. After centrifugation at 14000 rpm for 1 min, the aqueous phase was transferred to a clean eppendorf tube. The purified DNA sample was stored at 4°C or -20°C.

3.3.11 Site-directed PCR mutagenesis

Site-directed PCR mutagenesis was performed using two primers complementary to each other bearing the desired mutation. A 50 μl reaction is composed of 0.5 μl DNA, 1 μl forward primer (1 $\mu\text{g}/\mu\text{l}$), 1 μl reverse primer (1 $\mu\text{g}/\mu\text{l}$), 4 μl dNTPs (20 mM), 5 μl Pfu buffer (Promega), 1 μl Pfu DNA polymerase I (Promega, 3 $\text{u}/\mu\text{l}$) and 47.5 μl dH_2O . The T3 Thermocycler Biometra with a heated lid was used to perform the following PCR cycles:

95°C	2 min	
<hr/>		
95°C	30 sec	melting temperature
x°C	1 min	annealing temperature, depends on the T_m of the primers
69°C	y min	elongation time depends on the length of the DNA template (2 min per 1000 bp of sequence length)
<hr/>		
4°C	∞	

As a negative control, a PCR reaction without primers was performed. To remove the methylated DNA template from the PCR reaction, 1 μl *DpnI* (New England Biolabs, 20 $\text{u}/\mu\text{l}$) and 4.5 μl NE buffer 4 were added to 40 μl of the PCR reaction and digested for 5 h at 37°C. The remaining 10 μl of the PCR reaction were kept as an undigested control. 10 μl of the template-free PCR reaction were tested on a 1 % agarose gel (see 3.3.3), together with all control samples. 10 μl of digested DNA were used for transformation in competent *E. coli* cells (see 3.2.1.1).

3.3.12 Cassette cloning

For more extensive manipulation of DNA, cassette cloning was performed. Oligonucleotides containing the desired changes in DNA sequence were ordered from VBC biotech (see Table 2). Complementary oligonucleotides were phosphorylated and annealed (see chapter 3.3.7). Before ligation with these oligonucleotides (see chapter 3.3.9), the vector had to be restricted with appropriate restriction enzymes (see chapter 3.3.5), followed by dephosphorylation (see chapter 3.3.6) and gel extraction (see chapter 3.3.8). The ligation was then transformed into bacteria (see chapter 3.2.3).

3.3.13 DNA sequencing

DNA sequencing was performed by Gotthold Schaffner from the IMP sequencing service. For sequencing of the pCITE 1d vector, the primers TIM 550 and TIM 554 were used; for pET 11d vector sequencing the primers for T7 promoter and T7 terminator provided by the IMP sequencing service were used.

3.3.14 Primers

3.3.14.1 Primers used for site-directed PCR mutagenesis

ID	sequence	purpose
TIM 1528	5' GCTCTCGTGATCGCGAACATCAAGCAC 3'	primers to introduce W105A mutation into Lb ^{pro}
TIM 1529	5' GTGCTTGATGTTCCGGATCACGAGAGC 3'	
TIM 1635	5' ACCGGCATCGGCGCCGCTCGCGACCC 3'	primers to introduce T117A mutation into Lb ^{pro}
TIM 1636	5' GGGTCGCGAGGCGGCGCCGATGCCGGT 3'	
TIM 1655	5' GCTCTCGTGATCCGGAACATCAAGCAC 3'	primers to introduce W105R mutation into Lb ^{pro}
TIM 1656	5' GTGCTTGATGTTCCGGATCACGAGAGC 3'	
TIM 1657	5' GTTCAACGCAAGTTCAAATGATAAGGA 3'	primers to introduce L200F mutation into Lb ^{pro} cloned in pET 11d
TIM 1658	5' TCCTTATCATTTGAACTTGCGTTGAAC 3'	

3.3.14.2 Oligonucleotides used for cassette cloning

Table 3 Oligonucleotides used for cassette cloning

ID	sequence	purpose
TIM 1690	5' GTACGATCAAGAACCACTCAACGGGGAATGGAAA GCCAAGGTTCAACGCAAGCAAGCTCAAATGATAAG 3'	oligonucleotides to remove TAP tag from pMZI
TIM 1691	5' AATTCTTATCATTTGAGCTTGCGTTGAACCTT GGCTTTCCATTCCCCGTTGAGTGTTCTTGATC 3'	Lb ^{pro}

3.3.14.3 Primers used for sequencing

Table 4 Primers used for sequencing

ID	sequence	purpose
TIM 550	5' GGACGTGGTTTTTCCTTTG 3'	primers used for sequencing Lb ^{pro} cloned in pCITE 1d
TIM 554	5' ATTTAGGTGACACTATAG 3'	
TIM 1522	5' GACCGCTCGAGATGGAAGTACACTGTAC 3'	primers used for sequencing Lb ^{pro} cloned in pMZI
TIM 1523	5' CGCGCACATATGTTTGAGCTTGCGTTGAACC 3'	

3.4 RNA methods

3.4.1 *In vitro* transcription

First, the pCITE 1d vector was linearised by *SaI* digestion for 4 h at 37°C. *SaI* cleaves within the coding sequence of VP2, thereby clipping a part of VP2. This allows that self-processing of Lb^{pro}VP4/VP2 results in cleavage fragments of different size. 2 µl of the digestion were checked on a 1 % agarose gel (see 3.3.3) to verify whether linearisation was complete. The linearised plasmid was purified using Wizard SV Gel and PCR Clean-Up System (see 3.3.10.1). The purified DNA was directly eluted with 61 µl of dH₂O for the following *in vitro* transcription. A 100 µl transcription approach is composed of:

61	µl	eluted DNA
20	µl	Buffer 5x (Promega)
5	µl	100 mM DTT (Promega)
10	µl	2.5 mM NTP mix
3	µl	RNasin (Promega, 40 u/µl)
1	µl	T7 polymerase (Promega, 19 u/µl)
<hr/>		
100	µl	

The mix was incubated for 90 min at 37°C before adding 0.6 µl deoxyribonuclease (Invitrogen, 185.1 u/µl) and 1 µl RNasin (Promega, 40 u/µl). The mix was incubated for another 20 min at 37°C. The RNA was then extracted using Phenol/Chloroform extraction (see chapter 3.3.10.2). Afterwards, the RNA was precipitated with $\frac{1}{3}$ volume of 8 M NH₄Oac and 2.5 volumes of absolute ethanol. The precipitation mix was incubated for 15 min at -80°C. After centrifugation at 14000 rpm for 15 min at 4°C, the supernatant was discarded carefully with a pipette. The pellet was washed with 500 µl of 70 % ethanol and centrifugation was repeated as before. The supernatant was discarded carefully with a pump and the pellet was air-dried for 20 - 30 min. Finally, the pellet was resuspended in 25 µl of RNase-free water.

3.4.2 RNA gelelectrophoresis

After *in vitro* transcription, 2 µl of RNA were checked on a 1 % agarose gel containing 0.1 % of SDS (see 3.3.3). The RNA samples were mixed in $1/10$ volume of 10 x loading buffer. Separation of RNA fragments was performed at 90 to 110 V using a power pack 300 from Biorad. The agarose gel was washed twice in dH₂O for 15 min before incubation in ethidium bromide solution for 20 to 30 min. RNA bands were visualised via UV transillumination. The size marker consisted of 1 µg of *Hind*III digested λ-DNA (Promega).

10 x Loading Buffer: 1 mM EDTA, 0.1 % Orange G, 10 % Ficoll in 0.5 x TAE-buffer
Ethidium bromide solution: 10⁻⁴ % ethidium bromide in 0.5 x TAE
0.5 x TAE buffer: 20 mM Tris base, 5 mM sodiumacetate, 1 mM EDTA

3.4.3 *In vitro* translation

In vitro translation reactions were performed at 30°C in a total volume of 10 µl composed of:

4	µl	RRL (rabbit reticulocyte lysate)
2.5	µl	RNA
0.8	µl	translation mix lacking methionine
0.4	µl	³⁵ S-methionine
0.32	µl	2.5 M KCl
0.2	µl	2.5 mM MgAc ₂
1.78	µl	H ₂ O
<hr/>		
10	µl	

This translation reaction was multiplied by 9 for a time course experiment with 8 time points. After pre-incubation of the translation mix for 2 min at 30°C, the translation was started by the addition of 20 µl of RNA (eightfold). 10 µl aliquots were removed at the following time points: 0, 4, 8, 12, 20, 30 and 60 min after translation start. The aliquots were immediately transferred to 41 µl icecold stop solution. As a negative control, dH₂O was added to the translation mix instead of RNA. Translation products were analysed by SDS PAGE described by Dasso & Jackson (see 3.5.8.2) and fluorography (see 3.5.10). 10 µl of the translation reaction were loaded on the polyacrylamide gels.

Stop solution: 9 µl 25 mM methionine-cysteine mix, 225 µl 2 x Laemmli sample buffer and 135 µl dH₂O
2 x Laemmli sample buffer: 20 % glycerol, 10 % β-mercaptoethanol, 6 % SDS, 125 mM Tris, 0.01 % bromophenol blue, pH 6.8

3.5 Protein methods

3.5.1 Protein expression in HEK 293T cells

3.5.1.1 Ecdysone-Inducible Mammalian Expression System (Invitrogen)

The ecdysone-inducible mammalian expression system from Invitrogen was used for the transient expression of recombinant proteins in HEK 293T cells. Since mammalian cells are normally not responsive to the insect hormone ecdysone and do not contain the ecdysone receptor, basal levels of transcription are very low or absent. This expression system is based on the ability of the insect hormone 20-OH ecdysone to activate gene expression via the ecdysone receptor. In the presence of a ligand such as ecdysone or its analog ponasterone A, a heterodimeric ecdysone receptor, encoded by the pVgRXR vector, binds to a modified ecdysone response element on the pMZI vector and therefore activates transcription of the encoded recombinant protein.

3.5.1.2 Transfection and protein expression

One day prior to transfection, 2×10^6 cells were seeded in a 6-well-plate in antibiotic-free medium, so that the cells were 80 - 90 % confluent on the day of transfection. 1.6 μg of the pMZI vector as well as 1.6 μg of the pVgRXR vector from the ecdysone-inducible mammalian expression system (see chapter 3.5.1.1) were diluted in 200 μl of OptiMEM medium at RT and divided into 4 aliquots of 50 μl . 36 μl of Lipofectamine 2000 (Sigma) were diluted in 200 μl of OptiMEM medium and incubated at RT for 5 min. Subsequently, 50 μl of the lipofectamine solution were added to each aliquot of the DNA solution and incubated for 20 min at RT. Meanwhile, the cells were supplied with 1.5 ml of antibiotic-free DMEM, containing 2 % (v/v) FCS and 1% (v/v) glutamine. After incubation, the 100 μl aliquots of DNA-lipofectamine-mix were equally distributed over the wells. The cells of two wells were not transfected to serve as a negative control. The cells were incubated in a humidified chamber at 37°C for 4 h. Afterwards, the cells were trypsinised with 200 μl of trypsin/EDTA solution (Gibco) and neutralised with 800 μl of antibiotic-free DMEM, containing 10 % (v/v) FCS and 1% (v/v) glutamine. The cell suspension of two equally treated wells (transfected and non-transfected) were combined and seeded in a 100 mm cell culture dish. The final volume of 10 ml was filled with antibiotic-free DMEM, containing 10 % (v/v) FCS and 1 % (v/v) glutamine. The cells were incubated in a humidified chamber at 37°C overnight. The following day, the medium was changed to DMEM supplemented with 10 % FCS, 1 % glutamine and 50 units/ml of each penicillin and streptomycin. To start the induction of protein expression, 1 mM ponasterone A (Invitrogen) was added to the medium of one dish of transfected cells. Protein expression was induced for 36 to 48 h, dependent on the density of cells.

3.5.2 Protein expression in E. coli BL 21 (DE3) LysS

3.5.2.1 Protein expression in LB medium

Expression of recombinant proteins was performed in E. coli BL 21(DE3) LysS using pET 11d vectors. First, bacteria were transformed with the pET 11d vector containing cDNA coding for Lb^{pro} (see chapter 3.2.3). 100 ml of LB-Amp-Cam medium were then inoculated with a single colony and grown overnight at 37°C, shaking at 150 rpm. 900 ml of LB-Amp-Cam medium were inoculated with the overnight culture and incubated at 30°C on a shaker at 150 rpm. Once cell density had reached an OD₆₀₀ between 0.5 and 0.6 (after about 2 h of incubation), induction of protein expression was performed by the addition of 0.4 mM IPTG (Isopropyl β-D-1-thiogalactopyranoside). 25 ml of culture were removed as a non-induced fraction before IPTG induction. For protein expression, the culture was incubated at 110 rpm for 5 h at 30°C shaking. Cells were harvested by centrifugation at 5000 rpm for 15 min at 4°C on a Sorvall RC5C centrifuge. The cell pellet of the induced fraction was resuspended in 30 ml of Buffer A, the pellet of the non-induced fraction in 1 ml and stored at -80°C.

Buffer A: 50 mM Tris-HCl pH 8.0, 1 mM EDTA, 5 mM DTT, 5 % glycerol, 50 mM NaCl

3.5.2.2 Protein expression in minimal medium

Expression of recombinant proteins, single-labelled with ¹⁵N or double-labelled with ¹³C and ¹⁵N was performed in E. coli BL 21(DE3) LysS (see chapter 3.2.1.2) using pET 11d vectors (see chapter 3.3.1.1). After bacteria were transformed (see chapter 3.2.3), 10 ml of minimal medium were inoculated with a single colony and grown overnight at 37°C shaking at 160 rpm. On the next day, 990 ml of minimal medium were inoculated with the overnight culture. Once cell density had reached an OD₆₀₀ between 0.5 and 0.6 (after about 7 h of incubation), induction of protein expression was performed by the addition of 0.4 mM IPTG (Isopropyl β-D-1-thiogalactopyranoside). 25 ml of culture were taken away as a non-induced fraction before IPTG induction. For protein expression, the culture was incubated at 110 rpm overnight at 37°C shaking. Cells were harvested by centrifugation at 5000 rpm for 15 min at 4°C on a Sorvall RC5C centrifuge. The cell pellet of the induced fraction was resuspended in 30 ml of Buffer A, whereas the pellet of the non-induced fraction was resuspended in 1 ml and stored at -80°C.

Minimal medium: 33.7 mM Na₂HPO₄ · 2H₂O, 22 mM KH₂PO₄, 8.5 mM NaCl and 18.7 mM ¹⁵NH₄Cl, autoclaved and added to sterile filtered solution of 2 mM MgSO₄, 1 % trace elements, 0.4 % glucose or ¹³C labelled glucose, 0.3 mM CaCl₂, 1 µg/ml biotine, 1 µg/ml thiamine, and 100 µg/ml of ampicillin and 100 µg/ml chloramphenicol

Buffer A: 50 mM Tris-HCl pH 8.0, 1 mM EDTA, 5 mM DTT, 5 % glycerol, 50 mM NaCl

3.5.3 Preparation of HEK 293T cell extracts

After cells were washed with 3 ml of PBS, 0.5 ml of low-salt lysis buffer were supplied to the cells for 5 min. Then, the cells were scraped off the cell culture dish and incubated on ice for 20 min. Subsequently, the cells were centrifuged at 6000 g for 10 min at 4°C and the supernatant was collected as the cytoplasmic fraction. The pellet was washed with 0.5 ml low-salt lysis buffer and centrifuged. And the pellet was resuspended in 0.5 of high-salt lysis buffer. After sonication at a 10 % cycle for 20 sec using the homogeniser Sonoplus HD 200 from Bandelin combined with the probe tip MS 73D, the solution was centrifuged and the supernatant was collected as nucleic fraction. Protein fractions were further investigated by Western blot analysis (see chapter 3.5.11).

Low-salt-lysis buffer: 10 mM HEPES pH 7.9, 10 mM NaCl, 3 mM MgCl₂, 0.5 % Igepal-CA 630
High-salt-lysis buffer: 25 mM HEPES pH 7.9, 25 % glycerol, 0.42 M KCl, 1.5 M MgCl₂, 0.2 mM EDTA, 0.5 mM DTT

3.5.4 Preparation of BL 21(DE3) LysS cell extracts

The resuspended bacterial pellets were thawed on ice and cell disruption was completed by sonication with the homogeniser Sonoplus HD 200 from Bandelin in combination with the probe tip MS 73D. For the induced fraction, sonication was performed at a 40 % cycle, 4 times for 30 sec and finally one continuous cycle for 30 sec, on ice. The non-induced fraction was sonicated at a 20 % cycle, 3 times for 30 sec. The sample of the induced fraction was centrifuged at 18000 rpm for 30 min at 4°C in a Sorvall RC5C centrifuge to separate the soluble fraction (supernatant) from the insoluble one (pellet). The sample from the non-induced fraction was centrifuged in an eppendorf centrifuge at 14000 rpm for 20 min at 4°C. The supernatant from the induced fraction was kept for further protein purification steps, such as ammonium sulfate precipitation.

Buffer A: 50 mM Tris-HCl pH 8.0, 1 mM EDTA, 5 mM DTT, 5 % glycerol, 50 mM NaCl

3.5.5 Protein purification

3.5.5.1 Ammonium sulfate precipitation

The first step of protein purification of Lb^{pro} was precipitation by adding 30 % ammonium sulfate. Accordingly, the supernatant of the bacterial cell lysate was mixed with a saturated ammonium sulfate solution and gently stirred overnight at 4°C. After centrifugation at 20000 rpm in a Sorvall RC5C or RC5C plus centrifuge for 40 min at 4 °C, the supernatant was kept for further precipitation. Among other proteins Lb^{pro} precipitated upon the addition of 60 % saturated ammonium sulfate solution. Again, the mixture was gently stirred overnight at 4°C. After centrifugation at 20000 rpm for 30 min at 4°C, the supernatant was discarded and the pellet of a 1 l culture was resuspended in 8 ml of Buffer A.

Buffer A: 50 mM Tris-HCl pH 8.0, 1 mM EDTA, 5 mM DTT, 5 % glycerol, 50 mM NaCl

3.5.5.2 Dialysis

To desalt the protein sample after ammonium sulfate precipitation, the sample was dialysed against Buffer A. Therefore, the protein solution was transferred into a semi-permeable membrane bag made of cellulose acetate with a cut-off of 10 kDa. Dialysis bags were prepared as recommended by the manufacturer (Sigma). The sample was dialysed against 100 times the volume of Buffer A. Dialysis was performed at 4°C in a beaker under slow stirring of the bag from 3 h to overnight. During the dialysis process the buffer was changed 2 - 3 times.

Buffer A: 50 mM Tris-HCl pH 8.0, 1 mM EDTA, 5 mM DTT, 5 % glycerol, 50 mM NaCl

3.5.5.3 FPLC

Protein purification was performed using anion-exchange and size-exclusion chromatography on an ÄKTA FPLC (Fast Protein Liquid Chromatography) system from Amersham Biosciences. All used columns were purchased from Amersham Biosciences. For the collection of 2 ml fractions an automatic fraction collector was used. The handling of the columns was performed according to the instructions of the manufacturer. Fractions were analysed by SDS PAGE (see chapter 3.5.8.1).

3.5.5.3.1 Anion exchange chromatography

Proteins that differ in electrostatic interactions can be separated via anion-exchange chromatography. Therefore, a Mono Q HR 10/10 column was used. Before loading the protein sample, Buffer A was used to equilibrate the column. Buffer B was used as elution buffer creating a NaCl gradient. The gradient program was as follows: 5 column volumes (CVs) of 100 % of Buffer A, 2.5 CVs of 0-30% of Buffer B, 15 CVs of 30-60 % of Buffer B, 2 CVs of 60-100 % of Buffer B and 5 CVs of 100 % Buffer B.

Buffer A:	50 mM Tris-HCl pH 8.0, 1 mM EDTA, 5 mM DTT, 5 % glycerol, 50 mM NaCl
Buffer B:	50 mM Tris-HCl pH 8.0, 1 mM EDTA, 5 mM DTT, 5 % glycerol, 1 M NaCl

3.5.5.3.2 Size-exclusion chromatography

Proteins of different molecular size can be separated via size-exclusion chromatography. For preparative gelfiltration a HiLoad 26/60 Superdex 75 pg column was used. Analytical size-exclusion chromatography was performed on a HiLoad 16/60 Superdex 75 pg column. The samples were separated over 1.2 column volumes of Buffer A.

Buffer A:	50 mM Tris-HCl pH 8.0, 1 mM EDTA, 5 mM DTT, 5 % glycerol, 50 mM NaCl
-----------	--

3.5.6 Protein concentration

To concentrate protein samples Amicon Ultra Centrifugal Devices (Millipore) were used. The instructions of the manufacturer were followed. The centrifugations were performed at 4°C on an eppendorf centrifuge 5810 R.

3.5.7 Protein quantification

To quantify protein concentrations the Nanodrop spectrophotometer ND-1000 from Peglab was used according to the instructions of the manufacturer.

3.5.8 SDS PAGE (Sodiumdodecylsulfate Polyacrylamide Gelelectrophoresis)

3.5.8.1 SDS PAGE (Laemmli, 1970)

For separation of protein fractions, SDS PAGE was performed in the mini-PROTEAN® 3 system from Biorad, assembled according to the instructions of the manufacturer. Table 5 shows the composition of Laemmli separation gels with different percentages of polyacrylamide. The mix was poured and overlaid with isopropanol. After polymerisation, the gel was rinsed with dH₂O and the stacking gel was prepared. Afterwards, the gel unit was assembled and the tank was filled with Laemmli running buffer. Protein samples were mixed with 2 x Laemmli sample buffer and heated to 95°C for 5 min; 20 min in case of bacterial or cellular lysates. The samples were loaded on the gel and protein separation was performed at 20 mA using an electrophoresis power supply from ISCO. The prestained precision marker from Biorad was used as a size marker.

Table 5 Composition of 'Laemmli' separation gels and stacking gel

	Separation gel 15 % (ml)	Separation gel 17.5 % (ml)	Stacking gel (ml)
30 % Polyacrylamide	3	3.5	0.333
2.5 % Bisacrylamide	-	-	0.104
4 x LGS	1.5	1.5	-
4 x UGS	-	-	0.481
dH ₂ O	1.5	1	1.060
10 % APS	0.05	0.05	0.02
TEMED	0.005	0.005	0.002

LGS: lower gel solution; UGS: upper gel solution; APS: Ammoniumperoxidisulfate; TEMED: N,N,N',N'-Tetramethyl-ethylene diamine

LGS (lower gel solution):	1.5 M Tris base pH 8.8, 0.4 % SDS
UGS (upper gel solution):	0.5 M Tris base pH 6.8, 0.4 % SDS
2 x Laemmli sample buffer:	20 % glycerol, 10 % β-mercaptoethanol, 6 % SDS, 125 mM Tris, 0.01 % Bromophenol Blue pH 6.8
Laemmli running buffer:	25 mM Tris base, 0.2 M Glycine, 0.1 % (w/v) SDS

3.5.8.2 SDS PAGE (Dasso et al., 1989)

To separate *in vitro translation* products, the protocol of Dasso and Jackson was used in order to gain a higher resolution for proteins of small size. The composition of different separation gels is listed in Table 6. The composition of the stacking gel is the same as used for 'Laemmli' PAA gels (see chapter 3.5.8.1). The radioactively-labelled translation products were detected by fluorography (see chapter 3.5.10). The ¹⁴C-labelled protein marker CFA626 from Amersham Bioscience was used as size marker.

Table 6 Composition of 'Dasso & Jackson' separation gels

	Separation gel 6 % (ml)	Separation gel 17.5 % (ml)
30 % Polyacrylamide	1.2	3.5
2.5 % Bisacrylamide	0.209	0.158
4 x LGS	1.5	1.5
dH ₂ O	3.06	0.754
10 % APS	0.05	0.05
TEMED	0.005	0.005

LGS: lower gel solution; UGS: upper gel solution; APS: Ammoniumperoxidisulfate;
TEMED: N,N,N',N'-Tetramethyl-ethylene diamine

LGS (lower gel solution): 1.5 M Tris base pH 8.8, 0.4 % SDS

UGS (upper gel solution): 0.5 M Tris base pH 6.8, 0.4 % SDS

Dasso & Jackson
running buffer: 50 mM Tris base, 385 mM Glycine, 0.1 % (w/v) SDS

3.5.9 Coomassie Staining

The 'Laemmli' PAA gels were stained by incubation in coomassie staining buffer for 15 - 30 min. The gels were destained by transferring them to H₂O and boiling them for several times in the microwave. Gels were vacuum-dried on WhatmanTM 3MM paper for 1 h at 80°C using a Slab Gel Dryer SGD 4050 from Savant.

Coomassie staining buffer: 0.4 % (w/v) Biorad Coomassie Brilliant Blue R250, 45 % (v/v) methanol, 10 % (v/v) acetic acid

3.5.10 Fluorography

During *in vitro translation*, proteins were labelled with ^{35}S -methionine and separated on a 'Dasso & Jackson' PAA gel. After gelelectrophoresis, the gel was washed 2 times in enhancer solution for 15 min at RT. Thereby, the radiation is shifted to a wavelength which can be detected more sensitively by an autoradiography film. After vacuum-drying on WhatmanTM 3MM paper, the gel was exposed to a BioMax MR film (Kodak) or a CL-X PosureTM film (Thermo Scientific) for 20 - 90 h at -80°C .

Enhancer solution: 1 M sodium salicylate, 45 % methanol

3.5.11 Western blot analysis

For western blot analysis protein samples were separated by SDS PAGE (see chapter 3.5.8), together with a prestained precision protein marker (Biorad). Proteins were transferred to a PVDF ImmobilonTM-P Transfer Membrane (Millipore) that was activated with methanol before use. The western blot sandwich was composed of 2 pads and 3 pieces of WhatmanTM 3MM paper, which were pre-soaked in transfer buffer, enclosing the SDS gel and the transfer membrane. The TE 22 Mini Transfer Tank Unit from Hoefer scientific instruments was used for blotting. The transfer tank was filled with transfer buffer and blotting was performed overnight at 40 mA.

For immunoblot analysis the transfer membrane was incubated with blocking buffer for 30 min shaking at RT to block the non-specific binding sites. Subsequently, the membrane was incubated with the primary antibody shaking at RT for 1 h. After two times washing with PBST for 10 min, the membrane was incubated with the secondary antibody shaking at RT for 1 h. After two times washing with PBST, the immunolabelled proteins were detected.

For the detection of alkaline phosphatase (AP) conjugated secondary antibodies, the membrane was incubated with 5 ml alkaline phosphatase buffer supplemented with 25 μl NBT and 25 μl BCIP until proteins became visible (2 - 10 min). The colour reaction was stopped with dH_2O .

For horseradish peroxidase (HRP) conjugated antibodies, the detection was performed using the Super Signal[®] West Pico chemiluminescent substrate kit from Pierce. The membrane was covered with 1 ml of each of the two solutions of the detection kit and incubated for a few min. After removal of the solution, the membrane was wrapped in a clingfilm and exposed to an autoradiography film (BioMax MR film from Kodak or CL-X PosureTM film from Thermo Scientific).

Transfer buffer:	1 % (w/v) glycine, 20 % (v/v) methanol, 25 mM Tris base pH 8.8
Blocking buffer:	0.2 % Tween 20, 0.2 % I-Block (Tropix) in PBS
PBS(T):	1.4 mM KH ₂ PO ₄ , 2.7 mM KC, 4.3 mM Na ₂ HPO ₄ , 137 mM NaCl, (0.1 % Tween 20)
Alkaline phosphatase buffer:	5 mM MgCl ₂ , 100 mM NaCl, 100 mM Tris-HCl pH 9.6
NBT:	5 % (w/v) nitro blue tetrazolium in 90% dimethylformamide
BCIP:	2.5 % (w/v) 5-bromo-4-chloro-3-indolyl phosphate disodium salt in dH ₂ O

Table 7 Primary antibodies used for immunodetection

Primary antibody	dilution
rabbit anti eIF4GI (N-terminal, antiserum, gift from R. Rhoads, Shreveport, LA)	1:8000
rabbit anti Leader protease (antiserum)	1:2000
rabbit anti HRV14 (antiserum)	1:400
mouse anti α tubulin (monoclonal, Sigma)	1:30000
mouse anti lamin A/C (monoclonal, Mc Keon <i>et al.</i> , 1986)	1:30000

Table 8 Secondary antibodies used for immunodetection

Secondary antibody	dilution
anti rabbit alkaline phosphatase coupled (Sigma)	1:5000
goat anti mouse horseradish peroxidase coupled (Pierce)	1:20000

3.6 NMR (Nuclear Magnetic Resonance)

NMR (nuclear magnetic resonance) was chosen as technique to give information on the protein structure, molecular dynamics and quaternary interactions of Lb^{pro}. Further, measurements can be performed in solution, which reflect native physiological conditions. However, for NMR investigations protein concentrations of 1 mM are required, which exceeds the cellular concentrations by many times.

3.6.1 Principles

The fundament of NMR analysis is a quantum mechanical magnetic phenomenon of the nucleus, called spin. The spinning nucleus can be thought of as a rotating positive charge, creating a minute magnetic field. In NMR studies nuclei with a spin $\frac{1}{2}$, such as ^1H , ^{15}N and ^{13}C , are investigated. In the absence of an external magnetic field, the direction of the spin axis is random. If an external magnetic field is present, each nuclear magnet will adopt specific orientations. For spin $\frac{1}{2}$ -nuclei, two orientations are possible: a low-energy (or α) state, which is aligned parallel to the applied magnetic field, and a higher-energy (or β) state, which is aligned in an anti-parallel way. In the equilibrium, there are marginally more spins in the α -state than in the β -state. This small difference in populations gives rise to an NMR signal which makes NMR an insensitive spectroscopic method. Transitions between the α - and the β -state occur when an appropriate amount of energy (resonance) is supplied to the system. The energy is supplied in form of a pulse of electromagnetic radiation in the radio frequency (rf) range, which lies between 50 and 800 MHz. The higher the external magnetic field, the greater is the difference between the two transition states which results in more sensitive NMR signals.

The equilibrium is perturbed by rf pulses for a precise length of time. This leads to a rotation of the magnetisation vector by an angle, mostly 90° or 180° . Subsequently, the system returns to the equilibrium state by precession around the magnetic field which induces a detectable electric voltage. The detected time domain signals are transformed via Fourier transformation into a one-dimensional NMR spectrum.

3.6.1.1 Chemical shift

In the presence of an external magnetic field, the electrons of a nucleus generate a local magnetic field and thus shield the nucleus. The density of electrons around the nucleus is dependent on the electro-negativity of neighbour-atoms. If electrons are pulled away from the nucleus, there is less shielding and *vice versa*. Thus, the resonance of this nucleus is shifted to higher frequencies. Therefore, each nucleus has a unique chemical environment and specific absorption frequencies. The chemical shift of a nucleus is the difference between its own resonance frequency and that of a reference nucleus. The quantity is reported in parts per million (ppm) and given the symbol δ . Chemical shifts in proteins are influenced by non-covalent interactions such as hydrogen bonding, electrostatic and Van-der-Waals interactions. These interactions can give information on the local environment of the nucleus and thus allows conclusions about the secondary, tertiary as well as quaternary structure of the protein.

3.6.1.2 Spin relaxation

Spin relaxation describes the return of the spins to equilibrium after an rf pulse. The rate of relaxation is influenced by the physical properties and the dynamics of the molecules as well as the sample. There are two relaxation mechanisms that can be observed: spin-lattice or longitudinal relaxation (T_1) and spin-spin or transverse relaxation (T_2). The longitudinal relaxation time measures the average lifetime of nuclei in the higher energy level and is dependent on the gyromagnetic ratio and the mobility of the lattice. The transverse relaxation measures how efficient the exchange of energy between spins is. An isolated nuclear spin would present rather long relaxation times. Within molecules, relaxation can be induced by exchange of energy with the surrounding or with other spins in the same molecule. Therefore, relaxation rates give important information on molecular dynamics.

3.6.2 NMR sample

For NMR experiments Lb^{pro} mutant proteins were expressed in E. coli BL 21(DE3) LysS (see chapter 3.2.1.2) using pET 11d vectors (see chapter 3.3.1.1). Bacteria were grown in minimal medium containing the preferred isotopes for protein labelling (see chapter 3.5.2.2). The proteases were purified as described in Materials and Methods (see chapter 3.5.5). The isotope-labelled proteins were dialysed into NMR buffer and concentrated to 0.5 - 2 mM (see chapter 3.5.6) (see Table 9). Furthermore, 5 - 10 % (v/v) ²H₂O was added to the sample as internal standard.

The CBCA(CO)NH correlates the frequencies of a $^{13}\text{C}_\alpha$ and a $^{13}\text{C}_\beta$ with those of the amide proton and nitrogen of the next residue. In the HNCACB the frequencies of the amide proton and nitrogen are correlated with the $^{13}\text{C}_\alpha$ and $^{13}\text{C}_\beta$ of the preceding as well as to the same residue. Together, CBCA(CO)NH and HNCACB provide a further method for sequential assignment due to larger $^{13}\text{C}_\beta$ shift ranges.

In combination, HN(CO)CA/HNCA and CBCA(CO)NH/HNCACB, provide the basis for almost complete structure assignment.

4 Results

4.1 Investigating intramolecular self-processing of Lb^{pro}

In order to be able to investigate intramolecular self-processing of Lb^{pro} by NMR it is a prerequisite to inhibit dimer formation of Lb^{pro}. As several attempts to dissociate the dimer have failed so far (see chapter 1.5.1), we tried to dissociate the dimer via site-directed mutagenesis of residues involved in dimer formation. Thus, we were looking for Lb^{pro} mutants that were enzymatically active but remained monomeric. Essentially, mutations were introduced at two distinct sites of Lb^{pro}, either at the interface region or in the CTE. Wildtype Lb^{pro} (Lb^{pro} WT) and shortened Lb^{pro} (sLb^{pro}) served as reference proteins.

The enzymatic activity was analysed by an *in vitro* assay using rabbit reticulocyte lysates. At the same time, the oligomerisation state was analysed by size-exclusion chromatography.

4.1.1 Lb^{pro} wildtype and shortened Lb^{pro}

Wildtype Lb^{pro} (Lb^{pro} WT) and shortened Lb^{pro} (sLb^{pro}), lacking the last six amino acids of the CTE, were analysed as they serve as reference proteins for the Lb^{pro} mutants. It was shown that Lb^{pro} WT appears as a dimer, whereas sLb^{pro} appears in a monomeric state. The enzymatic activity of Lb^{pro} WT is measurable in *cis* and *trans*, whereas sLb^{pro} is only active in *trans* (Glaser *et al.*, 2001). The sLb^{pro} lacks the last six residues of the CTE, resembling the P region of the polyprotein cleavage sequence; there is thus no basis to investigate the self-processing activity. Furthermore, the dimerisation state of Lb^{pro} WT and sLb^{pro} was analysed.

4.1.1.1 Enzymatic activity of Lb^{pro} WT

The enzymatic activity of the Lb^{pro} mutants was investigated performing an *in vitro* assay. To this end, the desired mutations were introduced into the vector pCITE 1d Lb^{pro}VP4/VP2 by site-directed PCR mutagenesis (see chapter 3.3.11) using specific oligonucleotides (see chapter 3.3.14.1). After confirmation of the correct sequence of the mutagenised plasmids (see chapter 3.3.13), RNA coding for Lb^{pro}VP4/VP2 was transcribed *in vitro* (see chapter 3.4.1). Subsequently, *in vitro* translation was performed using the rabbit reticulocyte lysate system (see chapter 3.4.3). The translation mix contained ³⁵S-labelled methionine which was incorporated into the newly synthesised precursor protein Lb^{pro}VP4/VP2. The enzymatic activity was reflected in the rate at which Lb^{pro} cleaves the precursor protein into the cleavage products Lb^{pro} and VP4/VP2. In course of the translation process, aliquots were taken at defined time points and analysed by SDS PAGE, using the protocol of Dasso & Jackson (see chapter 3.5.8.2). ³⁵S-labelled proteins were visualised via fluorography (see chapter 3.5.10).

The kinetics of eIF4GI cleavage was analysed via western blot analysis of the *in vitro* translation sample (see chapter 3.5.11) using polyclonal α -eIF4GI primary antibodies (see Table 7) and α -rabbit alkaline phosphatase conjugated secondary antibodies (see Table 8).

Figure 10 shows the enzymatic activity of Lb^{PRO} WT, reflected in the kinetics of self-processing and eIF4GI cleavage. The high efficiency of the self-processing reaction of Lb^{PRO} WT is indicated by the low amount of uncleaved precursor Lb^{PRO}VP4/VP2. The cleavage products Lb^{PRO} and VP4/VP2 are visible for the first time after 4 to 8 minutes after translation initiation. Lb^{PRO} encoded by pCITE Lb^{PRO}VP4/VP2 has four methionines, whereas VP4/VP2 has only two. Therefore, the intensity of the Lb^{PRO} band is twice that of VP4/VP2. Furthermore, the majority of eIF4GI molecules is cleaved at the 8 minutes time point. The cleavage process is completed after 12 to 20 minutes after translation initiation. Aberrant cleavage products appear 30 and 60 minutes after translation initiation.

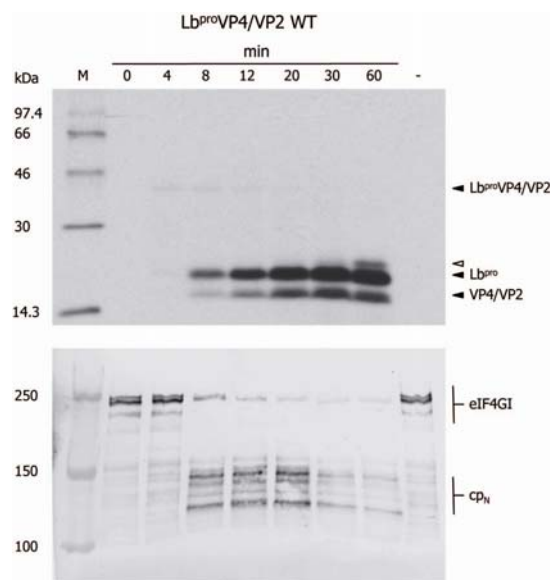


Figure 10 Enzymatic activity of Lb^{PRO} WT. Rabbit reticulocyte lysate was programmed with RNA (10 ng/ μ l) coding for Lb^{PRO}VP4/VP2 and incubated at 30°C. Negative controls (-) were prepared by addition of water instead of RNA and incubation at 30°C for 60 minutes. 10 μ l samples were taken at the indicated time points and protein translation was terminated by mixing the samples with an icecold mix of 25 μ l 2 x Laemmli sample buffer, 15 μ l H₂O and 1 μ l unlabelled methionine/cysteine (20 mM).

The **top panel** shows the self-processing activity of Lb^{PRO} WT on the precursor Lb^{PRO}VP4/VP2. Viral proteins were separated by SDS PAGE on a 17.5 % 'Dasso & Jackson' PAA-gel and visualised by fluorography. The fluorograph was exposed for 20 hours. The positions of uncleaved Lb^{PRO}VP4/VP2 and the cleavage products Lb^{PRO} and VP4/VP2 are marked. Aberrant cleavage products are marked with a white arrow.

The **bottom panel** shows the cleavage of eIF4GI. Cleavage products were separated by SDS PAGE on a 6 % 'Dasso & Jackson' PAA-gel and blotted on a PVDF membrane. For detection, a polyclonal α -eIF4GI primary antibody and an α -rabbit alkaline phosphatase conjugated secondary antibody were used. The multiple protein bands of eIF4GI are caused by translation initiation at different AUG codons.

Protein standards (kDa) are shown on the left.

4.1.1.2 Oligomerisation state of Lb^{pro} WT and sLb^{pro}

For the analysis of the oligomerisation state of the Lb^{pro} mutants, the proteases were expressed in *E. coli* BL21 (DE3) LysS cells (see chapter 3.5.2.1) using pET 11d vectors. Once again, the desired mutations were introduced by site-directed PCR mutagenesis (see chapter 3.3.11) using specific primers containing the desired mutations (see chapter 3.3.14.1). To ensure long-time stability of the samples the protease was inactivated by mutating the active site Cys 51 to Ala. This mutation results in the inactivation of the enzyme by removing the sulfhydryl group required for nucleophilic attack at the scissile peptide bond. Subsequently, the proteases were purified as described in Materials and Methods (see chapter 3.5.5).

In order to investigate the oligomerisation state of Lb^{pro} molecules, analytical size-exclusion chromatography was performed using a HiLoad 16/60 Superdex 75 pg column (see chapter 3.5.5.3.2). The molecular weight of a protein was estimated by comparing its elution volume with those of standard proteins of known molecular weight, such as ovalbumin (43 kDa), chymotrypsinogen A (25 kDa) and ribonuclease A (13.7 kDa) (Gel Filtration Calibration Kit LMW from GE Healthcare) (see Figure 11).

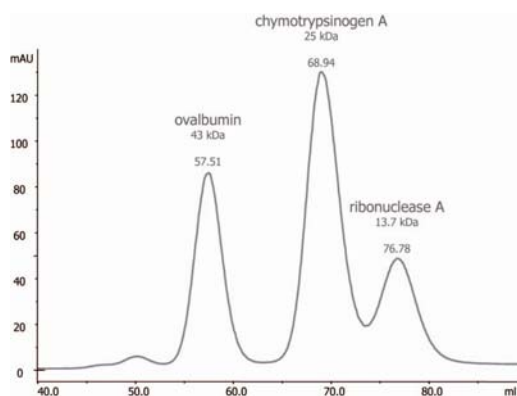


Figure 11 Chromatogram of standard proteins. Separation of proteins according to their size was achieved by size-exclusion chromatography using the HiLoad 16/60 Superdex 75 pg column (from Amersham Biosciences). 3 mg of each of the standard proteins ovalbumin (43 kDa), chymotrypsinogen A (25 kDa) and ribonuclease A (13.7 kDa) were analysed. The respective elution volumes (ml) are indicated.

As the elution volumes of proteins can slightly vary, each Lb^{pro} mutant was analysed together with ribonuclease A. Ribonuclease A has a known molecular weight of 13.7 kDa and is therefore used as an internal control. To make a comparison between the chromatograms of different Lb^{pro} mutants easier, the chromatogram of each Lb^{pro} mutant was overlaid with the chromatogram of the standard proteins. Subsequently, the chromatogram of the standard proteins was shifted along the X-axis and normalised to the ribonuclease A peak.

In Figure 12, the pure proteases are shown on a PAA gel. Although sLb^{pro} has a lower molecular weight than Lb^{pro} WT it appears to migrate more slowly. A similar effect was observed by Sangar and colleagues, as a result of the treatment of Lb^{pro} with carboxypeptidase B (Sangar *et al.*, 1988). This enzyme is specific for C-terminal basic amino acids. As the last six amino acids of the CTE contain three basic residues, this lack might be the reason why the mobility of sLb^{pro} is decreased on SDS PAGE.

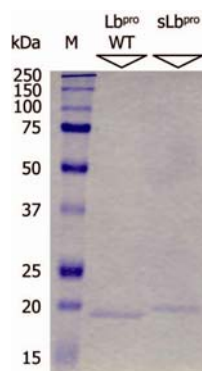


Figure 12 PAA gel showing the pure proteases Lb^{pro} WT and sLb^{pro}. The inactive forms of Lb^{pro} WT and sLb^{pro} were expressed in LB medium and purified using the methods described in Materials and Methods (see chapter 3.5.5). 2 µg of the pure protein sample are shown on a 17.5 % 'Laemmli' SDS gel. Protein standards (kDa) are shown on the left.

Following, the oligomerisation state was analysed via size-exclusion chromatography. Figure 13 shows the chromatograms of Lb^{pro} (WT) (A) and sLb^{pro} (B) compared to the chromatogram of the standard proteins.

As previously shown by Cencic and colleagues (Cencic *et al.*, 2007), Lb^{pro} WT elutes at about 58 ml. A comparison with the standard proteins reveals a molecular weight of about 40 kDa, representing the presence of a dimer (Figure 13A). In contrast, sLb^{pro} elutes at about 68 ml which corresponds to a molecular weight of about 20 kDa. This indicates the presence of a monomer (Figure 13B). The chromatogram of sLb^{pro} displays a lower amount of protein due to inaccurate loading of the protein to the column.

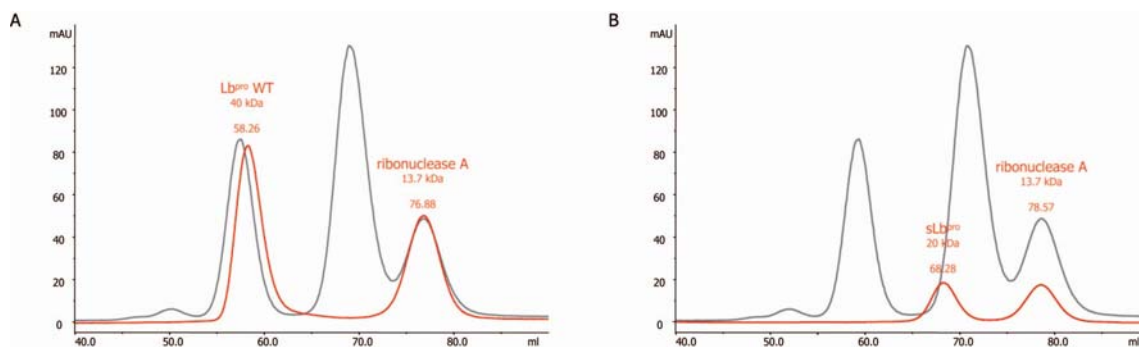


Figure 13 Chromatograms of Lb^{pro} WT and sLb^{pro}. Separation of proteins according to their size was achieved by size-exclusion chromatography, using the HiLoad 16/60 Superdex 75 pg column (from Amersham Biosciences). 1 mg of each Lb^{pro} WT and sLb^{pro} was analysed together with 2 mg ribonuclease A (13.7 kDa) used as an internal standard; the chromatogram of Lb^{pro} WT (A) and sLb^{pro} (B) is shown in red. The respective elution volumes (ml) are indicated. The chromatogram of standard proteins, shown in grey, was shifted along the X-axis to align the elution volume of ribonuclease A.

4.1.2 Effects of mutations at the interface on dimerisation

In order to inhibit dimer formation, we considered removing potential interactions between dimeric Lb^{pro} molecules by mutating specific residues. Based on the NMR studies by Cencic and colleagues (Cencic *et al.*, 2007), Trp 105 and Thr 117, located in the interface between dimeric Lb^{pro} molecules, were considered to be involved in dimer stabilisation (see Figure 14) (see chapter 1.5.1).

To analyse their importance in dimer formation, Trp 105 and Thr 117 were substituted with Ala either as single mutations or together as a double mutation to remove the putative attractive interactions between the two globular domains of dimerised molecules. Furthermore, Trp 105 was substituted with the large, positively charged amino acid Arg in an attempt to provoke repulsion between dimeric molecules. The enzymatic activity as well as the oligomerisation state of the Lb^{pro} interface mutants was examined.

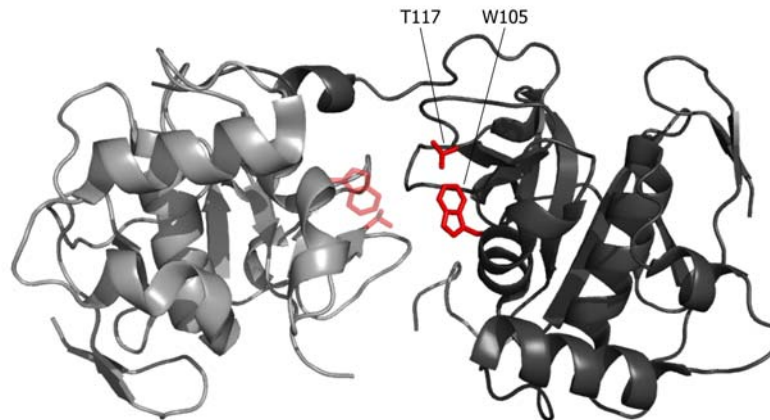


Figure 14 Mutated residues of Lb^{pro} interface mutants. The two Lb^{pro} molecules of the dimer are shown in light and dark grey. Trp 105 (W105) and Thr 117 (T117) (shown in red) are located in the interface between the two globular domains of dimeric molecules. Generated with PyMOL (DeLano, 2002) using the PDB ID code 1QQL.

4.1.2.1 Enzymatic activities of interface mutants

Figure 15 shows the kinetics of self-processing and eIF4GI cleavage of the various Lb^{pro} interface mutants. Lb^{pro} W105 (A) displays similar enzymatic activities compared to the wildtype. The cleavage products Lb^{pro} and VP4/VP2 are visible after 8 minutes of translation initiation and eIF4GI cleavage is completed at the 8 minutes time point.

The mutants Lb^{pro} T117A (B), Lb^{pro} L143A L200F (C) and Lb^{pro} W105R (D) display full activity in self-processing, as only a low amount of uncleaved precursor protein could be detected. The slight shift in mobility observed for Lb^{pro} T117A might be caused by the mutation. However, the slight delay in self-processing might result from a lower concentration of Lb^{pro} due to unfavourable conditions during the translation process. This is also reflected by a slight delay in eIF4GI cleavage. Nevertheless, the majority of the eIF4GI molecules are cleaved by the Lb^{pro} mutants at the 12 minutes time point.

In summary, all interface mutants were shown to be enzymatically active and showed little, if no difference to the wildtype.

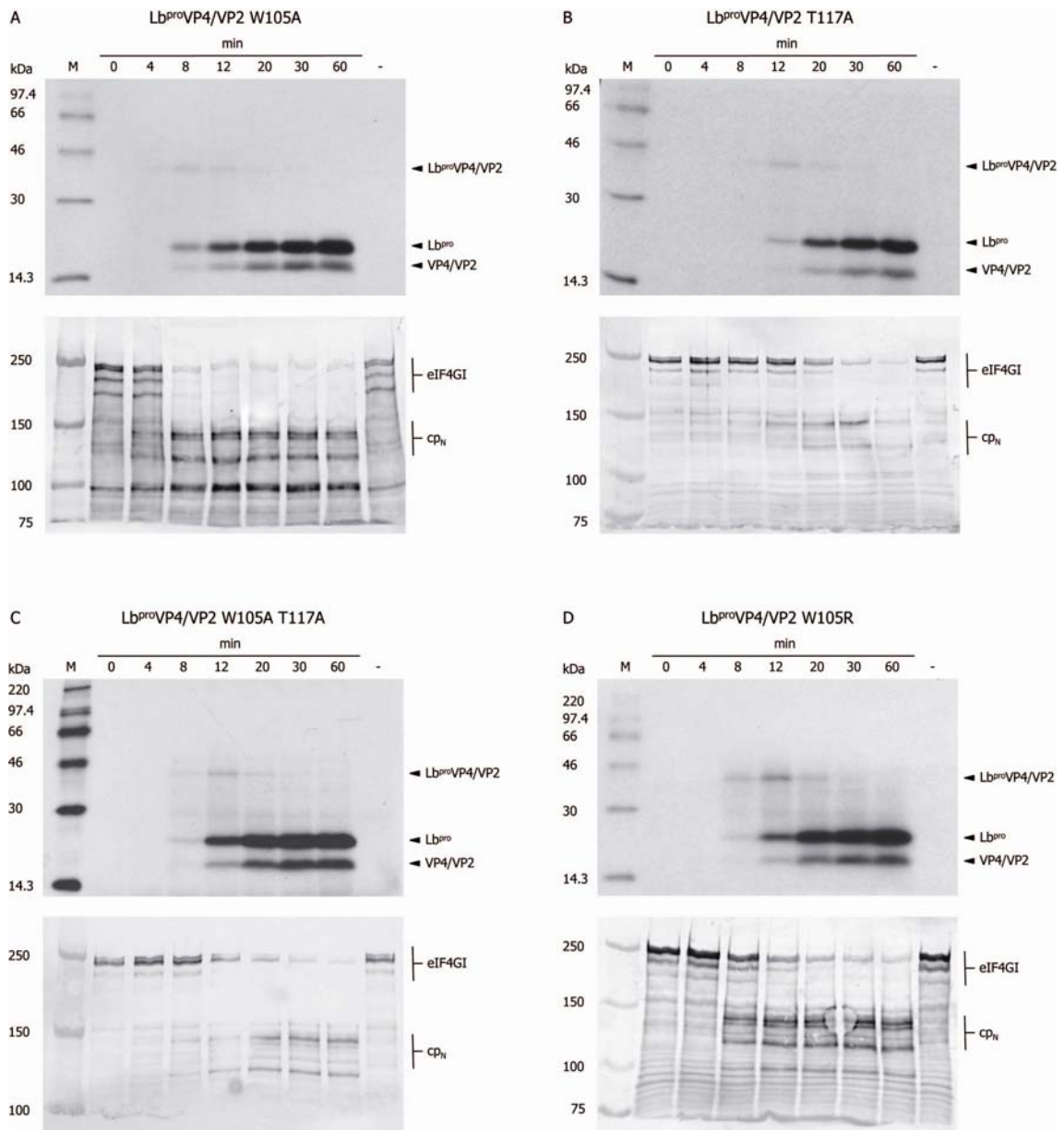


Figure 15 Enzymatic activity of Lb^{pro} interface mutants. The mutants Lb^{pro} W105A (A), Lb^{pro} T117A (B), Lb^{pro} W105A T117A (C) and Lb^{pro} W105R (D) are shown. Rabbit reticulocyte lysate was programmed with RNA (10 ng/ μ l) coding for $Lb^{pro}VP4/VP2$ and incubated at 30°C. Negative controls (-) were prepared by addition of water instead of RNA and incubation at 30°C for 60 minutes. 10 μ l samples were taken at the indicated time points and protein translation was terminated by mixing the samples with an icecold mix of 25 μ l 2 x Laemmli sample buffer, 15 μ l H_2O and 1 μ l unlabelled methionine/cysteine (20 mM).

Top panels show the self-processing activity of Lb^{pro} on the precursor $Lb^{pro}VP4/VP2$. Viral proteins were separated by SDS PAGE on 17.5 % 'Dasso & Jackson' PAA gels and visualised by fluorography. Fluorographs were exposed for 20 to 90 hours. The positions of uncleaved $Lb^{pro}VP4/VP2$ and the cleavage products Lb^{pro} and $VP4/VP2$ are marked.

Bottom panels show the cleavage of eIF4GI. Cleavage products were separated by SDS PAGE on 6 % 'Dasso & Jackson' PAA gels and blotted on a PVDF membrane. For detection, a polyclonal α -eIF4GI primary antibody and an α -rabbit alkaline phosphatase conjugated secondary antibody were used. The multiple protein bands of eIF4GI are caused by translation initiation at different AUG codons.

Protein standards (kDa) are shown on the left.

4.1.2.2 Oligomerisation state of interface mutants

In order to examine whether the mutations at the interface region had an effect on the oligomerisation state, the Lb^{pro} mutant proteins were expressed and analysed by size-exclusion chromatography. Figure 16 displays the PAA gel showing the pure proteins that were used for further analysis.

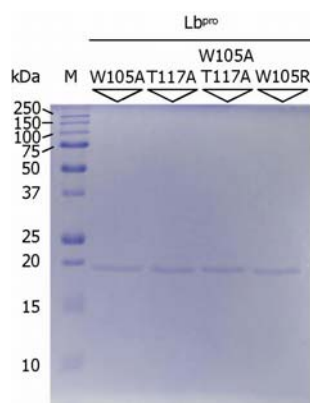


Figure 16 PAA gel showing the pure proteases Lb^{pro} W105A, Lb^{pro} T117A, Lb^{pro} W105A T117A and Lb^{pro} W105R. The inactive form of the mutant proteases was expressed in LB medium and purified using the methods described in Materials and Methods (see chapter 3.5.5). 2 µg of the pure protein sample are shown on a 17.5 % 'Laemmli' SDS gel. Protein standards (kDa) are shown on the left.

Figure 17 displays the elution profiles of the interface mutants Lb^{pro} W105A (A), T117A (B), W105A T117A (C) and W105R (D) that were compared with the chromatogram of the standard proteins. The interface mutants elute between 57.96 and 60.14 ml. These elution volumes are comparable with that of ovalbumin (43 kDa), suggesting a molecular weight of about 40 kDa. This and the fact that Lb^{pro} WT elutes at a similar volume of about 58 ml (see chapter 4.1.1.2) suggest that the interface mutant proteins appear in a dimeric state.

Altogether, the mutations in the interface region of dimeric Lb^{pro} molecules failed to affect both the enzymatic activity and dimer formation.

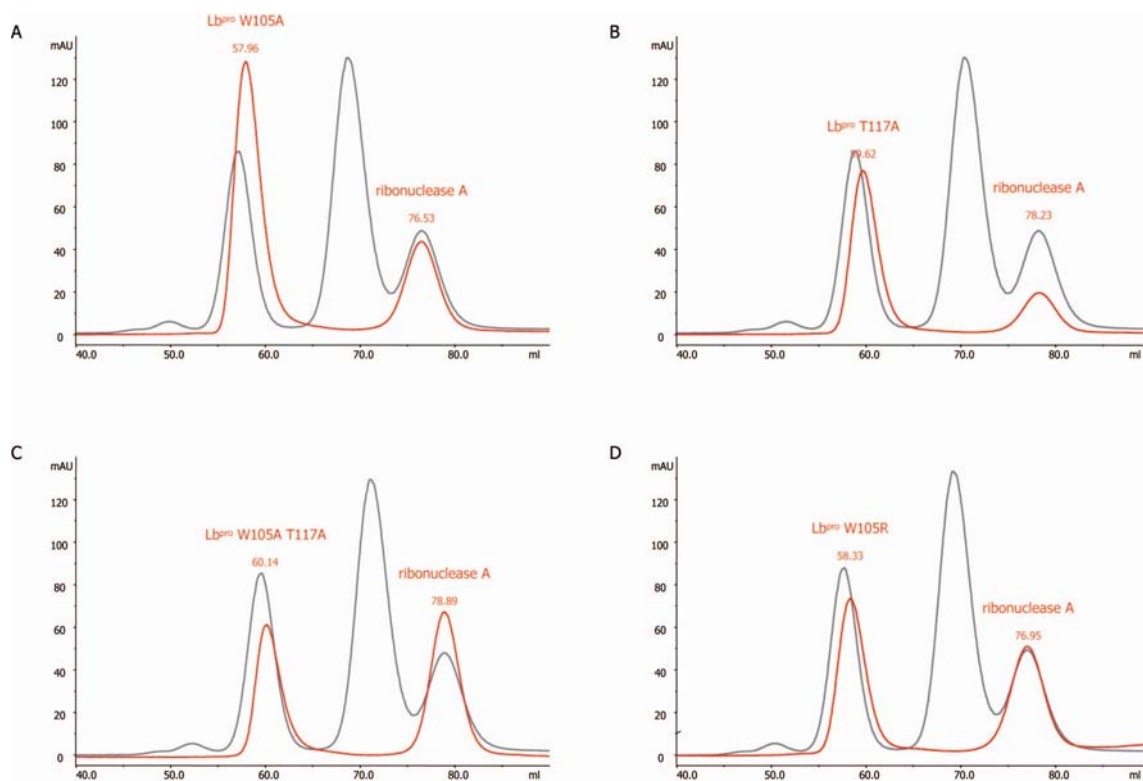


Figure 17 Chromatograms of Lb^{PRO} interface mutants. Separation of proteins according to their size was achieved by size-exclusion chromatography, using the HiLoad 16/60 Superdex 75 pg column (from Amersham Biosciences). 1 mg of each of the interface mutants was analysed together with 2 mg ribonuclease A (13.7 kDa) used as an internal standard; the chromatograms of Lb^{PRO} W105A (A), Lb^{PRO} T117A (B), W105A T117A (C) and Lb^{PRO} W105R (D) are shown in red. The respective elution volumes (ml) are indicated. The chromatogram of standard proteins, shown in grey, was shifted along the X-axis to align the elution volume of ribonuclease A.

4.1.3 Effects of mutations in the CTE on dimerisation

In further attempt to separate the dimer, residues of the CTE and the active site were chosen for mutagenesis. It was shown by Mayer and colleagues that the substitution of Leu 200 with Phe leads to a disruption of self-processing activity. However, the additional replacement of Leu 143 to Ala restored the enzymatic activity to wildtype levels (Mayer *et al.*, 2008).

As self-processing of Lb^{PRO} is impaired by the L200F mutation, we assumed that the dimerisation state might also be affected. Therefore, the enzymatic activity as well as the oligomerisation state of the mutants Lb^{PRO} L200F and Lb^{PRO} L143A L200F was analysed (see Figure 18).

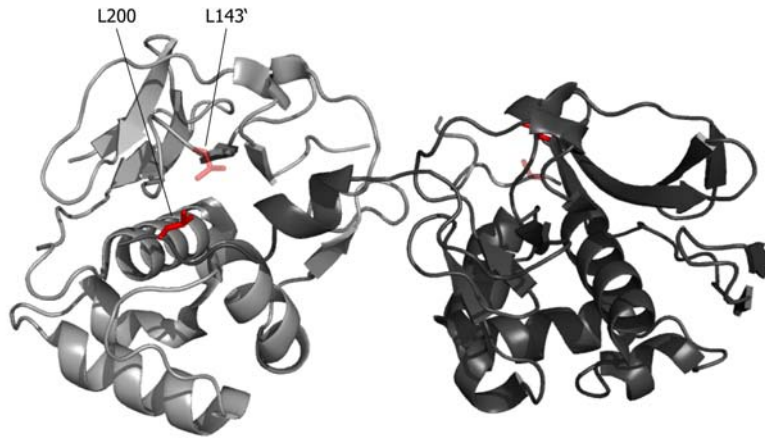


Figure 18 Mutated residues of Lb^{pro} CTE mutants. The two Lb^{pro} molecules of the dimer are shown in light and dark grey. Leu 200 (L200) of one molecule, reflecting the P₂ position, binds to the S₂ pocket of the neighbouring molecule, containing Leu 143' (L143') (shown in red). Generated with PyMOL (DeLano, 2002) using the PDB ID code

4.1.3.1 Enzymatic activities of CTE mutants

In Figure 19, the kinetics of self-processing and eIF4GI cleavage of the CTE mutants Lb^{pro} L200F (A) and Lb^{pro} L143A L200F (B) are shown. As demonstrated by Mayer and colleagues (Mayer *et al.*, 2008), the Lb^{pro} L200F self-processing is delayed compared to the wildtype (see chapter 4.1.1.1). The first cleavage products are detectable after 20 minutes of translation initiation and even after 60 minutes the precursor protein Lb^{pro}VP4/VP2 is not completely processed. However, the mutation L200F did not affect the cleavage rate of eIF4GI. 50 % cleavage could be detected at the 8 minutes time point and the reaction was completed after 12 minutes.

Interestingly, the additional mutation L143A fully restores the enzymatic activity. The first cleavage products of Lb^{pro} L143A L200F were detected after 8 minutes of translation initiation, resembling wildtype levels. The cleavage of eIF4GI is complete between 12 and 20 minutes after translation initiation, showing similar *trans* cleavage activity as Lb^{pro} WT.

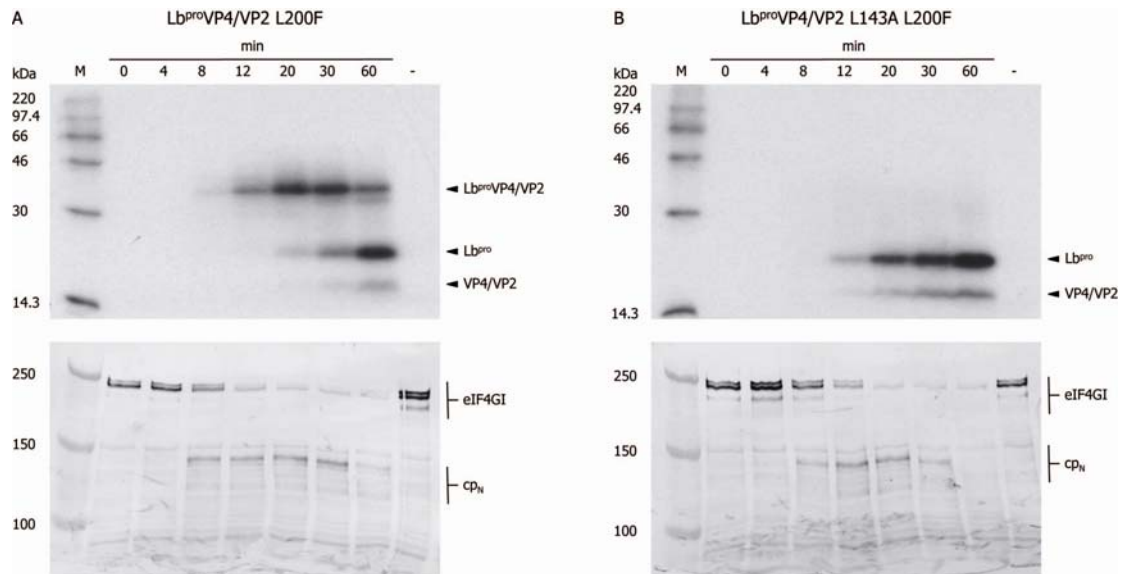


Figure 19 Enzymatic activity of Lb^{pro} CTE mutants. The mutants Lb^{pro} L200F (A) and Lb^{pro} L143A L200F (B) are shown. Rabbit reticulocyte lysate was programmed with RNA (10 ng/μl) coding for Lb^{pro}VP4/VP2 and incubated at 30°C. Negative controls (-) were prepared by addition of water instead of RNA and incubation at 30°C for 60 minutes. 10 μl samples were taken at the indicated time points and protein translation was terminated by mixing the samples with an icecold mix of 25 μl 2 x Laemmli sample buffer, 15 μl H₂O and 1 μl unlabeled methionine/cysteine (20 mM).

Top panels show the self-processing activity of Lb^{pro} on the precursor Lb^{pro}VP4/VP2. Viral proteins were separated by SDS PAGE on 17.5 % PAA gels and visualised by fluorography. Fluorographs were exposed for 20 to 90 hours. The positions of uncleaved Lb^{pro}VP4/VP2 and the cleavage products Lb^{pro} and VP4/VP2 are marked.

Bottom panels show the cleavage of eIF4GI. Cleavage products were separated by SDS PAGE on 6 % PAA gels and blotted on PVDF membrane. For detection, a polyclonal α-eIF4GI primary antibody and an α-rabbit alkaline phosphatase conjugated secondary antibody were used. The multiple protein bands of eIF4GI are caused by translation initiation at different AUG codons.

Protein standards (kDa) are shown on the left.

4.1.3.2 Oligomerisation state of CTE mutants

In order to investigate the oligomerisation state of Lb^{pro} L200F and Lb^{pro} L143A L200F, the Lb^{pro} mutant proteins were expressed and analysed by size-exclusion chromatography. The PAA gel showing the pure proteases used for size-exclusion chromatography is presented in Figure 20.

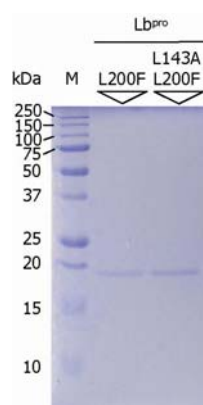


Figure 20 PAA gel showing the pure proteases Lb^{pro} L200F and Lb^{pro} L143A L200F. The inactive form of the mutant proteases was expressed in LB medium and purified using the methods described in Materials and Methods (see chapter 3.5.5). 2 µg of the pure protein sample are shown on a 17.5 % 'Laemmli' SDS gel. Protein standards (kDa) are shown on the left.

Figure 21 shows the elution profiles of the single mutant Lb^{pro} L200F and the double-mutant Lb^{pro} L143A L200F. The mutant Lb^{pro} L200F displays an elution volume of about 66.9 ml. A comparison with the chromatogram of standard proteins indicates a molecular weight of Lb^{pro} L200F of about 20 kDa. This and the fact that sLb^{pro} elutes at about 68.3 ml suggests that Lb^{pro} L200F is present in a monomeric state.

Interestingly, Lb^{pro} L143A L200F elutes at 66.4 ml which reflects an intermediate elution volume between the one of Lb^{pro} WT of about 58 ml and the one of sLb^{pro} of about 68 ml. This would suggest that Lb^{pro} L143A L200F also appears as a monomer. Furthermore, the alteration of the protein concentration from 50 nM to 25 nM did not affect the elution volume of Lb^{pro} L143A L200F, showing that the elution volume of Lb^{pro} L143A L200F is reproducible. As the additional mutation L143A restores the enzymatic activity of Lb^{pro} L143A L200F, we assumed that also the dimeric structure of the protein would be reconstituted. However, this assumption could not be confirmed by size-exclusion chromatography.

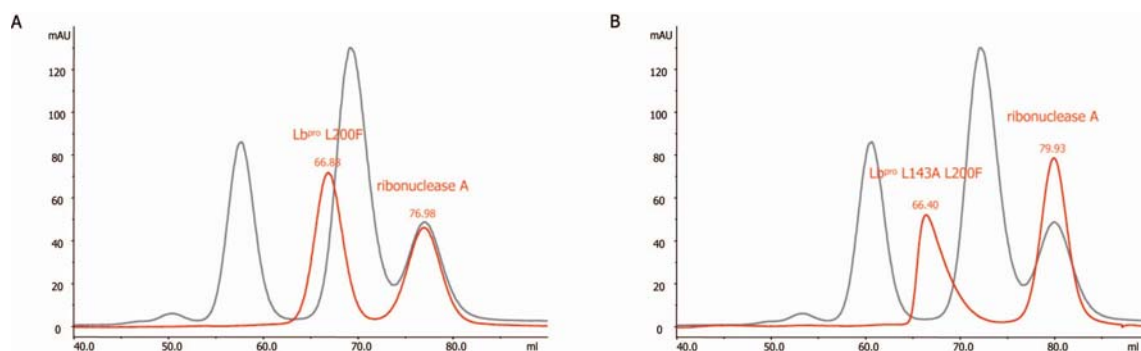


Figure 21 Chromatograms of Lb^{pro} CTE mutants. Separation of proteins according to their size was achieved by size-exclusion chromatography, using the HiLoad 16/60 Superdex 75 pg column (from Amersham Biosciences). 1 mg of each of the CTE mutants was analysed together with 2 mg ribonuclease A (13.7 kDa) used as an internal standard; the chromatograms of Lb^{pro} L200F (A) and Lb^{pro} 143A L200F (B) are shown in red. The respective elution volumes (ml) are indicated. The chromatogram of standard proteins, shown in grey, was shifted along the X-axis to align the elution volume of ribonuclease A.

4.1.3.3 NMR studies of CTE mutants

The mutants Lb^{pro} L200F and Lb^{pro} L143A L200F were analysed by NMR studies to gain further information about the oligomerisation state and the structural features of the proteins (see chapter 3.6). The T_2 transverse relaxation times of the ^{15}N labelled Lb^{pro} mutants were measured in order to determine the oligomerisation state (see chapter 3.6.3). Furthermore, a 2D ^1H - ^{15}N HSQC spectrum of the CTE mutants was recorded and compared to the spectra of Lb^{pro} WT and sLb^{pro} in order to determine any structural changes in the protein backbone structure (see chapter 3.6.3.1).

To this end, both mutant proteins were expressed in minimal medium containing ^{15}N (see chapter 3.5.2.2). Again, the protease was inactivated by mutating Cys 51 to Ala in order to ensure stability during NMR analysis. The proteases were purified as described in Materials and Methods (see chapter 3.5.5). The protein sample was dialysed into NMR buffer and concentrated (see chapter 3.6.2). Lb^{pro} L200F was concentrated to about 2 mM, whereas the Lb^{pro} L143A L200F reached a concentration of about 1 mM. The pure protein fractions used for NMR analysis are shown in Figure 22.



Figure 22 PAA-gel showing the pure proteases ^{15}N Lb^{pro} L200F and ^{15}N Lb^{pro} L143A L200F. The inactive form of the mutant proteases was expressed in minimal medium containing ^{15}N . The proteins were purified using the methods described in Materials and Methods (see chapter 3.5.5). 2 μg of the pure protein sample are shown on a 17.5 % 'Laemmli' SDS-gel. Protein standards (kDa) are shown on the left.

4.1.3.3.1 T_2 transverse relaxation times of CTE mutants

In order to determine the oligomerisation state of the CTE mutants more precisely, the ^{15}N T_2 transverse relaxation times for the mutants Lb^{pro} L200F and Lb^{pro} L143A L200F were measured. The ^{15}N T_2 transverse relaxation times of Lb^{pro} WT and sLb^{pro} were measured by Cencic and colleagues (Cencic *et al.*, 2007) who showed that the monomeric sLb^{pro} displays T_2 relaxation times that are about twice as long compared to the dimeric Lb^{pro} WT.

Figure 23 shows the ^{15}N transverse relaxation times of Lb^{pro} L200F compared to sLb^{pro} and Lb^{pro} L143A L200F compared to Lb^{pro} WT. Figure 23A shows an overlay of the T_2 values of Lb^{pro} L200F and sLb^{pro}. The compared T_2 relaxation times display similar values of about 60 milliseconds, suggesting the presence of a monomer. In fact, the unstructured CTE displays T_2 relaxation times that are substantially longer compared to the globular domain, exceeding the detection range. However, no signals were detected that could be assigned to the last 12 residues of the CTE. Relaxation rates could only be detected up to Asn 189.

Figure 23B shows a comparison of the ^{15}N T_2 transverse relaxation times of Lb^{pro} L143A L200F and Lb^{pro} WT. The compared relaxation times show T_2 values of about 30 milliseconds illustrating about half the value of Lb^{pro} L200F and sLb^{pro}. These findings suggest that the dimeric structure of Lb^{pro} L143A L200F is restored. However, the findings from size-exclusion chromatography, that Lb^{pro} L143A L200F appears as a monomer, could not be confirmed. This suggests that the quaternary structure of Lb^{pro} L143A L200F is different in size-exclusion experiments and in NMR analysis due to different protein concentrations.

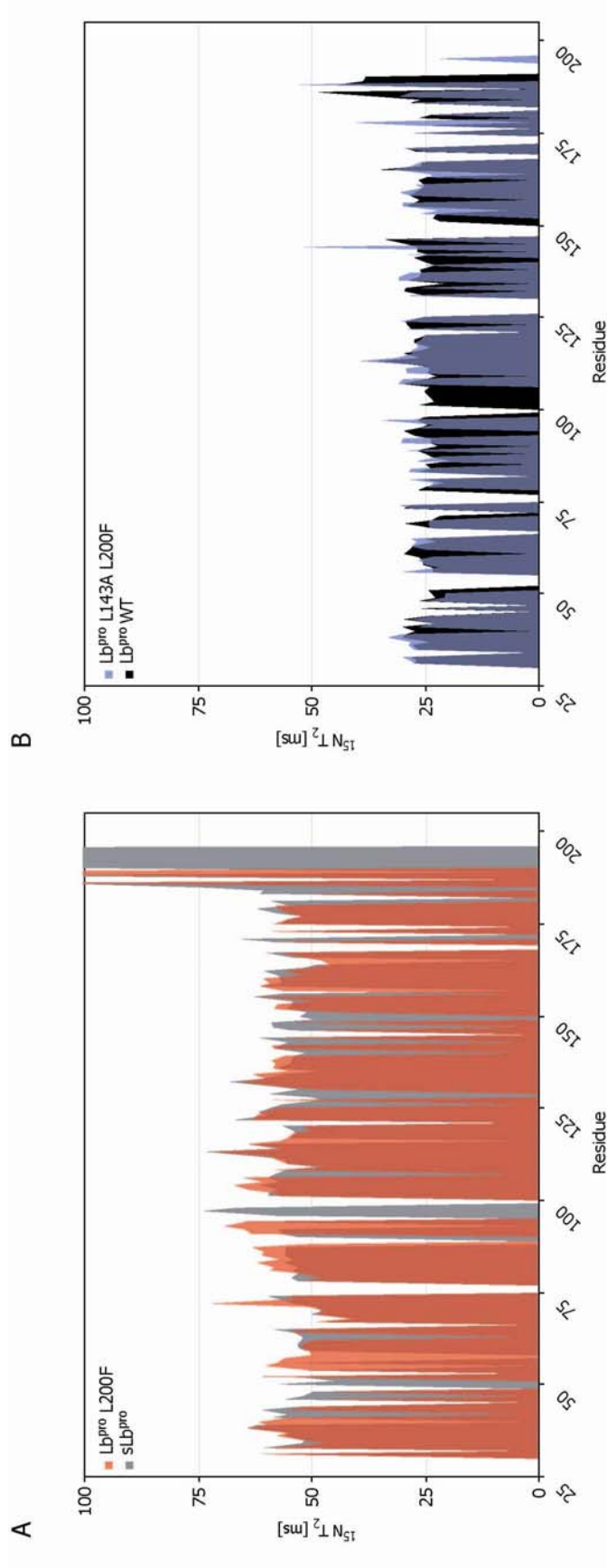


Figure 23 ^{15}N transverse relaxation times illustrating the oligomerisation state of the Lb^{pr} mutants. The relaxation times of Lb^{pr} L200F (red) compared to sLb^{pr} (grey) (A) and Lb^{pr} L143A L200F (blue) compared to Lb^{pr} WT (black) (B) are shown in milliseconds (ms). The ^{15}N transverse relaxation times were measured as described in Materials and Methods (see chapter 3.6.3). Signals for the last 12 residues of the CTE of Lb^{pr} L200F could not be detected. The roughly twofold difference in relaxation rates and the correlation with the compared spectra reveals that Lb^{pr} L200F appears as a monomer whereas Lb^{pr} L143A L200F appears as a dimer. The homologous assignments of sLb^{pr} and Lb^{pr} WT were used for Lb^{pr} L200F and Lb^{pr} L143A L200F.

4.1.3.3.2 2D ^1H - ^{15}N HSQC spectra of CTE mutants

Differences in the structure of the protein backbone between two protein variants can be examined by measuring the 2D ^1H - ^{15}N HSQC (see chapter 3.6.3.1). The spectrum shows signals that arise from the correlation of the frequency of the amide nitrogens with their protons. Therefore, every backbone amide gives rise to a signal. However, Pro residues can not be detected as they are an imide nitrogen rather than an amide. Furthermore, signals for Asn, Gln and Arg side chain amides as well as Trp indole are detectable.

Here, the ^1H - ^{15}N HSQC spectra of the Lb^{pro} mutants were compared to those determined for Lb^{pro} WT and sLb^{pro} by Cencic and colleagues (Cencic *et al.*, 2007). An overlay of the HSQC spectra of Lb^{pro} L200F and sLb^{pro} is shown in Figure 24. The compared spectra correlate to a high extent, as the majority of the signals show either no or only few differences. The signals displaying the greatest shifts (Asp 49, Trp 52, Val 127 and Gln 146) are pointed out with an arrow.

Table 10 shows the differences of the signals detected in the ^1H - ^{15}N HSQC spectrum for Lb^{pro} L200F compared to those of sLb^{pro}. Residues that were found to be shifted to the greatest extent are Asp 49 (0.60 ppm), Trp 52 (0.56 ppm), Val 127 (0.53 ppm) and Gln 146 (0.70 ppm). However, it was not possible to detect a signal for each residue of Lb^{pro} L200F. In particular, signals for the last 12 residues of the CTE were missing.

residue	$\Delta \delta$ (ppm)	residue	$\Delta \delta$ (ppm)	residue	$\Delta \delta$ (ppm)	residue	$\Delta \delta$ (ppm)	residue	$\Delta \delta$ (ppm)	residue	$\Delta \delta$ (ppm)		
Met 29	-	Asn 54	0.08	Thr 79	0.14	Ile 104	0.22	Gly 129	0.00	Val 154	0.00	Val 179	0.10
Glu 30	-	Ala 55	0.03	Leu 80	0.23	Trp 105	0.15	Thr 130	0.22	Thr 155	0.04	Phe 180	0.10
Leu 31	0.10	Ile 56	0.11	Glu 81	0.16	Asn 106	0.24	Asp 131	0.06	Ser 156	0.09	Val 181	0.14
Thr 32	0.19	Leu 57	0.13	Ala 82	0.10	Ile 107	0.09	Met 132	0.10	Asn 157	0.07	Pro 182	-
Leu 33	0.10	Gln 58	0.01	Ile 83	0.19	Lys 108	0.13	Cys 133	0.05	Gly 158	0.03	Tyr 183	0.13
Tyr 34	0.04	Leu 59	0.05	Lys 84	0.12	His 109	0.04	Leu 134	0.15	Trp 159	0.00	Asp 184	0.15
Asn 35	0.11	Phe 60	0.24	Gln 85	0.00	Leu 110	0.16	Ala 135	0.03	Tyr 160	0.05	Gln 185	0.23
Gly 36	0.05	Arg 61	0.15	Leu 86	0.12	Leu 111	0.10	Asp 136	0.13	Ala 161	0.05	Glu 186	0.21
Glu 37	0.05	Tyr 62	0.06	Glu 87	0.30	His 112	0.36	Phe 137	0.06	Ile 162	0.00	Pro 187	-
Lys 38	0.01	Val 63	0.09	Asp 88	0.00	Thr 113	0.44	His 138	0.13	Asp 163	0.14	Leu 188	0.20
Lys 39	0.03	Glu 64	0.05	Leu 89	0.01	Gly 114	0.13	Ala 139	0.05	Asp 164	0.12	Asn 189	0.01
Thr 40	0.05	Glu 65	0.13	Thr 90	0.12	Ile 115	0.24	Gly 140	0.09	Glu 165	0.16	Gly 190	-
Phe 41	0.10	Pro 66	-	Gly 91	0.00	Gly 116	0.10	Ile 141	0.16	Asp 166	0.09	Glu 191	-
Tyr 42	0.20	Phe 67	0.16	Leu 92	0.12	Thr 117	0.04	Phe 142	0.18	Phe 167	0.13	Trp 192	-
Ser 43	0.02	Phe 68	0.12	Glu 93	0.14	Ala 118	0.07	Leu 143	-	Tyr 168	0.00	Lys 193	-
Arg 44	0.12	Asp 69	0.12	Leu 94	0.00	Ser 119	0.29	Lys 144	0.00	Pro 169	-	Ala 194	-
Pro 45	0.00	Trp 70	0.03	His 95	-	Arg 120	0.10	Gly 145	-	Trp 170	0.12	Lys 195	-
Asn 46	0.16	Val 71	0.05	Glu 96	-	Pro 121	0.00	Gln 146	0.70	Thr 171	0.10	Val 196	-
Asn 47	0.17	Tyr 72	0.24	Gly 97	-	Ser 122	0.10	Glu 147	-	Pro 172	-	Gln 197	-
His 48	0.22	Ser 73	0.04	Gly 98	0.00	Glu 123	0.22	His 148	0.40	Asp 173	0.22	Arg 198	-
Asp 49	0.60	Ser 74	0.05	Pro 99	-	Val 124	0.03	Ala 149	-	Pro 174	0.00	Lys 199	-
Asn 50	-	Pro 75	-	Pro 100	-	Cys 125	0.05	Val 150	-	Ser 175	0.10	Phe 200	-
Ala 51	-	Glu 76	-	Ala 101	0.26	Val 126	0.00	Phe 151	0.13	Asp 176	0.55	Lys 201	-
Trp 52	0.56	Trp 77	-	Leu 102	0.42	Val 127	0.53	Ala 152	0.12	Val 177	0.10		
Leu 53	-	Leu 78	0.12	Val 103	0.20	Asp 128	0.00	Cys 153	0.06	Leu 178	0.10		

Residues for which no signal could be detected are indicated (-)

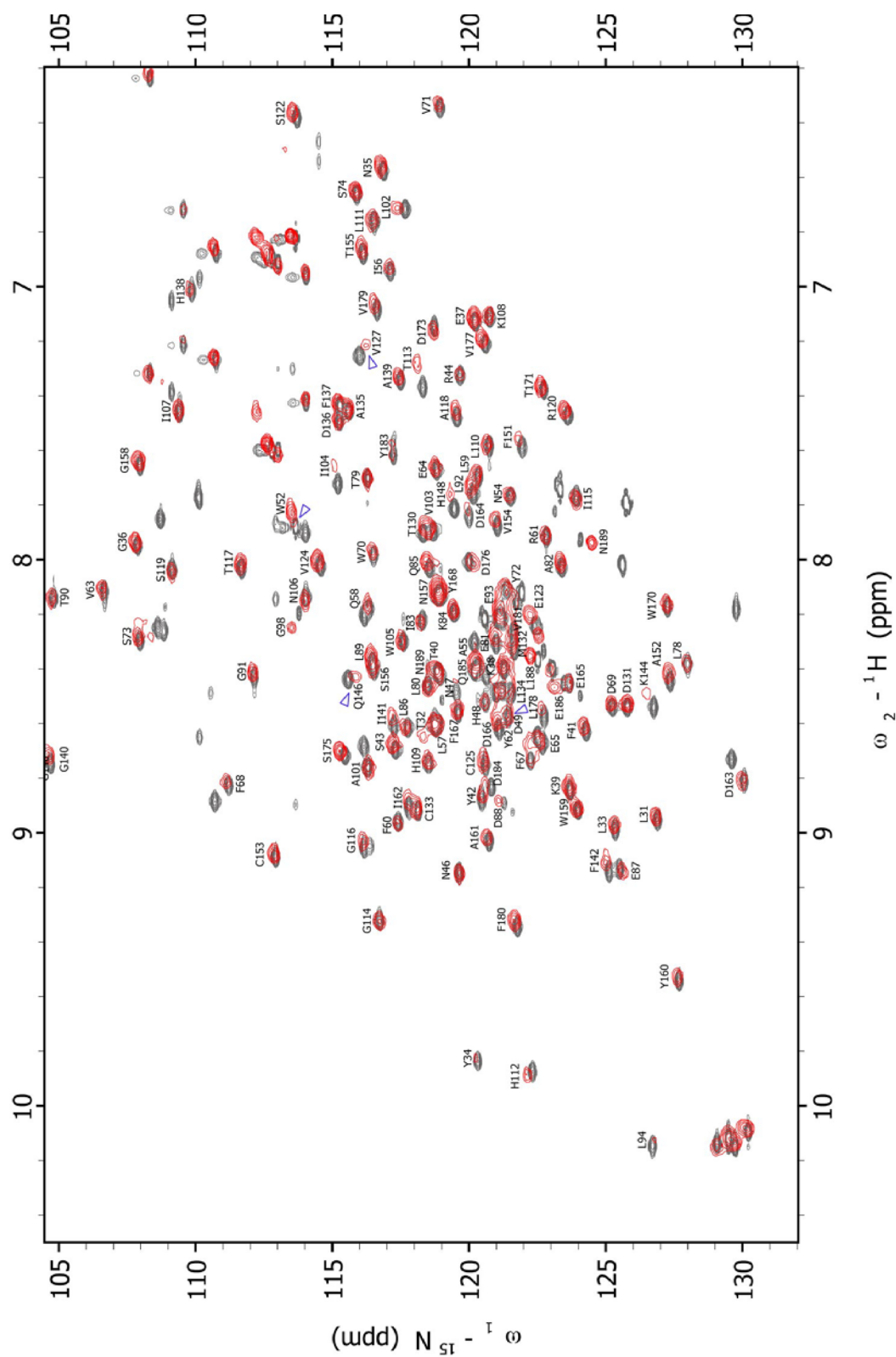


Figure 24 Overlaid ^1H - ^{15}N HSQC spectra of Lb^{pro} L200F (red) and sLb^{pro} (grey). The ^1H - ^{15}N HSQC spectrum was measured as described in Materials and Methods (see chapter 3.6.3). The overall correlation of the spectra suggests similar structures of Lb^{pro} L200F and sLb^{pro}. However, some signal shifts indicate distinct structural changes. The greatest signal shifts are indicated with a blue arrow. The homologous assignment of sLb^{pro} was used for Lb^{pro} L200F.

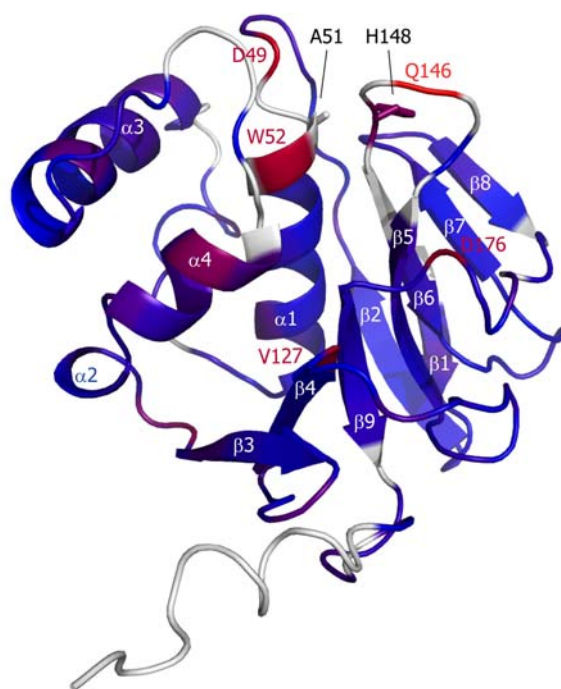


Figure 25 Differences in ^{15}N signal shifts between Lb^{pro} L200F and sLb^{pro} . Signal shifts of Lb^{pro} L200F detected in the ^1H - ^{15}N HSQC spectrum were mapped to the structure of the sLb^{pro} monomer. The chemical shift changes are colour-coded and range from low (0.00 ppm, blue) through medium (purple) to high (0.53-0.70 ppm, red). Residues for which no signal could be detected are shown in white. The active site residues Cys 51 (mutated to Ala) (A51) and His 148 (H148) are shown. Created with PyMOL (DeLano, 2002) using the PDB ID code 1QOL.

The residues of Lb^{pro} L200F that showed differences were mapped to the structure of sLb^{pro} as shown in Figure 25. Interestingly, the signals that show the greatest shifts mostly map to residues that are located in the substrate binding cleft.

There was no signal detected for the active site Ala 51 and also the signals of the flanking residues appeared to be either shifted or missing. Residues Asp 49 and Trp 52 of the active site display the greatest signal shifts within this region. In addition, the area around His 148 was found to show differences, including almost the entire loop connecting the sheets $\beta 5$ and $\beta 6$. Within this loop, the signal of Gln 146 appears to differ most. All residues of the helix $\alpha 4$ that are located at the surface appear to be changed by structural rearrangements. The β -sheet domain of Lb^{pro} L200F was found to be mainly unaffected by structural changes. Nevertheless, prominent signal shifts could be detected for Val 127 and Asp 176 building flanking residues of the binding cleft.

Although it was not possible to detect signals for the full-length CTE, it is likely that the observed signal shifts in the binding cleft are caused by a transient binding of the CTE to the active site of the same molecule.

Figure 26 shows an overlay of the ^1H - ^{15}N HSQC spectra of Lb^{pro} L143A L200F and Lb^{pro} WT. The comparison of the spectra showed an overall similarity of Lb^{pro} L143A L200F and Lb^{pro} WT. The signals which show the greatest shifts (Ala 118, Trp 170 and Tyr 183) are pointed out with an arrow.

Table 10 shows the differences of the signals detected in the ^1H - ^{15}N HSQC spectrum for Lb^{pro} L143A L200F compared to those of Lb^{pro} WT. The greatest signal shifts were detected for the residues Ala 118 (2.83 ppm), Trp 170 (6.07 ppm) and Tyr 183 (4.25 ppm).

Table 11 Shift differences ($\Delta \delta$) of Lb^{pro} L200F L143A compared to Lb^{pro} WT

residue	$\Delta \delta$ (ppm)	residue	$\Delta \delta$ (ppm)	residue	$\Delta \delta$ (ppm)	residue	$\Delta \delta$ (ppm)	residue	$\Delta \delta$ (ppm)	residue	$\Delta \delta$ (ppm)	residue	$\Delta \delta$ (ppm)
Met 29	-	Asn 54	-	Thr 79	0.05	Ile 104	-	Gly 129	-	Val 154	0.21	Val 179	0.36
Glu 30	-	Ala 55	-	Leu 80	0.10	Trp 105	-	Thr 130	-	Thr 155	0.23	Phe 180	0.43
Leu 31	0.20	Ile 56	0.04	Glu 81	0.20	Asn 106	-	Asp 131	0.31	Ser 156	0.12	Val 181	-
Thr 32	0.10	Leu 57	0.04	Ala 82	0.00	Ile 107	0.31	Met 132	-	Asn 157	-	Pro 182	-
Leu 33	0.01	Gln 58	0.00	Ile 83	0.12	Lys 108	0.28	Cys 133	0.49	Gly 158	0.20	Tyr 183	4.25
Tyr 34	-	Leu 59	0.06	Lys 84	0.20	His 109	0.00	Leu 134	-	Trp 159	0.13	Asp 184	0.00
Asn 35	0.20	Phe 60	0.10	Gln 85	0.14	Leu 110	0.24	Ala 135	0.23	Tyr 160	0.23	Gln 185	0.11
Gly 36	0.10	Arg 61	-	Leu 86	0.20	Leu 111	0.16	Asp 136	0.18	Ala 161	0.31	Glu 186	-
Glu 37	0.20	Tyr 62	0.20	Glu 87	0.14	His 112	0.68	Phe 137	0.32	Ile 162	-	Pro 187	-
Lys 38	0.20	Val 63	0.32	Asp 88	0.63	Thr 113	0.80	His 138	0.00	Asp 163	0.55	Leu 188	-
Lys 39	0.10	Glu 64	0.11	Leu 89	0.12	Gly 114	0.10	Ala 139	0.32	Asp 164	0.00	Asn 189	-
Thr 40	0.20	Glu 65	0.83	Thr 90	0.18	Ile 115	0.44	Gly 140	0.63	Glu 165	0.00	Gly 190	-
Phe 41	0.21	Pro 66	-	Gly 91	0.10	Gly 116	0.20	Ile 141	-	Asp 166	0.23	Glu 191	-
Tyr 42	0.23	Phe 67	-	Leu 92	0.36	Thr 117	0.32	Phe 142	0.60	Phe 167	0.10	Trp 192	-
Ser 43	0.13	Phe 68	0.31	Glu 93	0.20	Ala 118	2.83	Ala 143	0.25	Tyr 168	-	Lys 193	-
Arg 44	0.54	Asp 69	0.20	Leu 94	0.30	Ser 119	0.26	Lys 144	0.61	Pro 169	-	Ala 194	-
Pro 45	-	Trp 70	0.21	His 95	0.21	Arg 120	0.25	Gly 145	1.03	Trp 170	6.07	Lys 195	1.20
Asn 46	0.20	Val 71	0.00	Glu 96	0.26	Pro 121	-	Gln 146	0.19	Thr 171	0.39	Val 196	-
Asn 47	-	Tyr 72	-	Gly 97	0.43	Ser 122	0.15	Glu 147	-	Pro 172	-	Gln 197	-
His 48	0.10	Ser 73	0.12	Gly 98	-	Glu 123	-	His 148	-	Asp 173	-	Arg 198	-
Asp 49	0.22	Ser 74	0.20	Pro 99	-	Val 124	0.12	Ala 149	-	Pro 174	-	Lys 199	-
Asn 50	0.21	Pro 75	-	Pro 100	-	Cys 125	0.21	Val 150	-	Ser 175	0.00	Phe 200	-
Ala 51	-	Glu 76	-	Ala 101	-	Val 126	-	Phe 151	-	Asp 176	0.14	Lys 201	-
Trp 52	0.00	Trp 77	-	Leu 102	0.17	Val 127	-	Ala 152	-	Val 177	0.26		
Leu 53	-	Leu 78	0.11	Val 103	3.50	Asp 128	-	Cys 153	0.30	Leu 178	0.00		

Residues for which no signal could be detected are indicated (-)

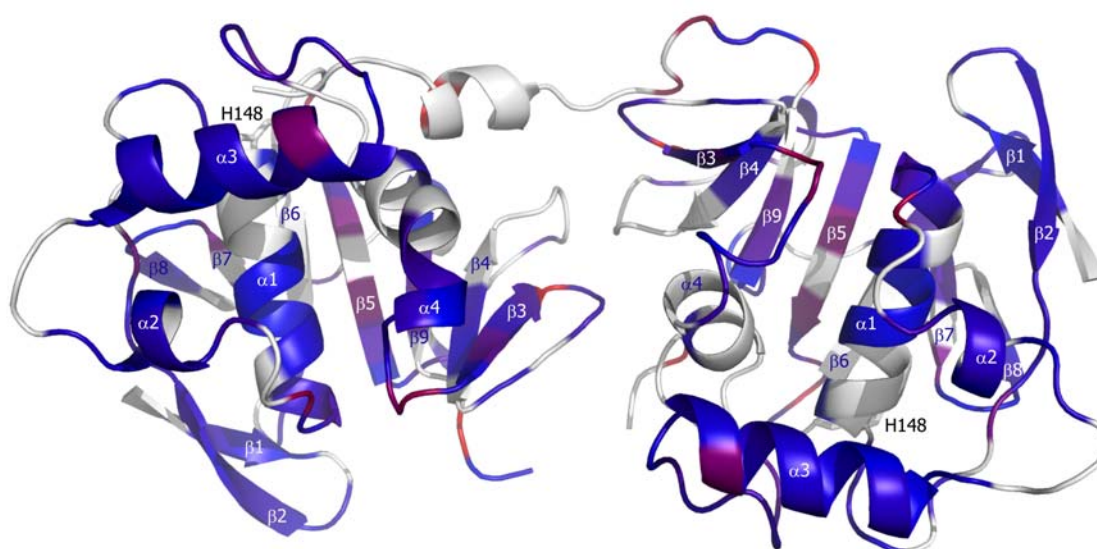


Figure 27 Differences in ^{15}N signal shifts between $\text{Lb}^{\text{pr}} \text{L143A L200F}$ and $\text{Lb}^{\text{pr}}\text{WT}$. Signal shifts of $\text{Lb}^{\text{pr}} \text{L143A L200F}$ detected in the ^1H - ^{15}N HSQC spectrum were mapped to the structure of the $\text{Lb}^{\text{pr}} \text{WT}$ dimer. The chemical shift changes are colour-coded and range from low (0.00 ppm, blue) through medium (purple) to high (1.03-6.07 ppm, red). Residues for which no signal could be detected are shown in white. The active site residues Cys 51 (mutated to Ala) (not visible) and His 148 (H148) are shown. Created with PyMOL (DeLano, 2002) using the PDB ID code 1QOL.

The overall changes found in the $\text{Lb}^{\text{pr}} \text{L143A L200F}$ spectrum were mapped to the structure of $\text{Lb}^{\text{pr}} \text{WT}$ as shown in Figure 27. This figure points out that the majority of the signals appear to be shifted in the rescue mutant $\text{Lb}^{\text{pr}} \text{L143A L200F}$. As the measurement of the T_2 relaxation times clearly suggests that $\text{Lb}^{\text{pr}} \text{L143A L200F}$ appears as a dimer, these findings indicate that the dimer is destabilised relative to the wildtype. Therefore, the additional mutation L143A could not completely restore the dimeric structure displaying the stability of a wildtype dimer.

The different oligomerisation states of $\text{Lb}^{\text{pr}} \text{L143A L200F}$ observed in size-exclusion chromatography and in NMR might be caused by the difference in protein concentration. It might be that the relatively low protein concentration of 50 nM used for size-exclusion chromatography allows the destabilised dimer to transiently dissociate into monomers, thus displaying an intermediate state of $\text{Lb}^{\text{pr}} \text{L143A L200F}$. The relatively high concentration of 1 mM used for NMR analysis might shift the of $\text{Lb}^{\text{pr}} \text{L143A L200F}$ intermediate into the dimeric state; however, the dimer appears rather destabilised.

4.1.3.3.3 3D triple resonance experiments of Lb^{pro} L200F

As the ¹H-¹⁵N HSQC spectrum of ¹⁵N labelled Lb^{pro} L200F suggested that the intramolecular binding of the CTE to the active site might be measurable, the assumed structural assignment of Lb^{pro} L200F should be confirmed by performing 3D triple resonance experiments (see chapter 3.6.3.2). To this end, inactive Lb^{pro} L200F was expressed in minimal medium containing ¹³C and ¹⁵N (see chapter 3.5.2.2). The purification of the protease was performed as described in Materials and Methods (see chapter 3.5.5). The protein sample was dialysed into NMR buffer and concentrated to about 0.5 mM (see chapter 3.6.2). A PAA gel showing the pure protein sample used for NMR analysis is displayed in Figure 28.

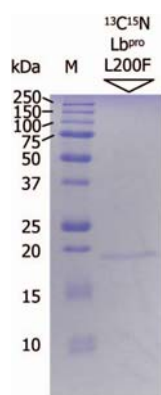


Figure 28 PAA gel showing the pure protease ¹³C ¹⁵N Lb^{pro} L200F. The inactive form of the mutant protease was expressed in minimal medium containing ¹³C and ¹⁵N. The protein was purified using the methods described in Materials and Methods (see chapter 3.5.5). 2 µg of the pure protein sample are shown on a 17.5 % 'Laemmli' SDS PAGE. The sample was further used for NMR experiments. Protein standards (kDa) are shown on the left.

As 0.5 mM lies below the optimal concentration for NMR analysis of 1 mM, the signals that could be detected were quite weak.

However, it could be shown that the ¹H-¹⁵N HSQC spectra of the double-labelled Lb^{pro} L200F is identical to the one of the single-labelled sample. The measurement of the HN(CO)CA/HNCA spectrum was also possible despite low protein concentration and the assignment of the backbone-^C_α's could be performed. Thereby, it could be shown that the signal assignment of the double labelled Lb^{pro} L200F is identical to the assumed one that was based on the assignment of sLb^{pro}. This confirms the finding observed for the single-labelled sample that there is a transient binding of the CTE to the active site of the same molecule. The only difference concerns residue Leu 188 for which two signals could be detected in the HN(CO)CA/HNCA spectrum.

Figure 29 demonstrates the assignment of residues Glu 186 to Asn 189 using Sparky software. For each of these residues a strip plot showing the HN(CO)CA and an HNCA spectrum is presented. In the HN(CO)CA spectrum the frequencies of an amide proton and nitrogen are correlated with those of the $^{13}\text{C}_\alpha$ of the preceding residue, whereas in the HNCA spectrum the frequencies of an amide proton and nitrogen are correlated with those of the $^{13}\text{C}_\alpha$ of the preceding residue as well as the same residue. Therefore, in the HN(CO)CA spectrum only the signal of the $^{13}\text{C}_\alpha$ of the preceding residue is detectable, whereas in the HNCA spectrum two signals for the $^{13}\text{C}_\alpha$ of the preceding residue and the observed residue are detectable. By this way, the chemical shifts of the protein backbone residues were assigned. The findings, that there are two signals detectable for Leu 188, might suggest that there are two different chemical environments provided to this residue.

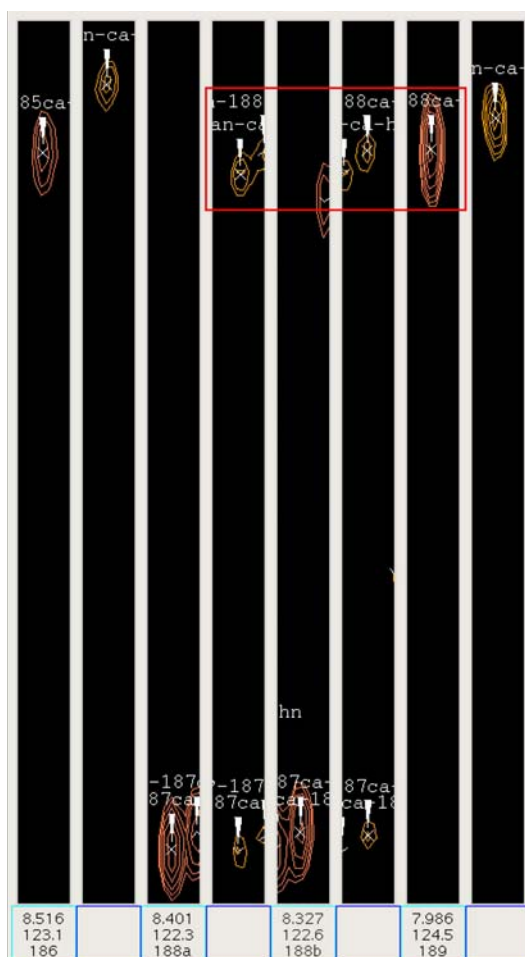


Figure 29 Backbone assignment using Strip Plots in Sparky. The proton (x-axis) and the carbon dimension (y-axis) of the amide region of the protein backbone is shown. The strip plots of an HN(CO)CA (cyan) and an HNCA spectrum (blue) of residues Glu 186 to Asn 189 are shown. The HN(CO)CA/HNCA spectrum was measured as described in Materials and Methods (see chapter 3.6.3). As Pro 187 does not contain an amide that can be detected, there is no strip plot available. For residue Leu 188, two peaks could be detected that are connected to Asn 189. Frequencies of the amide protons and the amide nitrogens that correlate are indicated by the red bar.

The two peaks for Leu 188 (named Leu 188a and Leu 188b) were also labelled in the ^1H - ^{15}N HSQC spectrum of Lb^{pro} L200F, as shown in Figure 30.

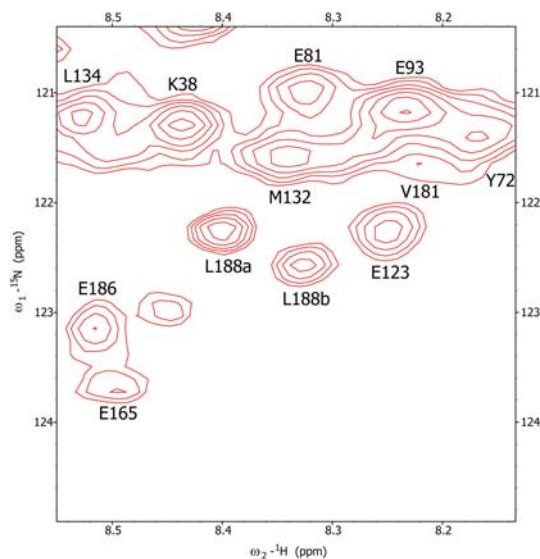


Figure 30 ^1H - ^{15}N HSQC spectrum of Lb^{pro} L200F showing two signals for Leu 188. The ^1H - ^{15}N HSQC spectrum was measured as described in Materials and Methods (see chapter 3.6.3). The two signals detected for Leu 188 are designated as L188a and L188b.

However, in the CBCA(CO)NH/HNCACB spectrum, the low protein concentration gave signals that were too weak to assign the side chain C_β 's.

4.2 Investigating the nuclear localisation of Lb^{pro}

De los Santos and colleagues recently presented experiments indicating that L^{pro} is found in the nucleus of infected cells. Assuming that Lb^{pro} enters the nucleus by a receptor-mediated mechanism, we analysed the sequence of Lab^{pro} in order to find a nuclear localisation signal (see Figure 31). Typically, a NLS is composed of one or more short sequences of the positively charged amino acids lysine and arginine. The only region of Lab^{pro} that exhibits a higher frequency of basic amino acids was found within the last nine amino acids of the CTE, **KAKVQRKLK**.

```
MNTTDCFIALVQAIREIKALFLSRTTGKMELTLYNGEKKTFYSRPNNHDN50  
CWLNAILQLFRYVEEPFDFWVYSSPENLTLEAIKQLEDLTGLELHEGGPP100  
ALVIWNIKHLLHTGIGTASRPSEVCMVDGTMCLADFHAGIFLKGQEHAV150  
FACVTSNGWYAIDDEDFYPWTPDPSDVLVFPYDQEPLNGEWKAKVQRKLL200  
K201
```

Figure 31 Amino acid sequence of FMDV O_iK Lab^{pro}. The positively charged amino acids Lys (K) and Arg (R) are shown in red. A higher frequency of basic residues is found within the last nine amino acids of the CTE, reflecting a putative nuclear localisation signal (highlighted in grey).

The first 28 amino acids do not contain a high rate of basic amino acids; therefore, we excluded that the N-terminus plays an important role in nucleocytoplasmic transport. Therefore, all experiments were performed using the Lb^{pro} form, lacking the first 28 amino acids of the N-terminus.

In order to confirm that Lb^{pro} really enters the nucleus and, if so, whether this is dependent on an NLS, an ecdysone-inducible mammalian expression system (see chapter 3.5.1.1) was used to express inactive Lb^{pro} in HEK 293T cells. Three different pMZI-constructs were used as shown in Table 12. The constructs pMZI TAP and pMZI Lb^{pro}-TAP were obtained from Carla Sousa. The TAP tag contains the sequence for Protein A which is able to bind immunoglobulins. Here, this feature is used to detect the TAP tag with an α -HRV14 antibody.

Assuming that the NLS of Lb^{pro} is located at the end of the CTE, a TAP tag directly fused to the C-terminal extension might shield the NLS, thus inhibiting the transport into the nucleus. Therefore, an additional pMZI Lb^{pro} construct was created lacking the TAP tag. To remove the TAP tag, the vector pMZI Lb^{pro}-TAP was cleaved with the enzymes *Bsi*MI and *Eco*RI, followed by the ligation with the oligonucleotides described in chapter 3.3.14.2. After confirmation of the correct sequence of the mutagenised plasmids (see chapter 3.3.13) they were used cell culture experiments.

Table 12 pMZI constructs

pMZI TAP	pMZI vector containing the sequence of the TAP tag
pMZI Lb ^{pro} -TAP *	pMZI vector containing the sequence of Lb ^{pro} fused to a TAP tag
pMZI Lb ^{pro} *	pMZI vector containing the sequence of Lb ^{pro}

* Lb^{pro} sequence contains the mutation C51A which inhibits enzymatic activity

HEK 293T cells were transiently transfected with each of the three different pMZI constructs together with the pVgRXR vector using Lipofectamine 2000. Protein expression was induced by adding 1 mM ponasterone A to the cell culture medium (see chapter 3.5.1.2). Cell extracts were separated into cytoplasmic and nucleic fractions using buffers of different salt and detergent concentrations (see chapter 3.5.3). The fractions were separated by 15 % SDS PAGE (see chapter 3.5.8.1) and blotted on a PVDF membrane (see chapter 3.5.11). The indicated proteins were detected using specific primary antibodies (see Table 7) and secondary antibodies either coupled to alkaline phosphatase or horseradish peroxidase (see Table 8). For each construct, the cells were treated with three different conditions: cells that were non-transfected (\emptyset), cells that were transfected with the plasmids, without the induction of ponasterone A (0) and cells that were transfected and induced with 1 mM ponasterone A (1).

To monitor the quality of fraction separation, proteins that are exclusively found in the cytoplasm or the nucleus were detected. To this end, α -tubulin was used as a marker for the cytoplasmic fraction, whereas lamin A/C was used for the nucleic fraction. As a control for the sensitivity of immunostaining, recombinant control proteins that had previously been expressed in bacteria were loaded (see chapter 3.5.2.1). For cell extracts containing TAP constructs, the protein HRV2 2A^{pro}-TAP was chosen as it also contains a TAP tag for detection. For cell extracts containing Lb^{pro}, Lb^{pro} WT from gelfiltration analysis (see chapter 4.1.1.2) was used as control protein.

Figure 32 shows the result of the transfection of HEK 293T cells with the vector pMZI TAP, only expressing the TAP tag as a control protein. The TAP tag was detected in the cytoplasmic fraction of transfected and induced cells (cytoplasm 1), but not in the control cells (cytoplasm \emptyset and 0). In addition, there was no TAP signal detected in the nucleic fractions (nucleus \emptyset , 0 and 1). The control proteins α -tubulin and lamin A/C indicate a sufficient separation of cytoplasmic and nucleic fractions. The detection of the control protein HRV2 2A^{pro} indicates proper immunodetection. It is important to mention that the protein concentration of the cytoplasmic and the nucleic fraction is substantially different as both fractions were brought to the same volume. As the signal detected in the cytoplasmic fraction is quite weak, it might be the case that a signal for the TAP tag in the nucleic fraction is not detectable because the protein concentration is too low.

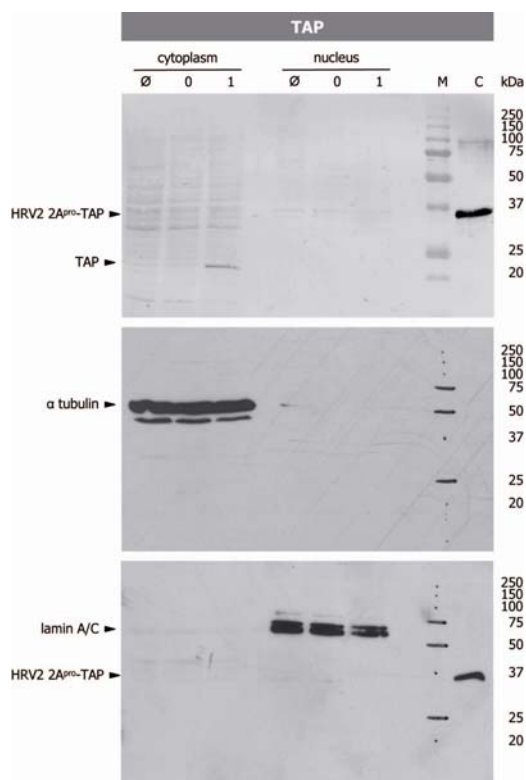


Figure 32 Immunoblot of HEK 293T fractions showing the expression of the TAP tag. HEK 293T cells were transfected and protein expression was induced for 36 to 48 hours. Cell extracts were separated into cytoplasmic and nucleic fractions. Proteins were separated on 15 % 'Laemmli' PAA gels and blotted on PVDF membranes. The TAP tag was detected using a polyclonal rabbit α -HRV14 primary antibody (1:400) and an α -rabbit alkaline phosphatase conjugated secondary antibody (1:5000). The primary antibody targets the protein A sequence which is part of the TAP tag. Tubulin was detected via a monoclonal mouse α - α -tubulin primary antibody (1:30000) and lamin A/C was detectable via a monoclonal mouse α -lamin A/C primary antibody (1:30000). For both, an α -mouse horseradish peroxidase coupled secondary antibody (1:20000) was used. Protein standards (kDa) are shown in lane M. Lane C shows the positive control for the immunoblot HRV2 2A^{pro}-TAP (0.1 μ g).

Figure 33 shows the result of the transfection of HEK 293T cells with the vectors pMZI Lb^{pro} (A) and pMZI Lb^{pro}-TAP (B). Figure 33A shows that Lb^{pro} could be detected in the cytoplasmic fraction of transfected and induced cells (cytoplasm 1), but not in the control cells (cytoplasm Ø and 0). Indeed, also a faint signal could be detected in the nucleic fraction (nucleus 1). The quality of immunostaining was confirmed by the detection of the control protein Lb^{pro} WT. However, the distribution of the control proteins α -tubulin and lamin A/C shows that the separation of the fractions was of lower quality, implying the possibility that there is contamination of the nucleic fraction with cytoplasmic material.

Figure 33B shows the localisation of Lb^{pro}-TAP in HEK 293T cells. A signal for TAP-fused Lb^{pro} was detected in the cytoplasm of transfected and induced cells (cytoplasm 1). A faint signal in the cytoplasmic fraction of transfected and non-induced cells resembles basal expression from the plasmid (cytoplasm 0). Interestingly, a faint signal for Lb^{pro}-TAP was also detectable in the nucleic fraction of transfected and induced cells (nucleus 1). Proper immunostaining was confirmed by the detection of the control protein HRV2 2A^{pro}-TAP. The distribution of the control proteins α -tubulin and lamin A/C shows that the separation of the cytoplasmic and nucleic fractions was adequate.

These findings show that Lb^{pro} is also detected in the nucleic fraction of cell extracts. However, as the amount of Lb^{pro} is not significant, this suggests that the signal evolves from a contamination with cytoplasmic material and is not related with receptor-mediated import of Lb^{pro} into the nucleus.

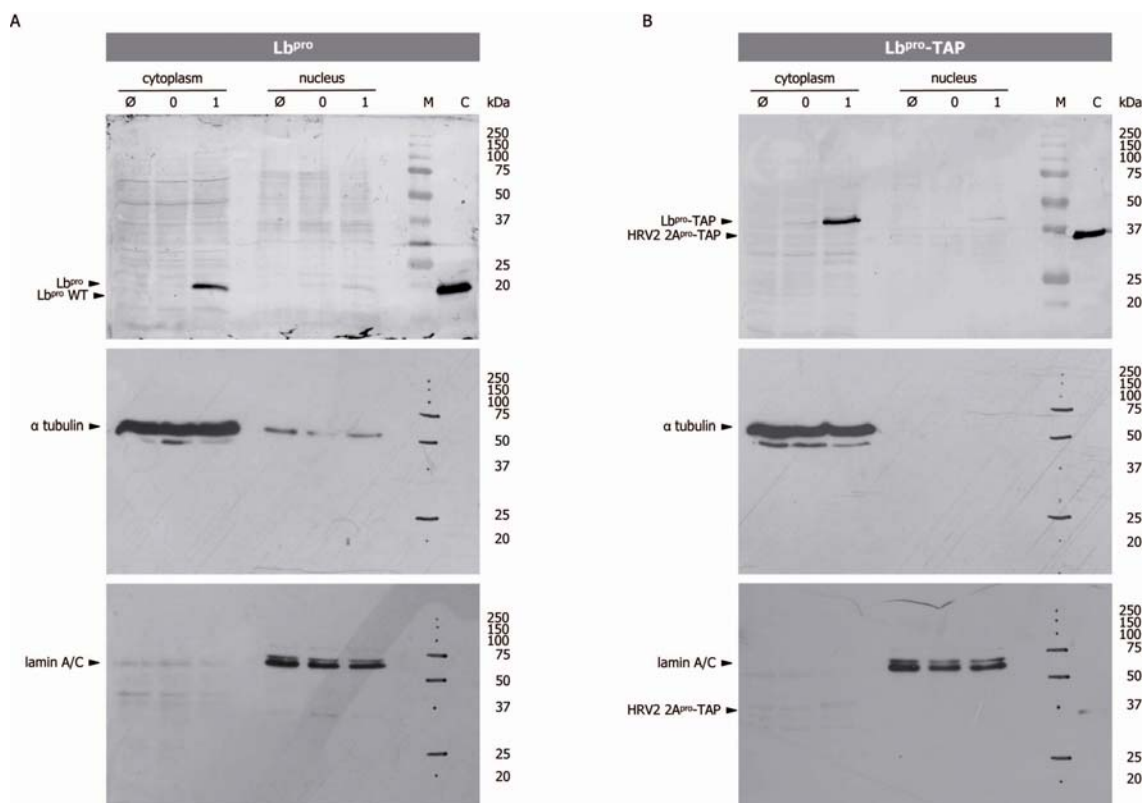


Figure 33 Immunoblot of HEK 293T fractions showing the expression of Lb^{pro} (A) and Lb^{pro}-TAP (B). HEK 293T cells were transfected and protein expression was induced for 36 to 48 hours. Cell extracts were separated into cytoplasmic and nucleic fractions. Proteins were separated on 15 % 'Laemmli' PAA gels and blotted on PVDF membranes. Lb^{pro} was detected using a rabbit α -L^{pro} antiserum (1:2000) and an α -rabbit alkaline phosphatase conjugated secondary antibody (1:5000). The TAP tag of Lb^{pro}-TAP was detected using a polyclonal rabbit α -HRV14 primary antibody (1:400) and an α -rabbit alkaline phosphatase conjugated secondary antibody (1:5000). The primary antibody targets the protein A sequence which is part of the TAP tag. Tubulin was detected via a monoclonal mouse α -tubulin primary antibody (1:30000) and lamin A/C was detected via a monoclonal mouse α -lamin A/C primary antibody (1:30000). For both, an α -mouse horseradish peroxidase coupled secondary antibody was used (1:20000). Protein standards (kDa) are shown in lane M. Lane C shows the positive control for the immunoblot; Lb^{pro} WT (0.1 mg) was used for Lb^{pro} containing fractions and for HRV2 2A^{pro}-TAP (0.1 mg) was used for Lb^{pro}-TAP containing fractions.

5 Discussion

5.1 Investigating intramolecular self-processing of Lb^{pro}

The self-cleavage reaction of Lb^{pro} is a crucial step during polyprotein processing. In this study, we consider that the self-processing reaction represents a target point to inhibit the formation of viable virus particles. A similar effect has been shown for the 2A protease of poliovirus (Crowder & Kirkegaard, 2005). The inhibition of the enzymatic activity of the viral protease 2A keeps it connected to VP1. Such, proteins can then dominantly interfere with the growth of viruses that are not defective in 2A protease activity.

Based on the findings of Crowder and Kirkegaard, we considered that the inhibition of Lb^{pro} self-processing would keep it connected to the capsid protein VP4; this would considerably interfere with proper capsid formation. It was previously shown that intramolecular self-processing is preferred over the intermolecular reaction (Cao *et al.*, 1995). Thus, these observations make the *cis*-cleavage mechanism interesting.

However, a closer investigation of *cis* self-processing was yet not possible as the Leader protease has been shown to form stable dimers in solution (Cencic *et al.*, 2007) making structural analysis difficult. In this study, we attempted to prevent dimer formation of Lb^{pro} by the introduction of site-directed mutations, whilst maintaining enzymatic activity. In the best case, the CTE of Lb^{pro} should remain devoid of mutations, as otherwise the interpretation of intramolecular self-processing would be difficult.

5.1.1 Interface mutants

Our first attempt to dissociate the Lb^{pro} dimer examined the residues Trp 105 and Thr 117, found in the interface region, which were thought to contribute to the stabilisation of dimeric molecules (Cencic *et al.*, 2007).

To this end, residues Trp 105 and Thr 117 were mutated to Ala either as single mutations or combined as a double mutation in order to remove putative stabilising interactions between dimeric molecules. The substitution of Trp 105 with the large, positively charged amino acid Arg was proposed to disrupt the dimer due to repulsion of the dimeric Lb^{pro} molecules.

All Lb^{pro} interface mutants displayed self-processing activities similar or slightly delayed to those of the wildtype. However, the analysis of the oligomerisation state revealed that all of the mutants show elution volumes similar to the wildtype, indicating the presence of a dimer. These findings show that the mutation of Trp 105 and Thr 117 to Ala or Arg was insufficient to disturb dimer formation.

The NMR structure was used to calculate the shortest distance from Trp 105 and Thr 117 of one Lb^{pro} molecule to the closest residues of the opposite molecule, as presented in Figure 34. It had been shown that one half of the dimer is rotated about 25-30° in the crystal structure due to crystallisation conditions (Cencic *et al.*, 2007); thus, the NMR data was used for calculations as the dimers are not rotated and the structure more closely reflects the native conditions. Interestingly, Arg 120' was found to be in close proximity to the opposite Trp 105 and Thr 117.

Figure 34A shows the distances between Trp 105 and residues Trp 105', Thr 117' and Arg 120' of the neighbouring molecule. Interestingly, Arg 120' is located closest to Trp 105, lying only 2.68 Å away, allowing the formation of Van der Waals interactions. The opposing Trp 105' lies 3.96 Å away, also allowing Van der Waals interactions to occur. The Thr 117 residues are located 6.07 Å apart, being out of range for any relevant interaction.

Figure 34B displays the shortest distances of Thr 117 to the residues of the neighbouring molecule constituted by Trp 105', Thr 117' and Arg 120'. These residues are the same as those found at close range to Trp 105. Again, Arg 120' is located closest to Thr 117, displaying a distance of 5.06 Å. However, as Trp 105' and Thr 117' are positioned more than 7 Å apart from Thr 117, none of the three residues is close enough to interact and contribute to the stabilisation of the dimer.

In respect of the structural data analysis, the substitution of Trp 105 with Ala would probably abrogate Van der Waals interactions. As Ala is a very small residue the distance to Arg 120' is increased, thus being out of range for any attractive interactions. As Thr 117 does not contribute to interactions between dimeric Lb^{pro} molecules, the substitution to Ala would not have any effect.

Due to the low number of interactions formed between residues of the interface, these mutations do not affect the stability of the dimer. This is reflected in the obtained results, namely no effect on self-cleavage nor on dimer formation.

In the mutant Lb^{pro} W105R, two Arg residues of each molecule from position 105 and 120 meet in the dimer interface and are supposed to induce repulsion due to the same electric charge. From structure analysis we would expect a distance of 2 – 4 Å between the opposite Arg residues. However, the analysis of Lb^{pro} W105R resembled full enzymatic activity and unchanged dimer formation.

As residues Trp 105 and Thr 117 do not essentially contribute to the stability of the dimer, we assumed that dimer stability might be mostly constituted by interactions between the CTE and the active site, as was investigated further (see chapter 5.1.2).

The assumption that Trp 105 and Thr 117 are important for dimer stability arose from NMR studies performed by Cencic and colleagues (Cencic *et al.*, 2007) (see chapter 1.5.1). However, our studies suggest that Trp 105 and Thr 117 do not contribute to interactions in the dimer interface. The reason for the signal shifts of Trp 105 and Thr 117 observed in NMR studies might have been caused by the competition of the model peptides with the CTE for the binding to the active site causing a reorientation of the interface residues. However, this does not explain why Arg 120' was not found to be shifted in these studies, though it displays a central position in the dimer interface.

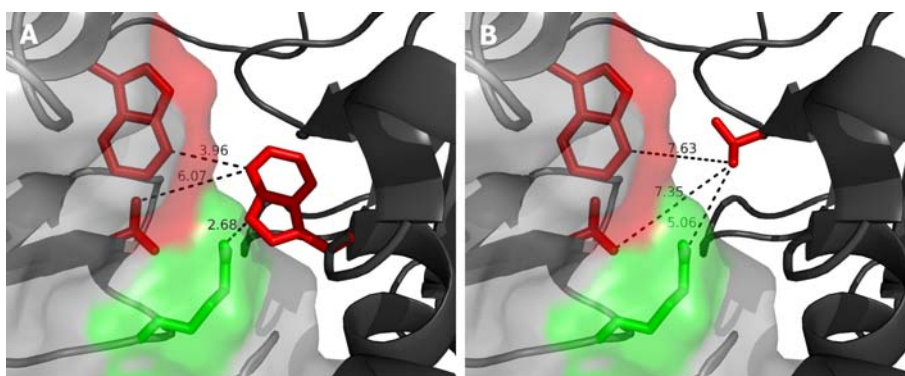


Figure 34 Distances between opposing residues in the dimer interface. The distances of the residues Trp 105 (A) and Thr 117 (B) of one molecule (black) to the closest residues of the second molecule (grey, surface) of the dimer are shown. Both residues are located in proximity to residues Trp 105' (red), Thr 117' (red) and Arg 120' (green) of the adjacent molecule. The closest distance between carbon or nitrogen atoms of the side chains were used for calculation. Distances are labelled (Å) and shown as dashed lines. Created with PyMOL (DeLano, 2002) using the PDB ID code 2JQF.

5.1.2 CTE mutants

The described investigations of the Lb^{pro} interface mutants suggested that the dimer is stabilised by the interactions between CTE and active site. Therefore, we considered investigating the mutant Lb^{pro} L200F, which was previously shown to be impaired in self-processing (Mayer *et al.*, 2008).

Our analysis of the enzymatic activity of Lb^{pro} L200F confirmed the findings of Mayer and colleagues that the substitution of Leu 200 to Phe impairs self-processing. Furthermore, we could show that eIF4GI cleavage was not affected by the substitution of Leu 200 with Phe. It was previously shown by Glaser and colleagues that Lb^{pro} is fully enzymatically active when it is still connected to the polyprotein (Glaser *et al.*, 2001). Therefore, self-processing is not a prerequisite for Lb^{pro} to cleave eIF4GI, when inhibited by this mutation.

Although the self-processing activity of Lb^{pro} L200F is impaired, the analysis of this mutant gave interesting insights in respect to intramolecular self-processing.

The oligomerisation state of Lb^{pro} L200F was analysed by size-exclusion chromatography and NMR analysis measuring the T₂ transverse relaxation times. Both investigations showed that Lb^{pro} L200F appears as a monomer showing that the single mutation L200F was sufficient to disrupt the dimer. This suggests that the dimer is exclusively stabilised by the interactions between CTE and active site, which corresponds with the findings that residues located at the interface of dimeric Lb^{pro} molecules do not contribute to the stabilisation of the dimer.

The analysis of the protein structure by measuring the ¹H-¹⁵N HSQC spectrum of Lb^{pro} L200F revealed that its structure is very similar to that of sLb^{pro}. Figure 35A shows the structure of the monomeric sLb^{pro}, onto which all signal shifts of Lb^{pro} L200F were mapped in a colour-coded manner. Interestingly, the majority of the signals that were either shifted or missing were observed for residues of the substrate binding cleft. Despite ¹³C labelling of Lb^{pro} L200F it was not possible to assign the full length CTE as there were no signals detectable for the last 12 C-terminal residues.

These results were compared to the model for intramolecular self-processing suggested by Guarne and colleagues (Guarne *et al.*, 1998) (see Figure 35B and C). In the model of Guarne and colleagues, the globular domain and the C-terminal residues Asp 184 to Asn 189 were taken from one molecule of the crystal structure (PDB ID code 1QOL). Lys 195 to Lys 201 illustrate the last seven residues of the CTE of a neighbouring molecule in the crystal (see Figure 35B). The stretch of Gly 190 to Ala 194 connecting Asn 189 and Lys 195 was modelled (see Figure 35C).

A comparison of the structural changes found in Lb^{pro} L200F with the model shows that differences in the signals were found in the area where the CTE protrudes from the globular domain as well as in the active site, reflecting a similar binding of the CTE to the active site as present in the dimer.

However, for the stretch of C-terminal residues Gly 190 to Ala 194 only a few effects on residues of the binding cleft could be detected that would indicate a tight binding of the CTE. This area of the molecule does not exhibit specific binding pockets for residues of the CTE. Therefore, there might be no close contact between the CTE and residues of the binding cleft resulting in signal changes. Nevertheless, signals for Trp 105' and Val 127' were found to be shifted which might result from interactions with certain residues of the stretch Gly 190 to Ala 194. Trp 105' shows a slight shift of 0.15 ppm that might be caused by the stacking interaction with the C-terminal residue Trp 192, as has been suggested in the model of Guarne and colleagues.

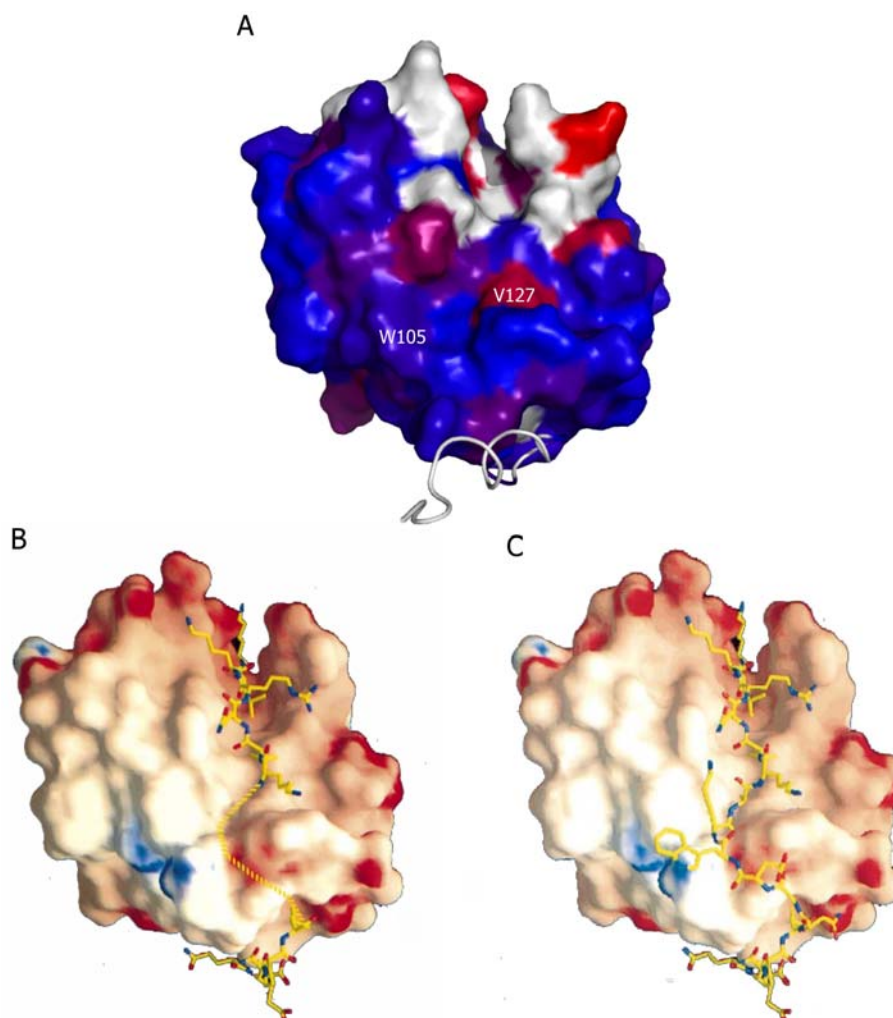


Figure 35 Model for intramolecular self-processing of Lb^{pro}. (A) Signal shifts of Lb^{pro} L200F detected in the 2D ¹H-¹⁵N spectrum are mapped on the structure of sLb^{pro}. The globular domain is shown as the surface, whereas the CTE is shown as a cartoon. The chemical shift changes are colour-coded and range from low (0.00 ppm, blue) through medium (purple) to high (0.53-0.70 ppm, red). Residues for which no signal could be detected are shown in white. Residues Trp 105 (W105) and Val 127 (V127) are labelled. Created with PyMOL (DeLano, 2002) using the PDB ID code 1QOL. (B) Model for self-processing of Lb^{pro} in *cis*. The electrostatic potential surface of the globular domain of Lb^{pro} is shown. The CTE, shown as sticks, is modelled into the binding cleft. Adapted from Guarne *et al.*, 1998.

Residue Val 127' was also found to be shifted to an extent of 0.53 ppm. This shift might be caused by interactions with Lys 195 at position P₇. However, the closest distance found in the NMR structure of the dimer between Val 127' and Lys 195 was 5.3 Å (see Figure 36). Therefore, interactions in form of Van der Waals interactions are not likely to occur. This might suggest that Lys 195 is oriented slightly differently in the self-processing reaction, enabling Lys 195 to interact with Val 127'.

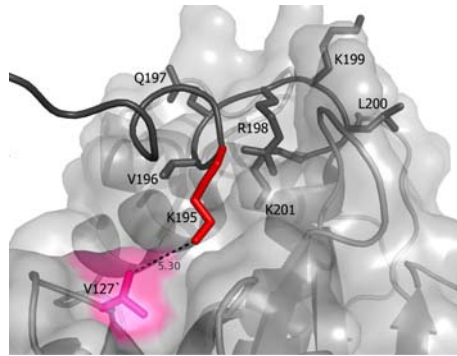


Figure 36 Distance between Val 127' and Lys 195 of the Lb^{pro} dimer. The CTE of one Lb^{pro} molecule (black) binds to the active site of the neighbouring molecule (grey, surface). The distance of 5.3 Å between Val 127' (V127') (pink) and Lys 195 (K195) (red) is labelled and indicated as dashed lines. Created with PyMOL (DeLano, 2002) using the PDB ID code 2JQF.

The fact that there are no signals detectable that could be assigned to the last 12 residues of the CTE might be caused by the rate of transient interaction between the CTE and the active site. If this interaction occurs in the time regime of a few hundred 'microseconds', the resulting signal suffers a broadening which renders it undetectable. This would explain why there are no C-terminal signals detectable. If this interaction occurs more slowly, for example in the 'milliseconds' range, there would be two signals detectable for each residue of the C-terminus for the free- and the bound-state of the CTE. If the interaction is more rapid, for example in the lower 'microseconds' range, only one averaged signal would be detectable.

In this respect, Pro 187 seems to play a crucial role, as C-terminal signals beyond this residue could hardly ever be detected. Further support concerning the importance of Pro 187 is given by the sequence alignment of different FMDV subtypes representing the seven serotypes, as shown in Figure 37. Residues Ile 141 to Lys 201 of the following FMDV subtypes are presented: Asia 1 subtype IND 97-03 (DQ989323), SAT 2 subtype 3kenya_11/60 (NC_003992), SAT 3 subtype 2sa57/59 (NC_011452), SAT 1 subtype 1bech (NC_011451), A subtype A10 (NC_011450), O subtype O1k (NC_004004) and C subtype C-S8 (AF274010). Interestingly, Pro 187 appears as the final conserved residue of the CTE. All preceding residues are conserved whereas the subsequent ones differ.

The two signals detectable for the C-terminal residue Leu 188 of the double labelled Lb^{pro} L200F might also be related to Pro 187. As the peptide bond of Pro can either exist in a *cis* or *trans* conformation, two different chemical environments could be provided for the adjacent residue. This might be the reason why there are two signals detectable for Leu 188.

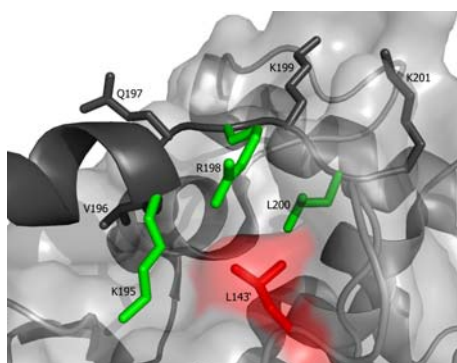


Figure 38 Contributions of Leu 143' to the interactions of the active site with the CTE. The Lb^{pro} dimer is formed by the binding of the CTE to the active site of the neighbouring molecule. The last seven residues of the CTE of one chain (black) are shown as sticks making interactions with the active site of the neighbouring molecule (grey, surface) (Santos *et al.*, 2009). Leu 143' (L143') (red) contributes to several interactions with residues of the CTE (green). It contributes to the S₂ and S₄ subsites, thereby binding Leu 200 (L200) (P₂) and Arg 198 (R198) (P₄). Furthermore, it forms Van der Waals interactions with Lys 195 (K195) (P₇). Created with PyMOL (DeLano, 2002) using the PDB ID code 1QOL.

5.2 Investigating the nuclear localisation of Lb^{pro}

The data presented by de los Santos and colleagues showed that in western blot analysis as well as in immunofluorescence studies L^{pro} localises to the nucleus of cells infected with wildtype virus (de Los Santos *et al.*, 2007). In this respect, the nuclear import could occur either by diffusion or NLS-mediated; however, we wanted to examine this further.

To this end, Lb^{pro} was expressed in HEK 293T cells either in a free form or as a fusion protein C-terminally coupled to the TAP tag. Both proteases were found in the cytoplasmic fraction; interestingly, a faint signal for both proteases could also be detected in the nucleic fraction. These findings could suggest that Lb^{pro} is able to enter the nucleus. However, it seems more likely that the signals detected in the nucleic fraction result from the contamination with cytoplasmic material. This statement is based on the quality of fraction separation as analysed by the detection of α -tubulin that should be found in the cytoplasmic fraction and lamin A/C that should be found in the nucleic fraction. However, as the separation was not 100 %, it is likely that the separation was not perfect, resulting in the contamination of the nucleic fraction with cytoplasmic material containing Lb^{pro} or Lb^{pro}-TAP.

A comparison with the data shown by de los Santos and colleagues supports the argument of cytoplasmic contamination. They similarly showed in western blot analysis that L^{pro} is found in the cytoplasmic, as well as to a lower extent in the nucleic fraction of whole virus (A12-IC) infected cells. The fact that a small portion of the viral capsid protein VP1, which is not thought to enter the nucleus, is found in the nucleic fraction also suggests a contamination with cytoplasmic material.

The TAP tag was expressed in HEK 293T cells as a control protein. The data shown here indicate that the TAP tag could be detected in the cytoplasmic fraction, but not in the nucleic fraction. However, as the signal in the cytoplasmic fraction is quite low, it is more likely that any signal in the nucleic fraction is too low for detection. Therefore, the investigation of the cellular localisation of the TAP tag did not give further information in regard to nucleocytoplasmic transport.

Thus, in western blot analysis we could not confirm the findings of de los Santos and colleagues that L^{pro} localises to the nucleus. Therefore, a closer investigation of the nucleocytoplasmic transport of Lb^{pro} was not possible. The reason for the differing results concerning the nuclear localisation of the Leader protease might be caused by the differences between the approach presented here and the one presented by de los Santos and colleagues.

The most obvious differences between these two approaches are displayed by the fact that in this study Lb^{pro} is expressed as single viral protein which is enzymatically inactive, whereas in the de los Santos approach the Leader protease is expressed in the course of a whole virus infection, being fully enzymatically active. In this regard, the enzymatic activity might be essential for Lb^{pro} to translocate to the nucleus. Although there are only eIF4GI and eIF4GII known that are cleaved by Lb^{pro}, there might be further cellular substrates which enable Lb^{pro} to enter the nucleus.

Another aspect is illustrated by the fact that the Leader protease of whole virus infected cells may benefit from effects caused by the other viral proteins. As the FMDV genome encodes 3C^{pro} as a second protease, its enzymatic activity might also play a role for the nuclear localisation of Lb^{pro}. It has been shown for poliovirus that 2A^{pro} is involved in the disruption of nucleocytoplasmic trafficking by cleaving two components, Nup 153 and Nup 62, of the nuclear pore complex (NPC) (Gustin & Sarnow, 2001). This permeabilisation of the nuclear envelope allows cytoplasmic proteins of 125 kDa to pass the nuclear pore and localise to the nucleus (Belov *et al.*, 2004). However, no similar mechanism has been determined during FMDV infection.

Another possibility how Lb^{pro} enters the nucleus might be a hitch-hiking mechanism. By the binding to a protein that contains a NLS, it could enter the nucleus without containing a NLS itself. It was shown for simian virus 40, which represents a large nucleoprotein complex, that only one nuclear localisation signal displayed by the capsid protein VP3 is sufficient for receptor-mediated transport of the whole complex through the nuclear pore (Nakanishi *et al.*, 2002). However, no further proteins, beside two homologues of eIF4G, have yet been shown to interact with Lb^{pro}.

In summary, we could not confirm the nuclear localisation of Lb^{pro}; therefore, it remains unclear whether Lb^{pro} enters the nucleus and if yes, by which mechanism.

6 Summary

Foot-and-mouth disease virus (FMDV), being a member of the picornavirus family, is a small, non-enveloped virus with a single-stranded RNA genome of positive polarity. The RNA genome is directly translated into a long polyprotein which is subsequently processed by viral proteases. The first protein encoded on this polyprotein is the Leader protease that can exist in two different forms, Lab^{pro} and Lb^{pro}, dependent on the translation initiation at two different start codons.

Lb^{pro} is a papain-like cysteine protease that frees itself from the polyprotein by cleavage between its own C-terminus and the N-terminus of the subsequent protein VP4. Lb^{pro} is a very specific protease cleaving only two cellular substrates, the two homologues of the eukaryotic translation initiation factor 4G (eIF4G), eIF4GI and eIF4GII. eIF4G plays an important role in eukaryotic translation initiation as it acts as a scaffold protein that binds together the capped mRNA and the ribosome. The term 'host cell shut off' describes the process during FMDV infection, at which eIF4G is cleaved by the Leader protease resulting in the inhibition of cellular cap-dependent translation initiation. However, the translation of the viral RNA remains unaffected as translation is initiated via an IRES (internal ribosome entry site).

The overall goal of this study is to inhibit the Lb^{pro} self-processing step. Consequently, Lb^{pro} would remain connected with the capsid protein VP4. As a result, VP4 would not be able to fit correctly into the viral capsid structure, thus inhibiting the formation of viable virus particles. Lb^{pro} self-processing can occur either inter- or intramolecularly; however, the *cis* cleavage reaction was shown to be preferred. Therefore, intramolecular self-processing of Lb^{pro} is an important target for the development of anti-virals.

Due to these facts, in this work we focused on the investigation of the intramolecular self-processing reaction of Lb^{pro} at the molecular level. It was observed that Lb^{pro} forms stable dimers in solution by inserting the C-terminal extension (CTE) of one molecule into the active site of the neighbouring molecule. Therefore, we tried to separate the dimer by site-directed mutagenesis in order to be able to investigate self-processing in *cis*. Mutations were introduced at two regions of the protease: the interface region between dimeric Lb^{pro} molecules and the CTE which binds to the active site of the neighbouring molecule.

As Trp 105 and Thr 117 were thought to contribute to the intermolecular interactions in the interface region between dimeric Lb^{pro} molecules, these residues were substituted either by Ala to remove potential attractive interactions or by Arg to provoke repulsion. However, the mutations W105A, T117A, W105A T117A and W105R in the interface region neither affected the enzymatic activity of Lb^{pro} nor could they inhibit dimer formation. Therefore, residues Trp 105 and Thr 117 do not appear to make crucial contributions to the stability of the dimer.

Interestingly, the single mutation of the C-terminal residue Leu 200 to Phe was sufficient to disrupt the dimer. Although monomeric Lb^{pro} L200F appeared delayed in self-processing, a transient binding of the CTE to the active site could be determined. Therefore, these findings

provide interesting insights concerning intramolecular self-processing. The data indicate that the last seven amino acids of the CTE are bound to the active site in a similar way as present in the dimer. However, it was not possible to detect signals for the last 12 residues of the CTE. This is probably caused by the rate of transient interaction between the CTE and the active site, which is difficult to detect by NMR.

The additional mutation L143A restores the self-processing activity as well as the dimeric structure of Lb^{pro} L200F, although the Lb^{pro} L143A L200F dimer appears rather destabilised.

Further investigations concerned the nuclear localisation of Lb^{pro}. It was considered that Lb^{pro} enters the nucleus via receptor-mediated transport. Therefore, enzymatically inactive Lb^{pro} was expressed in human cells. However, it was not possible to detect Lb^{pro} in the nucleus in appreciable amounts. Due to these findings, nuclear localisation and receptor-mediated nuclear transport of Lb^{pro} into the nucleus could not be confirmed.

7 Zusammenfassung

Das Maul-und Klauenseuchevirus (MKSU) stellt ein Mitglied der Picornavirus-Familie dar und ist ein kleines, nicht-umhülltes Virus mit einem einzelsträngigen RNA-Genom mit positiver Polarität. Das RNA-Genom wird direkt in ein Polyprotein translatiert, welches anschließend von viralen Proteasen prozessiert wird.

Das erste Protein dieses Polyproteins ist die Leader-Protease, die in Abhängigkeit von der Translationsinitiation an zwei verschiedenen Startkodons in den beiden Formen Lb^{pro} und Lb^{pro} vorkommen kann.

Lb^{pro} ist eine papain-ähnliche Cystein-Protease, die sich durch einen Schnitt zwischen dem eigenen C-Terminus und dem N-Terminus des nachfolgenden Proteins VP4 vom Polyprotein abspaltet. Lb^{pro} ist eine sehr spezifische Protease, die nur zwei zelluläre Substrate schneidet, nämlich die beiden Homologe des eukaryotischen Initiationsfaktors 4G (eIF4G), eIF4GI und eIF4GII. eIF4G spielt eine wichtige Rolle bei der eukaryotischen Translationinitiation, da es als Gerüstprotein dient und dadurch die „gecappte“ mRNA und das Ribosom zusammenführt. Der Begriff „Host cell shut off“ beschreibt den Vorgang während einer MKSV Infektion, bei dem eIF4G von der Leader Protease geschnitten wird und dadurch die zelluläre cap-abhängige Translationsinitiation verhindert wird. Dabei bleibt die Translation der viralen RNA allerdings unbeeinträchtigt, da die Translation durch eine IRES (internal ribosome entry site) eingeleitet wird.

Das letztendliche Ziel dieser Studie ist die Verhinderung der Selbst-Prozessierung von Lb^{pro} . Infolgedessen würde Lb^{pro} mit dem viralen Capsidprotein VP4 verbunden bleiben. Daher wäre VP4 nicht mehr in der Lage sich korrekt in die virale Capsidstruktur einzugliedern, weshalb die Bildung von lebensfähigen Viruspartikeln verhindert wäre. Die Selbstprozessierung von Lb^{pro} kann entweder inter- oder intramolekular ablaufen; allerdings wurde gezeigt, dass die *cis*-Spaltungsreaktion bevorzugt wird. Aus diesem Grund stellt die intramolekulare Selbst-Prozessierung von Lb^{pro} einen wichtigen Angriffspunkt für die Entwicklung von antiviralen Medikamenten dar.

Aufgrund dieser Fakten haben wir uns in dieser Arbeit darauf konzentriert die intramolekulare Selbst-Prozessierung von Lb^{pro} auf molekularer Ebene zu untersuchen. Es wurde beobachtet, dass Lb^{pro} durch Insertion des C-terminalen Fortsatzes in das aktive Zentrum des benachbarten Moleküls stabile Dimere in Lösung bildet. Daher haben wir versucht das Dimer durch zielgerichtete Mutagenese zu trennen um in der Lage zu sein die Selbst-Prozessierung in *cis* untersuchen zu können. Zwei Regionen der Protease wurden mutiert: die Grenzflächen-Region zwischen den dimeren Lb^{pro} Molekülen und der CTE, der an das aktive Zentrum des benachbarten Moleküls bindet.

Da angenommen wurde, dass Trp 105 und Thr 117 zu den intermolekularen Interaktionen in der Grenzflächen-Region zwischen dimeren Lb^{pro} Molekülen beitragen, wurden diese Aminosäuren entweder durch Ala ersetzt um potenzielle anziehende Interaktionen zu entfernen oder durch Arg um eine Abstoßung hervorzurufen. Die Mutationen W105A, T117A, W105A T117A und W105R in

der Grenzflächen-Region konnten weder die enzymatische Aktivität von Lb^{pro} beeinflussen, noch konnten sie die Bildung von Dimeren verhindern. Aufgrund dieser Tatsachen, scheinen die Aminosäuren Trp 105 und Thr 117 keinen maßgeblichen Beitrag zur Dimer-Stabilität zu leisten.

Interessanterweise war eine einzelne Mutation der C-terminalen Aminosäure Leu 200 zu Phe ausreichend um das Dimer zu trennen. Obwohl das monomere Lb^{pro} L200F eine verzögerte Selbst-Prozessierung aufweist, konnte eine transiente Binding des CTE an das aktive Zentrum festgestellt werden. Daher liefern diese Untersuchungen interessante Einblicke im Bezug auf die intramolekulare Selbst-Prozessierung. Die Daten zeigen, dass die letzten sieben Aminosäuren des CTE in einer ähnlichen Weise an das aktive Zentrum gebunden sind wie es im Dimer der Fall ist. Allerdings, war es nicht möglich Signale für die letzten 12 Aminosäuren des CTE zu detektieren. Dies wird wahrscheinlich durch die Frequenz der transienten Interaktion zwischen CTE und aktivem Zentrum bedingt, die mit Kernresonanzspektrometrie schwierig zu detektieren ist.

Die zusätzliche Mutation L143A stellt die Aktivität in der Selbst-Prozessierung wie auch die dimere Struktur von Lb^{pro} L200F wieder her, obwohl das Lb^{pro} L143A L200F Dimer destabilisiert erscheint.

Weitere Untersuchungen betrafen die nukleäre Lokalisation von Lb^{pro}. Es wurde angenommen, dass Lb^{pro} durch rezeptor-vermittelten Transport in den Zellkern eindringt. Aus diesem Grund wurde enzymatisch inaktives Lb^{pro} in humanen Zellen exprimiert. Allerdings war es nicht möglich Lb^{pro} in nennenswerten Mengen im Zellkern nachzuweisen. Aufgrund dieser Ergebnisse, konnte eine nukleäre Lokalisation und ein rezeptor-vermittelter Transport von Lb^{pro} in den Zellkern nicht bestätigt werden.

8 Appendix

8.1 Amino acids

A	Ala	alanine
C	Cys	cysteine
D	Asp	aspartic acid
E	Glu	glutamic acid
F	Phe	phenylalanine
G	Gly	glycine
H	His	histidine
I	Ile	isoleucine
K	Lys	lysine
L	Leu	leucine
M	Met	methionine
N	Asn	asparagine
P	Pro	proline
Q	Gln	glutamine
R	Arg	arginine
S	Ser	serine
T	Thr	threonine
V	Val	valine
W	Trp	tryptophan
Y	Tyr	tyrosine

8.2 Abbreviations

°C	degrees centigrade
µl	microliter
µM	micromolar
Amp	ampicillin
AP	alkaline phosphatase
APS	ammonium persulfate
ATP	adenosine triphosphate
BCIP	5-bromo-4-chloro-3-indolyl phosphate
bp	basepairs
CIP	calf intestine phosphatase
CITE	cap-independent translation enhancer
cp _N	cleavage products
cre	<i>cis</i> replicative element
CTE	C-terminal extension
dH ₂ O	deionised water
DMEM	Dulbecco's Modified Eagle Medium
DMSO	dimethyl sulfoxide
DNA	deoxyribonucleic acid
dNTP	deoxynucleotide triphosphate
DTT	dithiothreitol
EDTA	ethylenediaminetetraacetic acid
eIF	eukaryotic initiation factor
ER	endoplasmic reticulum
FCS	foetal calf serum
FMDV	foot-and-mouth disease virus
FPLC	fast protein liquid chromatography
g	gram
h	hour
HEK	human embryonic kidney
hpi	hours post infection
HRP	horseradish peroxidase
HRV	human rhinovirus
IPTG	isopropyl β-D-1-thiogalactopyranoside
IRES	internal ribosome entry site
kb	kilo bases
kDa	kilo Dalton
l	liter
Lab ^{pro}	Leader protease ab
LB	Luria Bertani

Lb ^{pro}	Leader protease b
LGS	lower gel solution
L ^{pro}	Leader protease
M	molar
MHz	megahertz
min	minute
ml	milliliter
mM	millimolar
mRNA	messenger ribonucleic acid
NBT	nitro blue tetrazolium
NLS	nuclear localisation signal
nm	nanometer
NMR	nuclear magnetic resonance
NMR	nuclear magnetic resonance
NPC	nuclear pore complex
NTP	nucleotide triphosphate
ORF	open reading frame
PABP	poly(A) binding protein
PAGE	polyacrylamide gelelectrophoresis
PBS	phosphate buffered saline
PBST	PBS-Tween
PCR	polymerase chain reaction
PNK	polynucleotide kinase
ppm	parts per million
RNA	ribonucleic acid
RNase	ribonuclease
rpm	rotations per minute
RRL	rabbit reticulocyte lysate
RT	room temperature
SDS	sodiumdodecylsulfate
SDS PAGE	SDS polyacrylamide gelelectrophoresis
sec	second
TAE	Tris-acetate-EDTA
TAP	tandem affinity purification
TE	trypsin/EDTA
TEMED	tetramethylethylenediamine
u	units
UGS	upper gel solution
UTR	untranslated region
UV	ultra-violet
V	volts

v	volume
VP	viral protein
VPg	viral protein genome
w	weigth
WT	wildtype

9 References

- Acharya R, Fry E, Stuart D, Fox G, Rowlands D and Brown F. 1989.** The three-dimensional structure of foot-and-mouth disease virus at 2.9 Å resolution. *Nature*, **337**:709-716.
- Alberts B. 2002.** *Molecular biology of the cell*, New York: Garland Science.
- Bachrach H L. 1968.** Foot-and-mouth disease. *Annu Rev Microbiol*, **22**:201-244.
- Baker N A, Sept D, Joseph S, Holst M J and McCammon J A. 2001.** Electrostatics of nanosystems: application to microtubules and the ribosome. *Proc Natl Acad Sci U S A*, **98**:10037-10041.
- Basavappa R, Syed R, Flore O, Icenogle J P, Filman D J and Hogle J M. 1994.** Role and mechanism of the maturation cleavage of VP0 in poliovirus assembly: structure of the empty capsid assembly intermediate at 2.9 Å resolution. *Protein Sci*, **3**:1651-1669.
- Belnap D M, McDermott B M, Jr., Filman D J, Cheng N, Trus B L, Zuccola H J, Racaniello V R, Hogle J M and Steven A C. 2000.** Three-dimensional structure of poliovirus receptor bound to poliovirus. *Proc Natl Acad Sci U S A*, **97**:73-78.
- Belov G A, Lidsky P V, Mikitas O V, Egger D, Lukyanov K A, Bienz K and Agol V I. 2004.** Bidirectional increase in permeability of nuclear envelope upon poliovirus infection and accompanying alterations of nuclear pores. *J Virol*, **78**:10166-10177.
- Berryman S, Clark S, Monaghan P and Jackson T. 2005.** Early events in integrin alphavbeta6-mediated cell entry of foot-and-mouth disease virus. *J Virol*, **79**:8519-8534.
- Bienz K, Egger D, Troxler M and Pasamontes L. 1990.** Structural organization of poliovirus RNA replication is mediated by viral proteins of the P2 genomic region. *J Virol*, **64**:1156-1163.
- Borman A M, Kirchwegger R, Ziegler E, Rhoads R E, Skern T and Kean K M. 1997.** eIF4G and its proteolytic cleavage products: effect on initiation of protein synthesis from capped, uncapped, and IRES-containing mRNAs. *RNA*, **3**:186-196.
- Cao X, Bergmann I E, Fullkrug R and Beck E. 1995.** Functional analysis of the two alternative translation initiation sites of foot-and-mouth disease virus. *J Virol*, **69**:560-563.
- Cencic R, Mayer C, Juliano M A, Juliano L, Konrat R, Kontaxis G and Skern T. 2007.** Investigating the substrate specificity and oligomerisation of the leader protease of foot and mouth disease virus using NMR. *J Mol Biol*, **373**:1071-1087.
- Chinsangaram J, Mason P W and Grubman M J. 1998.** Protection of swine by live and inactivated vaccines prepared from a leader proteinase-deficient serotype A12 foot-and-mouth disease virus. *Vaccine*, **16**:1516-1522.
- Chow M, Newman J F, Filman D, Hogle J M, Rowlands D J and Brown F. 1987.** Myristylation of picornavirus capsid protein VP4 and its structural significance. *Nature*, **327**:482-486.
- Davies G. 2002.** The foot and mouth disease (FMD) epidemic in the United Kingdom 2001. *Comp Immunol Microbiol Infect Dis.*, **25**:331-343.
- de Los Santos T, Diaz-San Segundo F and Grubman M J. 2007.** Degradation of nuclear factor kappa B during foot-and-mouth disease virus infection. *J Virol*, **81**:12803-12815.
- de los Santos T, Segundo F D, Zhu J, Koster M, Dias C C and Grubman M J. 2009.** A conserved domain in the leader proteinase of foot-and-mouth disease virus is required for proper subcellular localization and function. *J Virol*, **83**:1800-1810.
- DeLano D L. 2002.** The PyMOL molecular graphics system.
- Devaney M A, Vakharia V N, Lloyd R E, Ehrenfeld E and Grubman M J. 1988.** Leader protein of foot-and-mouth disease virus is required for cleavage of the p220 component of the cap-binding protein complex. *J Virol*, **62**:4407-4409.
- Donaldson A I. 1987.** Foot-and-mouth disease: the principal features. *Irish Vet. J.*, **41**:325-327.
- Donnelly M L, Luke G, Mehrotra A, Li X, Hughes L E, Gani D and Ryan M D. 2001.** Analysis of the aphthovirus 2A/2B polyprotein 'cleavage' mechanism indicates not a proteolytic reaction, but a novel translational effect: a putative ribosomal 'skip'. *J Gen Virol*, **82**:1013-1025.

- Etchison D and Fout S. 1985.** Human rhinovirus 14 infection of HeLa cells results in the proteolytic cleavage of the p220 cap-binding complex subunit and inactivates globin mRNA translation in vitro. *J Virol*, **54**:634-638.
- Etchison D, Milburn S C, Edery I, Sonenberg N and Hershey J W. 1982.** Inhibition of HeLa cell protein synthesis following poliovirus infection correlates with the proteolysis of a 220,000-dalton polypeptide associated with eucaryotic initiation factor 3 and a cap binding protein complex. *J Biol Chem*, **257**:14806-14810.
- Fenner F J, P. J. Gibbs, F. A. Murphy, R. Rott, M. J. Studdert, and D. O. White. 1993.** Veterinary virology. *Academic Press, New York*:403-430.
- Fields B N, Knipe D M and Howley P M. 2007.** *Fields' virology*, Philadelphia, Pa. ; London: Wolters Kluwer/Lippincott Williams & Wilkins.
- Foeger N, Glaser W and Skern T. 2002.** Recognition of eukaryotic initiation factor 4G isoforms by picornaviral proteinases. *J Biol Chem*, **277**:44300-44309.
- Gerber K, Wimmer E and Paul A V. 2001.** Biochemical and genetic studies of the initiation of human rhinovirus 2 RNA replication: purification and enzymatic analysis of the RNA-dependent RNA polymerase 3D(pol). *J Virol*, **75**:10969-10978.
- Glaser W, Cencic R and Skern T. 2001.** Foot-and-mouth disease virus leader proteinase: involvement of C-terminal residues in self-processing and cleavage of eIF4GI. *J Biol Chem*, **276**:35473-35481.
- Goodfellow I, Chaudhry Y, Richardson A, Meredith J, Almond J W, Barclay W and Evans D J. 2000.** Identification of a cis-acting replication element within the poliovirus coding region. *J Virol*, **74**:4590-4600.
- Gorlich D. 1997.** Nuclear protein import. *Curr Opin Cell Biol*, **9**:412-419.
- Gradi A, Foeger N, Strong R, Svitkin Y V, Sonenberg N, Skern T and Belsham G J. 2004.** Cleavage of eukaryotic translation initiation factor 4GII within foot-and-mouth disease virus-infected cells: identification of the L-protease cleavage site in vitro. *J Virol*, **78**:3271-3278.
- Gradi A, Imataka H, Svitkin Y V, Rom E, Raught B, Morino S and Sonenberg N. 1998a.** A novel functional human eukaryotic translation initiation factor 4G. *Mol Cell Biol*, **18**:334-342.
- Gradi A, Svitkin Y V, Imataka H and Sonenberg N. 1998b.** Proteolysis of human eukaryotic translation initiation factor eIF4GII, but not eIF4GI, coincides with the shutoff of host protein synthesis after poliovirus infection. *Proc Natl Acad Sci U S A*, **95**:11089-11094.
- Grubman M J. 1984.** In vitro morphogenesis of foot-and-mouth disease virus. *J Virol*, **49**:760-765.
- Guarne A, Hampoelz B, Glaser W, Carpena X, Tormo J, Fita I and Skern T. 2000.** Structural and biochemical features distinguish the foot-and-mouth disease virus leader proteinase from other papain-like enzymes. *J Mol Biol*, **302**:1227-1240.
- Guarne A, Tormo J, Kirchwegger R, Pfistermueller D, Fita I and Skern T. 1998.** Structure of the foot-and-mouth disease virus leader protease: a papain-like fold adapted for self-processing and eIF4G recognition. *Embo J*, **17**:7469-7479.
- Imataka H, Gradi A and Sonenberg N. 1998.** A newly identified N-terminal amino acid sequence of human eIF4G binds poly(A)-binding protein and functions in poly(A)-dependent translation. *Embo J*, **17**:7480-7489.
- Jackson T, Clark S, Berryman S, Burman A, Cambier S, Mu D, Nishimura S and King A M. 2004.** Integrin α v β 8 functions as a receptor for foot-and-mouth disease virus: role of the beta-chain cytodomain in integrin-mediated infection. *J Virol*, **78**:4533-4540.
- Kirchwegger R, Ziegler E, Lamphear B J, Waters D, Liebig H D, Sommergruber W, Sobrino F, Hohenadl C, Blaas D, Rhoads R E and et al. 1994.** Foot-and-mouth disease virus leader proteinase: purification of the Lb form and determination of its cleavage site on eIF-4 gamma. *J Virol*, **68**:5677-5684.
- Kolatkar P R, Bella J, Olson N H, Bator C M, Baker T S and Rossmann M G. 1999.** Structural studies of two rhinovirus serotypes complexed with fragments of their cellular receptor. *Embo J*, **18**:6249-6259.
- Kuehnel E, Cencic R, Foeger N and Skern T. 2004.** Foot-and-mouth disease virus leader proteinase: specificity at the P2 and P3 positions and comparison with other papain-like enzymes. *Biochemistry*, **43**:11482-11490.

- Lee Y F, Nomoto A, Detjen B M and Wimmer E. 1977. A protein covalently linked to poliovirus genome RNA. *Proc Natl Acad Sci U S A*, **74**:59-63.
- Luo M, Vriend G, Kamer G, Minor I, Arnold E, Rossmann M G, Boege U, Scraba D G, Duke G M and Palmenberg A C. 1987. The atomic structure of Mengo virus at 3.0 Å resolution. *Science*, **235**:182-191.
- Mason P W, Bezborodova S V and Henry T M. 2002. Identification and characterization of a cis-acting replication element (cre) adjacent to the internal ribosome entry site of foot-and-mouth disease virus. *J Virol*, **76**:9686-9694.
- Mason P W, Grubman M J and Baxt B. 2003. Molecular basis of pathogenesis of FMDV. *Virus Res*, **91**:9-32.
- Mayer C, Neubauer D, Nchinda A T, Cencic R, Trompf K and Skern T. 2008. Residue L143 of the foot-and-mouth disease virus leader proteinase is a determinant of cleavage specificity. *J Virol*, **82**:4656-4659.
- Medina M, Domingo E, Brangwyn J K and Belsham G J. 1993. The two species of the foot-and-mouth disease virus leader protein, expressed individually, exhibit the same activities. *Virology*, **194**:355-359.
- Morrell D J, Mellor E J, Rowlands D J and Brown F. 1987. Surface structure and RNA-protein interactions of foot-and-mouth disease virus. *J Gen Virol*, **68** (Pt 6):1649-1658.
- Nakanishi A, Shum D, Morioka H, Otsuka E and Kasamatsu H. 2002. Interaction of the Vp3 nuclear localization signal with the importin alpha 2/beta heterodimer directs nuclear entry of infecting simian virus 40. *J Virol*, **76**:9368-9377.
- Neff S, Sa-Carvalho D, Rieder E, Mason P W, Blystone S D, Brown E J and Baxt B. 1998. Foot-and-mouth disease virus virulent for cattle utilizes the integrin alpha(v)beta3 as its receptor. *J Virol*, **72**:3587-3594.
- O'Donnell V, Larocco M and Baxt B. 2008. Heparan sulfate-binding foot-and-mouth disease virus enters cells via caveola-mediated endocytosis. *J Virol*, **82**:9075-9085.
- O'Donnell V, LaRocco M, Duque H and Baxt B. 2005. Analysis of foot-and-mouth disease virus internalization events in cultured cells. *J Virol*, **79**:8506-8518.
- Olson N H, Kolatkar P R, Oliveira M A, Cheng R H, Greve J M, McClelland A, Baker T S and Rossmann M G. 1993. Structure of a human rhinovirus complexed with its receptor molecule. *Proc Natl Acad Sci U S A*, **90**:507-511.
- Palmenberg A C. 1982. In vitro synthesis and assembly of picornaviral capsid intermediate structures. *J Virol*, **44**:900-906.
- Pilipenko E V, Maslova S V, Sinyakov A N and Agol V I. 1992. Towards identification of cis-acting elements involved in the replication of enterovirus and rhinovirus RNAs: a proposal for the existence of tRNA-like terminal structures. *Nucleic Acids Res*, **20**:1739-1745.
- Pringle C R. 1997. Virus taxonomy 1997. *Arch Virol*, **142**:1727-1733.
- Rivera V M, Welsh J D and Maizel J V, Jr. 1988. Comparative sequence analysis of the 5' noncoding region of the enteroviruses and rhinoviruses. *Virology*, **165**:42-50.
- Rossmann M G, Arnold E, Erickson J W, Frankenberger E A, Griffith J P, Hecht H J, Johnson J E, Kamer G, Luo M, Mosser A G and et al. 1985. Structure of a human common cold virus and functional relationship to other picornaviruses. *Nature*, **317**:145-153.
- Saiz M, Gomez S, Martinez-Salas E and Sobrino F. 2001. Deletion or substitution of the aphthovirus 3' NCR abrogates infectivity and virus replication. *J Gen Virol*, **82**:93-101.
- Sangar D V, Clark R P, Carroll A R, Rowlands D J and Clarke B E. 1988. Modification of the leader protein (Lb) of foot-and-mouth disease virus. *J Gen Virol*, **69** (Pt 9):2327-2333.
- Sangar D V, Newton S E, Rowlands D J and Clarke B E. 1987. All foot and mouth disease virus serotypes initiate protein synthesis at two separate AUGs. *Nucleic Acids Res*, **15**:3305-3315.
- Sangar D V, Rowlands D J, Harris T J and Brown F. 1977. Protein covalently linked to foot-and-mouth disease virus RNA. *Nature*, **268**:648-650.
- Santos J, Gouvea I, Judice W, Izidoro M, Alves F, Melo R, Juliano M, Skern T and Juliano L. 2009. Hydrolytic Properties and Substrate Specificity of the Foot and Mouth Disease Leader Protease. *Biochemistry*.
- Sommergruber W, Zorn M, Blaas D, Fessl F, Volkmann P, Maurer-Fogy I, Pallai P, Merluzzi V, Matteo M, Skern T and et al. 1989. Polypeptide 2A of human rhinovirus

type 2: identification as a protease and characterization by mutational analysis. *Virology*, **169**:68-77.

Sonenberg N, Morgan M A, Merrick W C and Shatkin A J. 1978. A polypeptide in eukaryotic initiation factors that crosslinks specifically to the 5'-terminal cap in mRNA. *Proc Natl Acad Sci U S A*, **75**:4843-4847.

Toyoda H, Nicklin M J, Murray M G, Anderson C W, Dunn J J, Studier F W and Wimmer E. 1986. A second virus-encoded proteinase involved in proteolytic processing of poliovirus polyprotein. *Cell*, **45**:761-770.

Wimmer E. 1982. Genome-linked proteins of viruses. *Cell*, **28**:199-201.

Zeghouf M, Li J, Butland G, Borkowska A, Canadien V, Richards D, Beattie B, Emili A and Greenblatt J F. 2004. Sequential Peptide Affinity (SPA) system for the identification of mammalian and bacterial protein complexes. *J Proteome Res*, **3**:463-468.

Curriculum vitae

• Personal data

Name	Jutta Steinberger
Date of birth	7th February 1984
Adresse	Klosterweg 1, 3680 Persenbeug
Citizenship	Austria
Telephone nummer	0699 12584158
E-mail-adresse	jutta.steinberger@gmx.at



• Education

1990-1994	Elementary school in St. Martin
1994-1998	Secondary school in Amstetten
1998-2003	Commercial academy in Ybbs
2003-2004	'Individual diploma studies' at the University of Veterinary Medicine Vienna
2004-2005	'Biology' studies at the University of Vienna
2005-2009	'Genetics-Microbiology' studies at the University of Vienna

• Publications

Neubauer D, Steinberger J and Skern T. 2009. Picornaviruses. In *Viral Proteases and Antiviral Protease Inhibitor Therapy*, pp. 113-147.

• Attendance at Conferences

August 2008	Attendance and poster presentation at the VIZIER/SPINE2 workshop 'Structural virology', Vienna.
September 2008	Attendance and poster presentation at the annual meeting of the ÖGBM (Austrian society for biochemistry and molecular biology), Graz.

• Attendance at Trainings

February 2009	ÄKTA und UNICORN introductory course, Munich
---------------	--

Lebenslauf

• Persönliche Daten

Name	Jutta Steinberger
Geburtsdatum	07. Februar 1984
Adresse	Klosterweg 1, 3680 Persenbeug
Staatsbürgerschaft	Österreich
Telefonnummer	0699 12584158
E-Mail-Adresse	jutta.steinberger@gmx.at



• Ausbildung

1990-1995	Volksschule in St. Martin
1994-1999	Bundesgymnasium in Amstetten
1998-2003	Handelsakademie in Ybbs
2003-2004	„Individuelles Diplomstudium“ an der Veterinärmedizinischen Universität Wien
2004-2005	Diplomstudium „Biologie“ an der Universität Wien
2005-2009	Diplomstudium „Genetik-Mikrobiologie“ an der Universität Wien

• Veröffentlichungen

Neubauer D, Steinberger J and Skern T. 2009. Picornaviruses. In *Viral Proteases and Antiviral Protease Inhibitor Therapy*, pp. 113-147.

• Teilnahme an Konferenzen

August 2008	Teilnahme und Poster-Präsentation beim VIZIER/SPINE2 workshop „Structural virology“, Wien.
September 2008	Teilnahme und Poster-Präsentation an der Jahrestagung der österreichischen Gesellschaft für Biochemie und molekulare Biologie (ÖGBM), Graz.

• Teilnahme an Kursen

Februar 2009	ÄKTA und UNICORN Einführungskurs, München
--------------	---